DANMARKS OG GRØNLANDS GEOLOGISKE UNDERSØGELSE RAPPORT 2018/25

Final report of the activities ruby project

Formation, origin and fingerprinting of corundum (ruby and pink sapphire) from the Fiskenæsset complex and elsewhere in Greenland

Nynke Keulen (ed.)

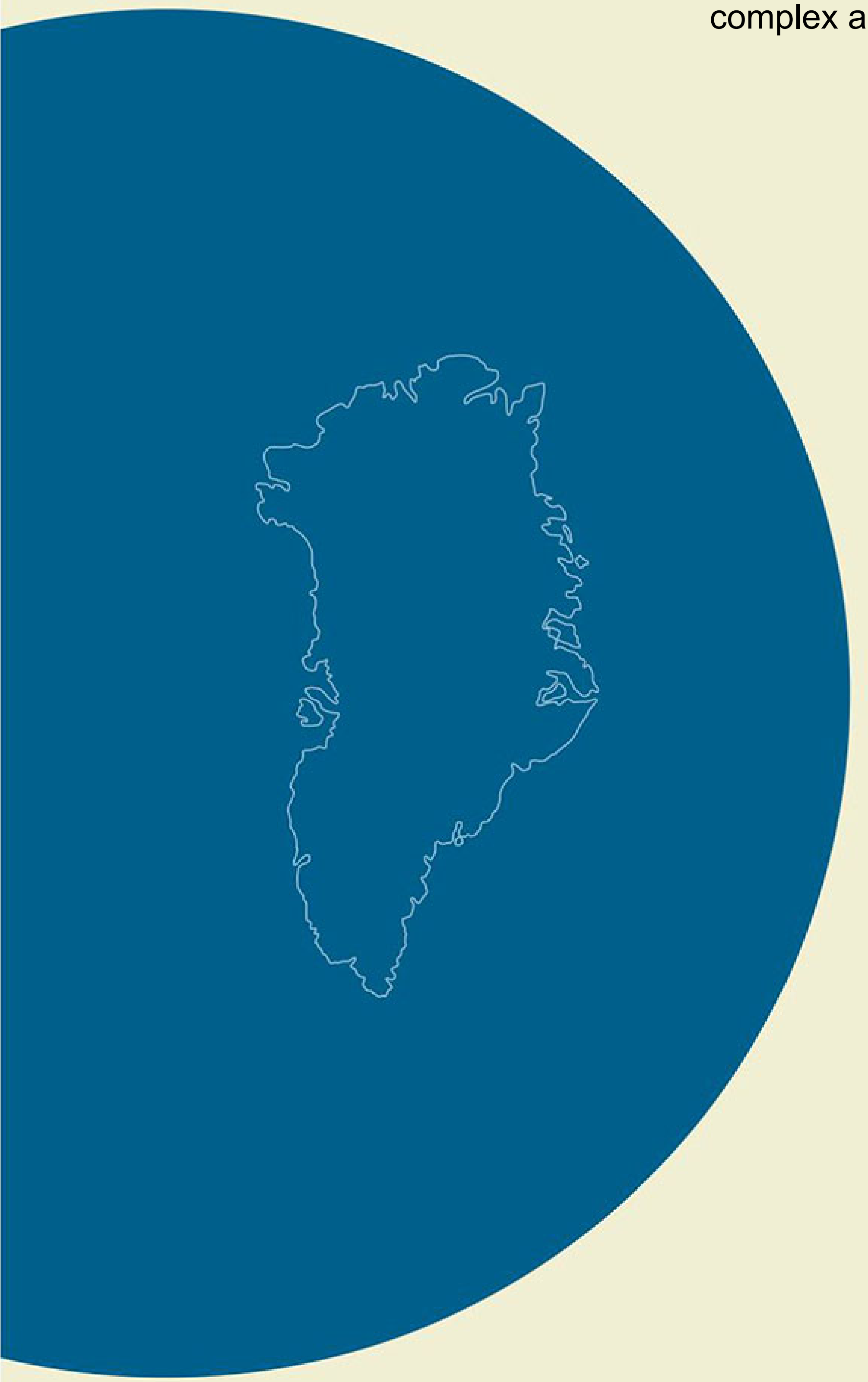

GEOLOGICAL SURVEY OF DENMARK AND GREENLAND
DANISH MINISTRY OF ENERGY, UTILITIES AND CLIMATE

G E U S

DANMARKS OG GRØNLANDS GEOLOGISKE UNDERSØGELSE RAPPORT 2018/25

Final report of the activities ruby project

Formation, origin and fingerprinting of corundum (ruby and pink sapphire) from the Fiskenæsset complex and elsewhere in Greenland

Nynke Keulen (ed.)

GEOLOGICAL SURVEY OF DENMARK AND GREENLAND
DANISH MINISTRY OF ENERGY, UTILITIES AND CLIMATE

G E U S

Contents

Executive Summary

Between 2011 and 2017 the Geological Survey of Denmark and Greenland, Copenhagen & Nuuk (GEUS) has evaluated the Greenlandic rubies as part of a collaboration project with and commissioned by the Ministry of Mineral Resources in Nuuk, Greenland. The investigations are mainly focused on characterisation of the Fiskenæsset complex (FC) ruby/sapphire, where a ruby mine is currently in operation at the most promising ruby outcrop in that area, Aappaluttoq, by the Greenlandic-Norwegian company Greenland Ruby. The license for this area was earlier held by the Canadian-Greenlandic company True North Gems Greenland (TNGG). The results for samples from the FC have been compared with samples from other areas in Greenland and abroad with the aim to find the characteristic fingerprint for the FC samples and to understand the ruby-formation process in the FC with the aim to find similar areas with rubies in the future. A pilot project was performed in 2010 by Per Kalvig and Dirk Frei from GEUS. Their samples have been re-analysed and re-interpreted and are included in this report.

In the course of this project, the following data has been collected and is reported and discussed in this report:

- Field report: describing the collection of samples in 2011 (Appendix A).
- Optical microscopy features: images of rubies of the FC showing internal features of the rubies and sapphires.
- Colour determination: Description of the colours of the rubies from the FC following the Munsell Notation.
- SEM inclusions: overview of the mineral inclusions found in corundum samples from the FC.
- Metamorphic history of the FC with a focus on the ruby-forming reaction. Microprobe analyses on thin sections from the FC and whole rock geochemistry for a few samples.
- LA-ICP-MS: trace element composition for all samples from the FC, other localities in Greenland and from a range of other countries.
- µXRF: pilot study on the trace element composition with data on 11 samples.
- LIBS: pilot study on the trace element composition with data on 14 samples.
- Oxygen isotopes: analyses of the oxygen isotope results for samples from the FC and elsewhere.
- Raman and fluorescence spectroscopy: pilot study on the possibilities to use these methods to fingerprint corundum.
- Multivariate statistics: pilot investigation using the software Siro-SOM.
- A blind test of the fingerprinting by trace elements.
- An investigation of the effects of LA-ICP-MS analyses on the surface of polished gemstones.

Ruby formation in the FC, including Aappaluttoq result from a metasomatic reaction of anorthite-rich rocks (anorthosite and leucogabbro) and ultramafic rocks, triggered by the intrusion of pegmatites shortly after peak metamorphic conditions (ca. 640°C and 7 kbar; 2.72-2.70 Ga). The anorthite component of the plagioclase is the source for the aluminium and oxygen

in the rubies, while important trace colouration elements, including Cr, are derived from the Archaean ultramafic rocks. In the FC, the presence of pegmatite with a special composition (halide anion- and/or K-enriched), ultramafic rocks and anorthosite-rich rocks define, together with the correct pressure and temperature conditions, whether the ruby-forming reaction will take place in ruby-bearing ultramafic complexes.

The most suitable trace elements to define the origin of the FC rubies (including Aappaluttoq) are Cr, Ga, V, Fe, and Ti. Rubies from the FC yield high Cr, intermediate Fe, rather low V, and low Ga and Ti concentrations compared to abundances in rubies from international deposits. In addition, Mg, Si, Ca, Na, Ba, Zr, K and Sr are common trace element in FC rubies. Values for Aappaluttoq agree well with previous studies and compare well to other high-quality localities in the FC. There is an overlap in trace element composition with some other samples derived from similar outcrops with ruby-bearing ultramafic complexes such as Umba, Seza Kofi and Longido, and with the placer deposit derived of possibly the same primary rocks like Andilamena (Madagascar). Rubies from other Greenlandic localities near Maniitsoq are slightly enriched in Ta, Nb and locally Pb, while those from the Tasiilaq area are relatively enriched in Sn, Sr, Nb, Ta and Pb, but show lower Cr/Ga values than FC ruby samples.

The obtained $\delta^{18}O$ values (1.62-4.20‰) for the FC and Nattivit area in the Tasiilaq area are low compared to most other analysed deposits outside Karelia (NW Russia) and Madagascar. Rubies from other ultramafic rock complexes including Tanzania (Winza, Tunduru, and Songea), and Kapisilit, Westgreenland, as well as samples derived from xenoliths in basalts display slightly higher $\delta^{18}O$ values.

The investigation of optical features and inclusions derived from the FC, including Aappaluttoq reveal that typical features include growth zonation, negative crystals, rutile and boehmite needles, milky zones, and zonal clouds combined with the typical mineral inclusions biotite, Ca-rich amphiboles (anthophyllite, pargasite), rutile, zircon, spinel, sapphirine, and anorthite. While rutile is a very common inclusion mineral, and biotite and spinel occur frequently, the other minerals are rarer. The combined presence of several inclusion minerals and other optical features is required for a successful fingerprinting.

For the most beneficial fingerprinting, the three described fingerprinting techniques (trace elements, oxygen isotopes, optical features) should be combined. As the geological history of the FC is relatively unique – only few other anorthosite-ultramafic rock complexes metamorphosed at granulite-upper amphibolite facies yield high-quality rubies – fingerprinting of these Greenland rubies is possible with only few possibilities for overlapping alternative localities.

1. Introduction

1.1 Included material

This final report contains the integrated results of five earlier reports and two scientific papers:

Kalvig, P. & Keulen, N. 2011: Aktiviteter i Rubinprojektet, 2011 – Samarbejdsprojekt med Råstofdirektoratet. Denmark og Grønlands Geologiske Undersøgelse Rapport **2011/138**, 41pp.

Keulen, N. & Kalvig, P. 2013: Report on the activities in the ruby project 2012. A joint project with the Bureau of Minerals and Petroleum. Danmarks og Grønlands Geologiske Undersøgelse Rapport **2013/9**, 24pp.

Keulen, N. & Poulsen M.D. 2014: Report on the activities in the ruby project 2011-2013. Danmarks og Grønlands Geologiske Undersøgelse Rapport **2014/36**, 44pp.

Keulen, N., Poulsen, M.D. & Salimi, R. 2016: Report of the activities in the ruby project 2014. Danmarks og Grønlands Geologiske Undersøgelse Rapport **2016/20** 29pp.

Keulen, N. 2017: Data collected in the ruby project. Danmarks og Grønlands Geologiske Undersøgelse Rapport **2017/14**. GEUS, 1 pp. + USB stick.

Keulen, N. & Kalvig, P. 2013: Fingerprinting of corundum (ruby) from Fiskenæsset, West Greenland. In: Bennike, O., Garde, A.A, & Watt, W.S. (eds): Review of Survey Activities 2012. Geological Survey of Denmark and Greenland Bulletin 28, 53-56. (Included as Appendix B)

Keulen, N., Thomsen, T.B., Schumacher, J.C., Poulsen M.D., Kalvig, P., Vennemann, T. & Salimi, R. Formation, origin and geographic typing of corundum (ruby and pink sapphire) from the Fiskenæsset complex, Greenland. Submitted to Lithos.

Furthermore, the results of the Laser-Induced Breakdown Spectroscopy analyses are presented here. The analyses were carried out by Simon Hansen Serre, GEUS and have not been reported previously, nor are they included in the submitted paper.

1.2 Background for the investigations

Fingerprinting of gemstones, including rubies, is performed for economic, political, and scientific reasons. The country of origin of a gemstone is a factor determining its market value, irrespective of quality aspects like colour, cut, or clarity. Rubies from Myanmar, for example, are valued higher than rubies from other countries, even if they have exactly the same physical properties (Rossman 2009). Governments have an interest in whether gemstones were mined in their own country for taxation reasons. Some gemstones come from conflict zones, or areas with high rates of child-labour, which is less attractive to certain potential customers. Trade with stones from some of these areas can have been banned intermittently for political reasons.

Fingerprinting and the geochemical investigations of the rubies may indicate the provenance of placer deposits (Giuliani *et al.* 2007; Kochelek *et al.* 2015), which yield information on sedimentary and tectonic processes during the geological history of the area or point to hitherto unknown source areas where rubies still might be found in-situ. Geochemical analyses also give information on the processes forming the rubies, and as many rubies worldwide are found in placer deposits or in xenoliths, these processes are not always clearly understood. In this report, we combine metamorphic petrology observations on rocks hosting in-situ-formed rubies and geochemical observations on the same rubies in order to connect the ruby-forming metamorphic reactions with the unique fingerprint for these minerals.

The metamorphic and geochemical investigations described and discussed in here focus on the ruby deposits in the FC in southern West-Greenland, where an open-pit ruby mine recently opened (Figure 1). The FC comprises a ca. 550 m thick series of intrusive sheets of anorthosite, leucogabbro, gabbro, and ultramafic rocks (Myers 1985; Windley *et al.* 1973) that intruded into a sequence of amphibolites, which in places can be found as only mildly deformed metavolcanic rocks. This can e.g.be seen in the Bjørnesund Supracrustal Belt and at Pikiniq (located ca. 20 km east of the village of Fiskenæsset) (Keulen *et al.* 2014b). The amphibolites show mixed geochemical evidence for being subduction-related, as well as being associated with a Mid Oceanic Ridge setting (Polat *et al.* 2009; Szilas *et al.* 2012). Ultramafic rocks in the FC occur as complete units or as 10-100 m long lenses-shaped bodies that consist of either nearly monomineralic clinopyroxenite with minor plagioclase and titanite, or dunite with mainly olivine and minor Fe-hydroxides, chlorite, plagioclase and spinel. The intrusive age of the FC was determined on magmatic zircons to ca. 2.97-2.95 Ga (Keulen *et al.* 2010; Polat *et al.* 2010), which is consistent with whole-rock Sm-Nd isotope data including both intrusive and extrusive units and yield an errorchron age of 2973 ± 28 Ma (Polat *et al.* 2010). With an initial εNd value of +3.3, the FC was likely derived directly from the ambient depleted mantle at that time. The FC is surrounded by orthogneiss and dissected by intrusive sheets of mainly tonalitic and granodioritic composition that have a protolith age of 2.917 ± 0.005 Ga-2.878 ± 0.006 Ga (Keulen *et al.* 2014b; Kokfelt *et al.* 2011; Friend and Nutman 2001). During the latest Mesoarchaean and the Neoarchaean the FC near the village of Fiskenæsset was metamorphosed at lower granulite-facies conditions, whereas further to the south and east mid- to upper amphibolite-facies conditions were reached (McGregor and Friend 1992; Schumacher *et al.* 2011).

Field observations demonstrate that the ruby-forming reaction in the FC typically occurs directly at the contact between ultramafic rock (typically peridotite or dunite), which commonly were hydrated prior to the ruby-forming reaction, and an anorthite-rich rock (anorthosite, leucogabbro). The reaction is triggered by a generation of pegmatites dated to 2.72-2.70 Ga (Keulen *et al.* 2014b), during which those pegmatites change in composition from regular granodioritic to tonalitic sheets into a nearly pure anthophyllite or phlogopite rock. It is possible that these pegmatites either contain K-enriched fluids or that the pegmatite fluids were enriched in, e.g. B, F or Cl, as associated minerals in the reaction zone are ruby, cordierite, spinel, sapphirine, calcic amphibole, sillimanite and kornerupine. Resulting reaction zones are typically between ca. 50 cm and 5 m wide. The presence of the ultramafic rocks in the ruby-forming reaction zone causes a distinct trace element signature for the FC rubies (Keulen and Kalvig 2013). Here, we provide further details on the unique geochemical signature of the FC rubies and determine if these features can be used to fingerprint rubies derived from this deposit. In general, little information is available on the geochemical fingerprint of other Greenland ruby occurrences, thus we also present data from the occurrences at

Maniitsoq NW, Kangerdluarssuk (Maniitsoq), Storø, Kapisillit, Ujarassuit Nunaa and Nattivit. As far as we currently know, these other occurrences are small and foremost of economic interest to small-scale mining projects. However, they yield a wealth of scientific information, as they all occur in a setting with ultramafic rocks involved in the ruby-formation, but nevertheless show different metamorphic reactions and fingerprints compared to the FC occurrences.

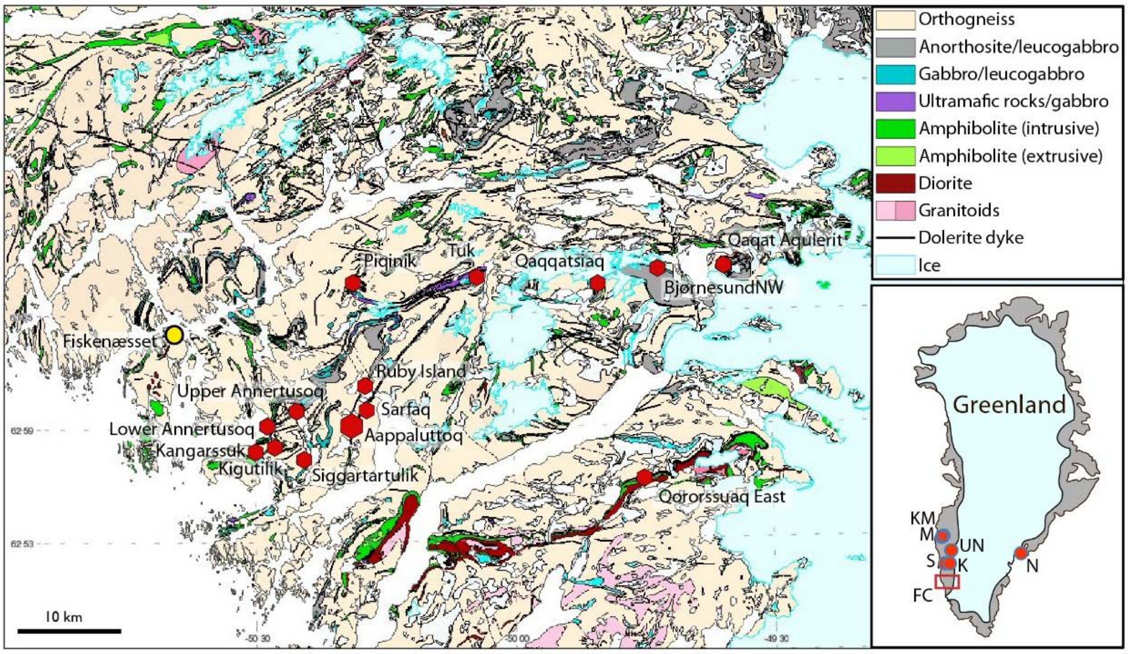

Figure 1. *Simplified geological map of the Fiskenæsset complex indicating the localities of the analysed samples (red diamonds) and the village of Fiskenæsset (yellow dot). Map modified from Keulen et al. 2011. Insert shows the location of the Greenlandic samples outside the Fiskenæsset complex (FC, red square); KM = Kangerdluarssuk near Maniitsoq, M = Maniitsoq NW, UN = Ujarassuit Nunaa, N = Nattivit, S = Storø, K = Kapisilit.*

In this report, we refer to all red and pink corundum as ruby and to all corundum of other colours as sapphire(s), irrespective of the quality (gem, semi-gem or non-gem) of the minerals. All analyses are performed on non-treated, unheated, raw material, unless indicated. Throughout this report we also excluded the prefix meta- for anorthositic, dioritic, ultramafic and (leuco)gabbroic rocks, despite their clear metamorphic overprint. This is common practice for rocks of the Greenlandic North Atlantic Craton.

2. Analytical methods

2.1 Sample set

The samples investigated in this study are from the FC, from the ruby occurrences in Greenland shown in Figure 1, and from deposits outside Greenland (here labelled as international samples). For electron microprobe analyses (EMPA) and whole-rock geochemistry ruby-bearing rock samples were investigated, while the other analyses, i.e. Laser Ablation Inductively Coupled Plasma Mass Spectrometry trace element investigations (LA-ICP-MS), oxygen isotope geochemistry, optical microscopy and scanning electron microscope (SEM), mineral inclusion analyses were performed on individual rubies, which were separated from their parent rock by crushing and hand-picking. Table 1 lists all samples and the analyses performed on them.

2.2 Electron Microprobe Analyses (EMPA)

Mineral analyses of thin sections of eight ruby-bearing rock samples from the FC were performed by electron microprobe, using Copenhagen University's JEOL JXA-8200 Superprobe, fitted with five wavelength dispersive spectrometers (WDS) and one energy dispersive spectrometer (EDS). Rubies, their reaction rims, and the surrounding minerals were analysed for their major element properties (Si, Al, Fe, Mn, K, Ca, Mg, Cr, and Ni). The electron microprobe was operated at 15 kV acceleration voltage, 1.5×10^{-8} A beam current, and an approximately 5 µm beam diameter. Modelling of the phase relations to obtain the pressure- (p) and temperature-(T) conditions, was done using the Perple_X software suite (Connolly 2005).

2.3 Whole-rock geochemistry

Whole-rock geochemistry was carried out on five samples of varied mineralogy to characterise the bulk composition of these rocks. The analyses were carried out by Activation Laboratories, Ontario, Canada, using their Research Lithium Metaborate/Tetraborate Fusion – ICP/MS analytical package.

2.4 Trace element geochemistry by laser-ablation ICP-MS

Trace element concentrations of rubies were determined on ruby mineral separates in polished mounts by isotopic analyses using LA-ICP-MS at the Geological Survey of Denmark and Greenland (GEUS). The analyses focused on red, transparent raw material (ruby) without many inclusions, but other material, especially with different colours, was also investigated. A NWR213 frequency-quintupled Nd:YAG solid state laser system from New Wave Research/ESI, employing two-volume cell technology, was coupled to an ELEMENT 2 double-focusing single-collector magnetic sector field-ICP-MS from Thermo-Fisher Scientific.

Table 1. *Sample list showing the localities and indicating the applied analytical techniques for the samples in this study. Sample numbers are GEUS' sample numbers following the GGU numbering system. Abbreviations: EMPA+WRG = Electron Microprobe Analyses and Whole-Rock Geochemistry, LA-ICP-MS = Laser Ablation Inductively Coupled Plasma Mass Spectrometry trace element investigations, Oxygen = Oxygen isotope geochemistry, Optical = optical microscopy, SEM-EDS = Scanning Electron Microscope Energy Dispersive Spectrometry. Sample 545601 has been heat-treated, the other samples are untreated. Samples with ? before their locality name cannot be guaranteed to originate from this locality.*

Sample no.	Country	Region	Locality	Latitude	Longitude	EMPA+ WRG	LA-ICP-MS	Oxygen	Optical	SEM-EDS
477395	Greenland	Fiskenæsset	Aappaluttoq	63.01089	-50.3197		X	X		
521101	Greenland	Fiskenæsset	Aappaluttoq	63.01067	-50.3206		X			X
521103	Greenland	Fiskenæsset	Aappaluttoq	63.01067	-50.3206	X				
521104	Greenland	Fiskenæsset	Aappaluttoq	63.01067	-50.3206		X		X	X
521105	Greenland	Fiskenæsset	Aappaluttoq	63.01067	-50.3206	X	X			X
521106	Greenland	Fiskenæsset	Aappaluttoq	63.01067	-50.3206	X	X			X
521107	Greenland	Fiskenæsset	Aappaluttoq	63.01067	-50.3206		X			
521108	Greenland	Fiskenæsset	Aappaluttoq	63.01067	-50.3206		X		X	X
521109	Greenland	Fiskenæsset	Aappaluttoq	63.01067	-50.3206		X		X	X
521110	Greenland	Fiskenæsset	Aappaluttoq	63.01067	-50.3206		X			X
521111	Greenland	Fiskenæsset	Aappaluttoq	63.01067	-50.3206		X			X
521113	Greenland	Fiskenæsset	Aappaluttoq	63.01067	-50.3206		X			
521114	Greenland	Fiskenæsset	Aappaluttoq	63.01067	-50.3206	X				
521115	Greenland	Fiskenæsset	Aappaluttoq	63.01067	-50.3206	X				
521119	Greenland	Fiskenæsset	Aappaluttoq	63.01067	-50.3206	X				
521120	Greenland	Fiskenæsset	Aappaluttoq	63.01067	-50.3206		X		X	
521121	Greenland	Fiskenæsset	Aappaluttoq	63.01067	-50.3206		X			X
497394	Greenland	Fiskenæsset	Annertusoq	63.01186	-50.4313		x			
521123	Greenland	Fiskenæsset	Upper Annertusoq	63.01189	-50.4293		X		X	X
521127	Greenland	Fiskenæsset	Upper Annertusoq	63.01189	-50.4293		X			X
521130	Greenland	Fiskenæsset	Lower Annertusoq	63.00697	-50.4788		X			X
513743	Greenland	Fiskenæsset	BjørnesundNW	63.1268	-49.7408		X	X		
521131	Greenland	Fiskenæsset	BjørnesundNW	63.12672	-49.746		X			X
521132	Greenland	Fiskenæsset	BjørnesundNW	63.12672	-49.746		X			X
521133	Greenland	Fiskenæsset	BjørnesundNW	63.12672	-49.746	X				
521134	Greenland	Fiskenæsset	BjørnesundNW	63.12672	-49.746		X		X	
521135	Greenland	Fiskenæsset	BjørnesundNW	63.12672	-49.746		X			
497386	Greenland	Fiskenæsset	Pikiniq	63.1279	-50.2897		X	X		

511163	Greenland	Fiskenæsset	Pikiniq	63,12443	-50.292		X			X
459991	Greenland	Fiskenæsset	Kangaarsuk	62.97925	-50.5273		X			
521149	Greenland	Fiskenæsset	Kigutilik	62.98878	-50.4794		X			X
160098	Greenland	Fiskenæsset	Qaqqat Akuleriit	63.14028	-49.5828		X			
497391	Greenland	Fiskenæsset	Qaqqat Akuleriit	63.14028	-49.5828		X			
160063	Greenland	Fiskenæsset	Qaqqatsiaq	63.12601	-49.8232		X			
510132	Greenland	Fiskenæsset	Qaqqatsiaq	62.95398	-49.728		X			X
508660	Greenland	Fiskenæsset	QoororsuaqEast	63.12601	-49.8232		X			X
497393	Greenland	Fiskenæsset	Ruby Island/ Tarsiusarsuaq	63.03617	-50.2864		X	X		
521142	Greenland	Fiskenæsset	Ruby Island/ Tarsiusarsuaq	63.03617	-50.2864		X		x	X
521144	Greenland	Fiskenæsset	Ruby Island/ Tarsiusarsuaq	63.03617	-50.2864	X				
459905	Greenland	Fiskenæsset	Sarfaq	63.013	-50.3166		X			
497392	Greenland	Fiskenæsset	Siggartatulik	62.98481	-50.4269		X	X		
521138	Greenland	Fiskenæsset	Siggartatulik	62.98671	-50.4197		X			X
521140	Greenland	Fiskenæsset	Siggartatulik	62.98671	-50.4197		X			X
521159	Greenland	Fiskenæsset	Siggartatulik	62.98671	-50.4197				X	
521160	Greenland	Fiskenæsset	Siggartatulik	62.98671	-50.4197				X	
476373	Greenland	Fiskenæsset	Tuk	63.13972	-50.0611		X			
289933	Greenland	Maniitsoq	Maniitsoq	65.54922	-52.4164		X	X		
339590	Greenland	Maniitsoq	Kangerdsluarssuk	65.54922	-52.4164		X			
339592	Greenland	Maniitsoq	Kangerdsluarssuk	65.54922	-52.4164		X			
339598	Greenland	Maniitsoq	Kangerdsluarssuk	65.54922	-52.4164		X			
339599	Greenland	Maniitsoq	Kangerdsluarssuk	65.54922	-52.4164		X			
339611	Greenland	Maniitsoq	Kangerdsluarssuk	65.54922	-52.4164		X			
339612	Greenland	Maniitsoq	Kangerdsluarssuk	65.54922	-52.4164		X			
339613	Greenland	Maniitsoq	Kangerdsluarssuk	65.54922	-52.4164		X			
224779	Greenland	Nuuk	Kapisillit	64.29465	-49.9801		X	X		
497396	Greenland	Nuuk	Storø	64.39791	-51.0411		X	X		
545609	Greenland	Nuuk	Storø	64.4375	-51.0412		X			
569728	Greenland	Nuuk	Storø	64.4269	-51.0203		X			
545632	Greenland	Nuuk	Ujarassuit Nunaa	64.94583	-50.0472		X			
545632	Greenland	Nuuk	Ujarassuit Nunaa	64.94583	-50.0472		X			
319411	Greenland	Tasiilaq					X			
497397	Greenland	Tasiilaq	Nattivit	62.95398	-49.728		X	X		

562714	Greenland	Tasiilaq	Nattivit	65.618	-38.4709		X			
562726	Greenland	Tasiilaq	Nattivit	65.618	-38.4709		X			
562727	Greenland	Tasiilaq	Nattivit	65.62101	-38.4855		X			
562737	Greenland	Tasiilaq	Nattivit	65.618	-38.4709		X			
545604	Cambodia		Pailin				X			
545607	Cambodia		?Pailin				X			
545608	Cambodia		?Pailin				X			
545626	Ethiopia						X			
545627	India						X			
497399	Macedonia						X			
545602	Madagascar		?Ilakaka				X			
545629	Madagascar						X			
545630	Madagascar						X			
545631	Madagascar						X			
545625	Myanmar	?Mong Hsu					X			
545624	Myanmar		Mogok North				X			
545622	Myanmar		Mogok West				X			
545621	Sri Lanka		?Pel Madulla				X			
1A-545613	Greenland	Fiskenæsset	Aappaluttoq				X			
1B-545613	Greenland	Fiskenæsset	Aappaluttoq				X			
1C-545613	Greenland	Fiskenæsset	Aappaluttoq				X			
2A-545614	Greenland	Fiskenæsset	Kigutilik				X			
2B-545614	Greenland	Fiskenæsset	Kigutilik				X			
3A-545615	Greenland	Fiskenæsset	Siggartatulik				X			
3B-545615	Greenland	Fiskenæsset	Siggartatulik				X			
4A-545616	Greenland	Fiskenæsset	Ruby Island				X			
4B-545616	Greenland	Fiskenæsset	Ruby Island				X			
5A-545617	Greenland	Fiskenæsset	Qaqqatsiaq				X			
5B-545617	Greenland	Fiskenæsset	Qaqqatsiaq				X			
6A-545618	Greenland	Fiskenæsset	Lower Annertusoq				X			
6B-545618	Greenland	Fiskenæsset	Lower Annertusoq				X			
6C-545618	Greenland	Fiskenæsset	Lower Annertusoq				X			
7A-545619	Greenland	Fiskenæsset	Upper Annertusoq				X			

The mass spectrometer was equipped with a Fassel-type quartz torch shielded with a grounded Pt electrode and a quartz bonnet. Operating conditions and data acquisition parameters are listed in Table 2.

To ensure stable laser output energy, a laser warm-up time of min. 15 minutes were applied before operation, providing stable laser power and flat craters by a “resonator-flat” laser beam. The mass spectrometer was run for at least one hour prior to analyses to stabilize the background signal. Samples and standards were carefully cleaned with ethanol before loading to remove surface contamination. After sample insertion, the ablation cell was purged with the helium carrier gas for a minimum of 20 minutes to minimize gas blank level. The helium was mixed with argon gas ca. 0.5 m before introduction into the plasma.

The ICP-MS was optimised for dry plasma conditions through continuous linear ablation of the NIST-612 glass standard. The signal-to-noise ratios were maximized for isotopes in the middle and heavy mass range (i.e. ^{49}Ti to ^{208}Pb) while opting for low element-oxide production levels by minimizing the $^{254}UO_2/^{238}U$ ratios. Instrumental drift was minimized by following a double standard-sample-standard analysis protocol, bracketing 10 sample analyses by measurements of the BCR-2 basalt and the NIST-612 glass standards. The BCR-2 standard was used for Fe determination, and the NIST-612 glass standard for all other elements. The quality of the measurements was controlled by analyses of the respective standards and the NIST-614 glass was measured regularly during the analyses, yielding typical 2σ accuracies of 4-20%.

Data were acquired from single spot analysis of 25 µm, using a pulse rate of 10 Hz and a nominal laser fluence of ca. 10 J/cm^2. Total acquisition time for single analyses were 80 s, including 30 s gas blank measurement followed by laser ablation for 30 s and washout for 20 s. Factory-supplied software was used for the acquisition of the time-resolved data, obtained through pre-set spot locations. Data reduction and determination of concentrations was calculated off-line through the software Iolite using the Trace_Elements_IS routine (Hellstrom *et al.* 2008, Paton *et al.* 2011).

2.5 Oxygen isotope geochemistry

The oxygen isotope composition (^{16}O, ^{18}O) of 10 Greenlandic ruby samples were measured at the University of Lausanne, Switzerland, using a method similar to the one described by Sharp (1990), Rumble and Hoering (1994) and Kasemann *et al*. (2001). Several ruby minerals from each rock sample were crushed and representative pieces were selected for analysis. Between 1 and 2.5 mg of sample was loaded onto a small Pt-sample holder and pumped out to a vacuum of about 10^{-6} mbar. After pre-fluorination of the sample chamber overnight, the samples were heated with a CO_2-laser in 50 mbars of pure F_2. Excess F_2 was separated from the O_2 produced by conversion to Cl_2 using KCl held at 150°C. The extracted O_2 was collected on a molecular sieve (5A) and subsequently expanded into the inlet of a Finnigan MAT 253 isotope ratio mass spectrometer. Oxygen isotope compositions are given in the standard δ-notation, expressed relative to VSMOW in permil (‰). Replicate oxygen isotope analyses of the standard used (NBS-28 quartz; n = 3) has an average precision of ± 0.1‰ for $\delta^{18}O$. The accuracy of $\delta^{18}O$ values is better than 0.2‰ compared to accepted $\delta^{18}O$ values of 9.64‰ for the NBS-28 standard.

Table 2. *Operating conditions and data acquisition parameters for the LA-ICP-MS trace elements analyses. Not all samples were analysed for B, ^{47}Ti, Mo, and Hf.*

Laser system	**New Wave Research UP213 solid state ND:YAG laser with aperture imaging**
Laser wavelength	213 nm (Nd:YAG)
Laser mode	Q-switched (Nd:YAG)
Nominal pulse width	2 ns (Nd:YAG)
Repetition rate	10 Hz
Spot sizes (diameter)	25 µm
Energy density on sample	10 J/cm^2 (homogonized energy distribution)
Ablation cell	Standard, two-volume cell
Ablation cell gas flow rates	380 ml/min He
Tubing for gas flow	Tygon S-50 HL (5 mm i.d.)
Laser beam focus	Fixed sample surface
ICP-MS	**Thermo-Fisher Scientific ELEMENT 2 double focusing sector-field ICP-MS**
Interface cones	Ni sampler and skimmer cone
Detector type	Single-collector discrete dynode electron multiplier
Detector mode	Cross-calibrated pulse counting and analogue
Detector vacuum	10-7 mbar (during analysis)
Argon gas flow rates(l/min):	
Plasma	16
Auxiliary	0.90
Sample	0.955
RF power	1110 W
Lenses (V):	
Extraction	-2000
Focus	-870
X-Defelction	3.00
Y-Defelction	-3.40
Shape	109
SEM potential	2315 V
Data acquisition and processing	
Isotopes measured (sampling times in ms in brackets)	^{25}Mg (25), ^{27}Al (5), ^{29}Si (15), ^{49}Ti (25), ^{51}V (25), ^{52}Cr (25), ^{55}Mn (10), ^{57}Fe (25), ^{64}Zn (10), ^{65}Cu (25), ^{71}Ga (30), ^{72}Ge (10), ^{88}Sr (15), ^{90}Zr (10), ^{93}Nb (10), ^{120}Sn (10), ^{133}Cs (10), ^{137}Ba (10), ^{139}La (15), ^{140}Ce (15), ^{181}Ta (15), ^{208}Pb (10). *^{11}B (10), ^{47}Ti (xx), ^{98}Mo (10), ^{178}Hf (15).*
Settling times	1 ms; 7-33 ms at magnet jumping (10 jums
Dead time	25 ns
Integration window	10% except Ga (60%) and V, Cr, Mn, Fe, Cu, Zn, Mo, Sn, Cs and Ba (80%)
Samples per peak	1
Acquisition mode	Time resolved analysis
Scan type	E-scan
Detection type	Both
Integration type	Average
Mass resolution	300 (low)
Oxide production rate	Tuned to ≤ 0.7% UO$_2$ (254UO$_2$/238U)
Analysis duration	30 s. blank, 30 s. ablation and 20 s. washout.
Software for data reduction	Iolite vers. 2.2 (Hellstrom et al. 2008)
External standardization	BCR-2 and NIST-6 12 glasses
Internal standard isotope	^{27}Al

2.6 Optical features

The fingerprinting optical features, like inclusions and growth phenomena, of rubies from the FC were investigated at the Geological Survey of Denmark and Greenland (GEUS) using a Leica M80 stereomicroscope equipped with Leica DFC295 camera and Leica Application Suite 3.7 software. Images were made on unpolished ruby minerals applying naturally smooth crystal facets. Both heavily included and near inclusion-free samples were investigated.

The colour and transparency of 27 ruby samples Greenland, including the FC, were determined applying the Munsell colour description and the Gemological Institute of America colour grade system (Gemval 2014), and a relative scale for transparency, respectively.

2.7 Mineral inclusion investigation by SEM-EDS

Inclusions in the rubies were investigated at GEUS using a Philips XL40 SEM equipped with two EDS detectors: a Thermo Nanotrace 30 mm^2 window and a Pioneer Voyager 2.7 10 mm^2 window Si(Li) detector. Ruby grains were crushed to smaller pieces, mounted in epoxy, polished and carbon-coated. Inclusions are visible as different shades of grey with the SEM's back scattered electron (BSE) detector. Approximately 30 pieces per sample were investigated. The tungsten filament of the SEM was operated with an acceleration voltage of 17 kV, a filament current of typically 50-70 µA, and the sample was placed at a distance of 10 mm from the detector. The Noran System SIX software package was used to collect X-ray spectra of inclusions in the ruby and to recalculate the data following the Proza (φρZ) data correction and the filtering quantification technique.

EDS analysis is a grain surface technique; therefore inclusions-rich were selected to study the range of types of inclusions in the rubies and sapphire. Mineral classification is based on EDS data alone, no further detailed petrography was undertaken to classify the inclusions. In cases of overlapping chemistry, the most likely mineral classification is applied. For example is TiO_2 the chemical formula for rutile, brookite and anatase. Rutile however, is the most likely mineral inclusion in rubies, as it is a high-temperature metamorphic mineral, which brookite and anatase are not.

2.8 Micro-XRF method

Micro-X-ray fluorescence (µXRF) is an elemental analysis method, which can examine very small sample areas. µXRF uses direct X-ray excitation to induce characteristic X-ray fluorescence radiation from the sample for elemental analysis. Unlike conventional XRF, which has a typical spatial resolution ranging from several hundred micrometres to millimetres, µXRF uses X-ray optics to restrict the excitation beam size or to focus the excitation beam to a small spot on the sample surface so that small features on the sample can be analysed. The term “micro” indicates that localized regions of the sample can be analysed into a spatial resolution on the micrometre scale, down to about 10 micrometre.

With the µXRF instrument, the elemental compositions of a sample and the related spatial distribution are accessible. The µXRF analytical method can be used to measure all elements in the periodic system between Na-U, and the sample material can be solids, liquids and powder. The spatial resolution is between micrometres to mm scale (Beckhoff *et al*. 2006), while the typical spot size is between 20-300 micrometre, depending on the distance between the sample and the capillary optics. The µXRF instrument applied on the rubies from the FC (from the localities Bjørnesund, Ruby Island, Kigutilik, Upper Annertusoq and Lower Annertusoq) is a Bruker M4 Tornado based at the Roskilde University (currently at the National History Museum, Copenhagen). The M4 Tornado is equipped with a large high-speed stage and supports 2D-analysis of inorganic, organic and liquid samples.

In this study we compare the quality of µXRF analyses with LA-ICP-MS trace element analyses to test whether µXRF could be a less destructive alternative.

2.9 Laser-Induced Breakdown Spectroscopy

The third method to analyse for trace elements was Laser-Induced Breakdown Spectroscopy (LIBS) applying equipment from the Department of Plant and Environmental Sciences at Copenhagen University (group of Søren Husted). Samples were analysed for all trace elements and a range of trace elements was observed.

2.10 Raman spectroscopy

The Raman effect of minerals is based on molecular vibrations in a crystal, which are activated by monochromatic light, e.g. from a laser. The inelastic scattering of the monochromatic light causes a shift in the energy of the laser photons, called a Raman shift. The peaks in the Raman shift spectrum occur at specific values for the studied crystal. Corundum has seven specific phonons (Raman peaks) with bands at 378, 418, 432, 451, 580, 645, and 756 cm^{-1}. Which peaks occur, depends on the orientation of the crystal with respect to the monochromatic light (Porto & Krishnan 1967). Hence, usually only three or four of the seven known peaks occur. In case the crystal contains impurities, in the form of trace elements or as tiny mineral inclusions, extra peaks occur in the Raman spectrum. These peaks have been used to characterise rubies and especially (blue) sapphire occurrences.

Raman and fluorescence spectroscopy analyses were carried out in cooperation with Rolf W. Berg, Department of Chemistry, DTU (Technical University of Denmark). Analyses were performed with a visible light argon-ion laser with a wavelength of 532 nm on a LABRAM Raman Spectrometer (Horiba Jobin-Yvon, Villeneuve d'Ascq, France).

2.11 Fluorescence spectroscopy

The fluorescence of a sample depends on the ability of the sample to emit light as a result of an electromagnetic radiation. In the case of these fluorescence spectroscopy analyses, a laser with visible light was used (532 nm). The fluorescence effect is caused by the absorption of photons in the sample, which is exciting the sample, causing molecular vibrations. The sample emits energy again, usually of a lower frequency, which can be measured. The fluorescence of corundum strongly depends on the amount of Cr present in the crystal structure, pure Al_2O_3 is non-luminescent and a higher amount of the trace element Fe reduces the fluorescence. Ruby has two typical lines, R1 and R2, which are placed at 692.6 and 694.2 nm at room conditions.

Analyses were performed with a visible light argon-ion laser with a wavelength of 532 nm on a LABRAM Raman Spectrometer (Horiba Jobin- Yvon, Villeneuve d’Ascq, France).

2.12 Multivariate statistics

2.12.1 Principle component analysis

Multivariate statistical analysis is an often-applied technique for examining relationships among multiple variables at the same time. This type of analysis is, among others, used in studies that involve more than one independent variable and can be used as a prediction tool. The provenance of ruby/sapphire can be defined by a range of features, like characteristic trace element distribution, oxygen isotope signature, or distinct inclusions of minerals or fluids, or by distinctive peaks in a spectrum obtained with spectrometry. Ideally each feature will give a range of possible provenance areas, while a combination of several features (principally, as many as possible) will restrict the number of possible areas. In the ideal case the area of origin of the ruby/sapphire can be fingerprinted by a combination of independent techniques.

For this multivariate statistics study on the Greenlandic ruby and pink sapphire, a principal component analysis (PCA) has been performed. For the analysis the software SiroSOM, developed by CSIRO, Australia has been applied. PCA is an often-applied technique for visualizing high dimensional data. PCA reduces the dimensionality (the number of variables) of a dataset by maintaining as much variance as possible. This is done by rotating the original data space such that the axes of the new coordinate system point to the directions of highest variance of the data. These axes of variance are termed principal components (PCs) and are ordered by degree of variance: The first component, PC1, represents the direction of the highest variance of the data. The direction of the second component, PC2, represents the highest of the remaining variance orthogonal to the first component (e.g. Scholz 2006).

SOM in SiroSOM stands for Self Organising Maps. This is a visualisation tool for PCA. The software defines clusters of samples with a high similarity when all variables are taken in account. These are then plotted near each other on a map of all samples. The maps are wrapping around horizontally and vertically; this means that samples in the upper left and upper right corner are very similar, just like samples from the top left and bottom left part of the map.

2.12.2 Samples and applied data sets

For this multivariate statistics study the results for 70 ruby and pink sapphire samples have been used. From this set, 50 samples have been analysed at GEUS for their trace element composition, of these 36 samples from Greenland and 14 samples from other countries. Furthermore, trace element geochemistry data from 20 samples described in literature have been used to supplement the data set with more international occurrences (Calligaro 1999; Calvo del Castillo *et al.* 2009; Pornwilard 2011; Rakontondrazafy 2008; Schwarz 2008; Keulen *et al.* unpublished data). Data for Mg, Si, Ti, V, Cr, Fe and Ga have been applied in this multivariate study; these elements occur in significant quantities in ruby/sapphire and are traditionally found to be good indicators of provenance.

The trace element geochemistry data has been supplemented with data for oxygen isotopes from the following three studies: The Greenlandic data originates from Kalvig & Keulen (2011), while most of the international data is taken from Giuliani *et al.* (2005), supplemented with newer data for Madagascar (Giuliani *et al.* 2007) and Tanzania (included this report).

Because nearly none of the samples were analysed for trace element geochemistry and oxygen isotopes in the same study, the matching between oxygen isotope data and geochemistry data is not necessarily optimal. For example for all the Aappaluttoq samples, the same oxygen isotope value δ^{18}O =4.20‰ has been applied, as this is the only value available to us. In cases where more than one oxygen isotope value was available, the average of the analyses on the ruby/sapphire has been applied. Despite the disadvantages that come with the stable oxygen isotope data, we find it useful to include this independent dataset.

2.13 Trace element fingerprinting blind test

Asta F. Jørgensen, MSc-student at Copenhagen University, was given four samples for a blind test. She analysed the samples on the ICP-MS and compared the analytical results with literature data and the GEUS corundum dataset. The four samples were chosen as follows: one sample that was bought at a market in Pailin, Cambodia, (545608-unknown 1) and was claimed to be derived from that area, one from Storø, Godthåbsfjorden, Greenland, (545609-unknown 2), one sample from Aappaluttoq (521111-unknown 3), one from the FC locality Qaqqatsiaq, (160063-unknown 4).

3. Results

3.1 Metamorphic petrology

3.1.1 Mineralogy

The mineral assemblages of the ruby-bearing rocks from the FC are consistent with pressure-temperature conditions of the upper-amphibolite to lower-granulite facies. Various combinations of the following minerals: Ca-amphibole, Fe-Mg amphibole (ortho-amphibole or cummingtonite), phlogopite, anorthite-rich plagioclase, cordierite, sapphirine, sillimanite, and ruby are the common peak or near-peak metamorphic minerals (Figure 2, Table 3). Orthopyroxene was identified in one sample (521144). Spinel or chromite is present in a few samples. Retrograde chlorite is a common constituent; the compositions of the retrograde sheet silicates are highly variable. Some of these are extremely Al-rich, and these may represent mixed-layer structures or, possibly, sub-microscopically intergrown chlorite with hydrous, Al-rich sheet silicate.

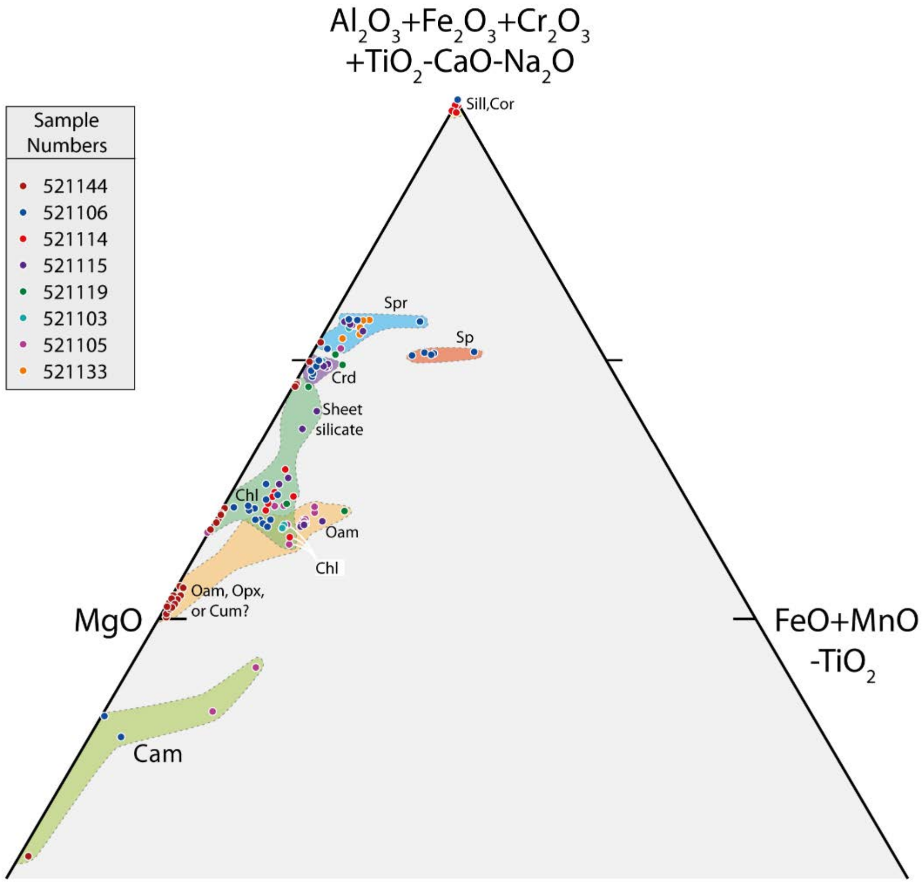

Figure 2. *Plot of mineral compositions on an AFM ternary diagram with A=$Al_2O_3+Fe_2O_3+Cr_2O_3+TiO_2-CaO-Na_2O$; M=MgO; F=$FeO+MnO-TiO_2$ all in molecular proportions. Abbreviations: Cam = Ca-amphibole; Chl = chlorite; Cor = corundum; Crd = cordierite; Cum = cummingtonite; Oam = ortho-amphibole; Opx = orthopyroxene; Sill = sillimanite; Sp = spinel; Spr = sapphirine.*

Figure 2 shows representative mineral compositions from ruby-bearing and related rocks. These analyses indicate that most of the minerals are enriched in Mg relative to Fe. The only exceptions are the spinel and one sapphirine analyses that are closely associated spatially with the spinel in sample 521106. The other notable compositional feature is the variation of Al content in the amphiboles. Most of the orthorhombic amphiboles are enriched in both Na and Al and would be classified as gedrite. However, in sample 521114, all of the minerals are exceptionally rich in Mg, and, here, orthorhombic amphibole is very low in Al and is closer to the end-member anthophyllite composition. The Ca-amphibole shows a wide range of Al and Na contents, typical for the hornblende solid solution series (Table 3).

3.1.2 Whole-rock compositions

The results of the whole-rock geochemical analyses are given in Appendix C. Whole-rock compositions of selected samples are shown as normative mineral assemblages in Figure 3. Figure 3A shows an important distinction between two broad classes of compositions, where one group is corundum normative, and the other is diopside normative. Figure 3B shows the whole-rock compositions with schematic compositional fields for Ca-amphibole (Cam) and Fe-Mg amphibole (Oam) along with compositions of measured Ca-amphibole and Fe-Mg amphibole (small, filled-white circles in the black fields). The variation in Figure 3 suggests that parts of the process that modified these bulk compositions affects the Ca/Al ratio of the rocks by the production of calcic amphibole. Appendix D shows the normalized rare earth elements for the analysed samples from the FC.

3.2 Trace element geochemistry

Trace element contents were measured by LA-ICP-MS on 35 ruby samples from the FC, 21 samples from other areas in Greenland and, 22 samples from international ruby deposits (Table 1). The results of these analyses are listed can be found in Table 4.

Compared to ruby derived from other areas, the FC rubies have high Cr, intermediate Fe, rather low V, and low Ga and Ti concentrations of trace elements. The Cr/Ga vs Fe/Ti diagram (Figure 4A) is one of the most commonly used trace element diagrams to determine the geological typing of ruby (Saminpanya et al. 2003). The figure uses the ratios among the four most abundant trace elements in rubies. Rakontondrazafy et al. (2008) introduced three fields into the diagram, viz. for marbles, metamorphic rocks and mafic deposits (i.e. basalt- and syenite-hosted sapphire and ruby). In Figure 4, we rectified the positions of the boundaries for the three fields for the usage of ppm (weight) instead of wt%-oxides as used in the early versions of the plot (Sutherland et al. 1998). The FC samples were divided into three groups: Aappaluttoq samples, for samples derived from the site where the ruby mine is located; Aappaluttoq-best samples, for those samples with a fine red or pink colour and high level of clarity from the mining site; and samples from the other localities in the FC combined (Fiskenæsset). The samples from the FC, including all Aappaluttoq samples, plot around the border of the metamorphic field, thus away from the marble and magmatic fields (Figure 4A). The samples are characterised by a high Fe/Ti ratio compared to other samples, mainly due to a low Ti content and suggest that upper Fe/Ti boundary for metamorphic rubies on the discriminant diagram (Figure 4A) should be placed at higher values.

Table 3. *Representative electron microprobe analyses of minerals.*

Abbreviations: Ged=gedrite, Anth=anthophyllite, Hbl=hornblende, Opx=orthopyroxene, Crd=cordierite, Spr=sapphirine, Cor=corundum, Plg=plagioclase, Al-sil=aluminosilicate, Phl=phlogopite or biotite, Chl=chlorite, Ru=rutile

AmphBasis=cations used to estimate ferric iron. Minimum estimates based on stoichiometry were used: All Ferrous = cations based on 23 oxygen; 15eNK = total cations exclusive of K and Na normalized to equal 15.

sample				**52115**			
wt %	Ged	Crd	Spr	Cor	Al-sil	Plg	Phl
SiO2	44.91	47.38	12.27	0.04	36.36	43.34	38.40
TiO2	0.32	0.01	0.01	0.00	0.00	0.00	1.30
Al2O3	19.31	33.28	64.18	99.73	61.98	33.90	18.29
Cr2O3	0.00	0.00	0.00	0.01	0.03	0.00	0.01
FeO	9.19	1.72	5.19	0.36	0.39	0.04	5.78
MnO	0.18	0.04	0.00	0.04	0.08	0.00	0.00
MgO	22.19	12.38	17.81	0.00	0.00	0.00	21.24
CaO	0.53	0.03	0.02	0.02	0.05	18.36	0.04
Na2O	1.84	0.24	0.00	0.00	0.02	1.28	0.60
K2O	0.03	0.00	0.00	0.01	0.02	0.02	8.59
Total	98.49	95.07	99.48	100.21	98.92	96.94	94.24
Oxygen	23	18	20	3	5	8	11
AmphBasis	15eNK						
Si	6.158	4.907	1.446	0.001	0.994	2.069	2.748
Al	3.121	4.062	8.912	1.993	1.996	1.907	1.543
Ti	0.033	0.000	0.001	0.000	0.000	0.000	0.070
Cr	0.000	0.000	0.000	0.000	0.001	0.000	0.001
Fe3	0.003	0.000	0.196	0.005	0.009	0.002	0.000
Mg	4.536	1.912	3.128	0.000	0.000	0.000	2.266
Fe	1.051	0.149	0.315	0.000	0.000	0.000	0.346
Mn	0.021	0.003	0.000	0.001	0.002	0.000	0.000
Ca	0.078	0.003	0.003	0.000	0.001	0.939	0.003
Na	0.489	0.047	0.000	0.000	0.001	0.118	0.083
K	0.005	0.000	0.000	0.000	0.001	0.001	0.784
Sum	15.494	11.084	14.000	2.000	3.004	5.036	7.843
Xmg	0.812	0.928	0.908				0.868
Xan						0.887	

sample					**521106**				
wt %	Ged	Hbl	Crd	Spr	Cor	Sp	Plg	Chl	Phl
SiO2	44.94	45.66	50.42	11.48	0.02	0.00	45.98	29.42	40.02
TiO2	0.21	0.37	0.04	0.05	0.01	0.02	0.01	0.04	0.79
Al2O3	18.05	14.91	35.36	62.43	97.92	45.25	33.96	25.56	18.57
Cr2O3	1.11	0.50	0.02	1.62	0.81	23.38	0.00	0.57	0.31
FeO	6.01	3.98	0.87	2.73	0.29	15.82	0.09	3.61	3.38
MnO	0.07	0.05	0.00	0.00	0.04	0.08	0.07	0.02	0.00
MgO	24.27	18.94	13.86	17.32	0.00	14.10	0.02	27.75	23.65
CaO	0.59	12.53	0.01	0.02	0.00	0.00	18.08	0.02	0.08
Na2O	1.97	1.83	0.23	0.01	0.00	0.17	1.29	0.00	0.85
K2O	0.02	0.11	0.01	0.00	0.00	0.03	0.00	0.01	7.97
Total	97.24	98.88	100.83	95.66	99.09	98.85	99.50	87.01	95.61
Oxygen	23	23	18	20	3	4	8	14	11
AmphBasis	15eNK	15eNK							
Si	6.176	6.287	4.904	1.403	0.000	0.000	2.128	2.760	2.778
Al	2.923	2.420	4.053	8.995	1.984	1.500	1.853	2.827	1.519
Ti	0.022	0.038	0.003	0.005	0.000	0.000	0.000	0.003	0.041
Cr	0.121	0.054	0.002	0.157	0.011	0.520	0.000	0.043	0.017
Fe3	0.033	0.367	0.000	0.036	0.004	0.000	0.004	0.000	0.000
Mg	4.972	3.888	2.010	3.156	0.000	0.591	0.001	3.882	2.447
Fe	0.658	0.091	0.071	0.243	0.000	0.372	0.000	0.283	0.196
Mn	0.008	0.006	0.000	0.000	0.001	0.002	0.003	0.002	0.000
Ca	0.087	1.849	0.001	0.002	0.000	0.000	0.897	0.002	0.006
Na	0.525	0.489	0.044	0.003	0.000	0.009	0.116	0.001	0.114
K	0.003	0.019	0.001	0.000	0.000	0.001	0.000	0.002	0.706
Sum	15.528	15.508	11.088	14.000	2.000	2.995	5.001	9.803	7.824
Xmg	0.883	0.977	0.966	0.928		0.614		0.932	0.926
Xan							0.886		

sample			**521144**		
wt %	Anth	Hbl	Opx	Spr	Chl
SiO2	59.77	49.04	57.51	13.70	30.62
TiO2	0.19	0.80	0.07	0.04	0.09
Al2O3	4.11	10.18	2.35	63.75	20.25
Cr2O3	0.02	0.07	0.00	0.53	0.11
FeO	0.24	0.35	0.71	0.29	0.30
MnO	0.03	0.03	0.00	0.00	0.01
MgO	31.71	21.51	39.23	21.83	34.72
CaO	0.11	13.40	0.14	0.01	0.06
Na2O	0.51	1.07	0.00	0.00	0.04
K2O	0.05	0.21	0.00	0.02	0.00
Total	96.74	96.66	100.01	100.16	86.20
Oxygen	23	23	6	20	14
AmphBasis	All Ferrou	All Ferrous			
Si	7.844	6.824	1.933	1.578	2.869
Al	0.636	1.670	0.093	8.656	2.236
Ti	0.019	0.084	0.002	0.003	0.007
Cr	0.002	0.008	0.000	0.048	0.008
Fe3	0.000	0.000	0.000	0.000	0.000
Mg	6.204	4.462	1.966	3.749	4.849
Fe	0.026	0.040	0.020	0.028	0.023
Mn	0.003	0.004	0.000	0.000	0.000
Ca	0.016	1.998	0.005	0.002	0.006
Na	0.130	0.288	0.000	0.000	0.008
K	0.008	0.037	0.000	0.002	0.000
Sum	14.887	15.416	4.019	14.067	10.006
Xmg	0.996	0.991	0.990	0.993	0.995

sample				**521119**			
wt %	Ged	Crd	Spr	Al-sil	Plg	Chl	Phl
SiO2	41.54	49.70	11.24	36.28	43.87	41.69	39.38
TiO2	0.09	0.03	0.00	0.04	0.04	0.02	0.55
Al2O3	17.97	34.86	62.69	61.57	33.40	30.09	19.81
Cr2O3	0.19	0.00	0.13	0.03	0.00	0.10	0.08
FeO	9.98	1.73	4.69	0.36	0.33	1.14	5.55
MnO	0.27	0.16	0.01	0.05	0.00	0.05	0.06
MgO	20.58	11.92	17.28	0.02	0.44	13.10	21.94
CaO	0.45	0.01	0.05	0.00	15.49	0.77	0.04
Na2O	2.09	0.27	0.02	0.00	1.73	0.28	0.90
K2O	0.00	0.03	0.00	0.01	0.27	0.03	8.24
Total	93.15	98.71	96.11	98.36	95.57	87.25	96.55
Oxygen	23	18	20	5	8	14	11
AmphBasis	15eNK						
Si	6.069	4.950	1.368	0.997	2.110	3.686	2.737
Al	3.094	4.092	8.993	1.993	1.893	3.135	1.623
Ti	0.010	0.002	0.000	0.001	0.001	0.001	0.029
Cr	0.021	0.000	0.012	0.001	0.000	0.007	0.005
Fe3	0.135	0.000	0.264	0.008	0.013	0.000	0.000
Mg	4.482	1.770	3.136	0.001	0.032	1.727	2.273
Fe	1.085	0.144	0.214	0.000	0.000	0.084	0.323
Mn	0.033	0.014	0.001	0.001	0.000	0.003	0.004
Ca	0.070	0.001	0.007	0.000	0.798	0.073	0.003
Na	0.592	0.052	0.006	0.000	0.161	0.048	0.121
K	0.000	0.004	0.000	0.000	0.017	0.003	0.731
Sum	15.592	11.030	14.000	3.002	5.025	8.767	7.847
Xmg	0.805	0.925	0.936			0.954	0.876
Xan					0.818		

sample			**521103**			
wt %	Ged	Crd	Spr	Al-sil	Plg	Phl
SiO2	45.63	50.04	12.89	37.02	44.41	39.50
TiO2	0.29	0.00	0.04	0.01	0.03	0.91
Al2O3	18.81	34.03	66.00	62.51	36.01	19.22
Cr2O3	0.25	0.01	0.33	0.17	0.00	0.10
FeO	7.08	1.15	3.45	0.30	0.03	4.14
MnO	0.12	0.01	0.03	0.00	0.00	0.00
MgO	23.29	12.66	18.59	0.01	0.00	22.68
CaO	0.60	0.02	0.01	0.04	19.50	0.26
Na2O	2.07	0.18	0.00	0.00	0.64	0.73
K2O	0.00	0.01	0.00	0.02	0.00	6.99
Total	98.14	98.11	101.33	100.07	100.62	94.53
Oxygen	23	18	20	5	8	11
AmphBasis	All Ferrous					
Si	6.223	4.996	1.484	1.000	2.041	2.764
Al	3.024	4.004	8.956	1.990	1.950	1.585
Ti	0.030	0.000	0.003	0.000	0.001	0.048
Cr	0.027	0.001	0.030	0.004	0.000	0.005
Fe3	0.000	0.000	0.040	0.000	0.001	0.000
Mg	4.735	1.884	3.191	0.000	0.000	2.366
Fe	0.808	0.096	0.292	0.007	0.000	0.242
Mn	0.014	0.001	0.002	0.000	0.000	0.000
Ca	0.087	0.002	0.001	0.001	0.960	0.020
Na	0.547	0.035	0.000	0.000	0.057	0.099
K	0.000	0.002	0.001	0.001	0.000	0.624
Sum	15.495	11.020	14.000	3.003	5.011	7.754
Xmg	0.854	0.951	0.916			0.907
Xan					0.944	

sample		**521112**		
wt %	Ged	Cor	Plg	Chl
SiO2	45.10	0.00	44.59	26.99
TiO2	0.28	102.50	0.00	0.01
Al2O3	19.12	0.06	35.15	17.79
Cr2O3	0.01	0.09	0.01	0.00
FeO	9.26	0.20	0.05	32.51
MnO	0.11	0.00	0.00	0.00
MgO	22.30	0.00	0.00	4.51
CaO	0.51	0.01	18.98	0.27
Na2O	2.22	0.03	0.95	0.10
K2O	0.02	0.00	0.01	0.04
Total	98.93	102.89	99.74	82.22
Oxygen	23	3	8	14
AmphBasis	All Ferrous			
Si	6.166	0.000	2.066	3.155
Al	3.081	0.002	1.920	2.451
Ti	0.029	1.995	0.000	0.001
Cr	0.001	0.002	0.001	0.000
Fe3	0.000	0.000	0.002	0.000
Mg	4.545	0.000	0.000	0.786
Fe	1.059	0.004	0.000	3.178
Mn	0.013	0.000	0.000	0.000
Ca	0.075	0.000	0.942	0.033
Na	0.588	0.001	0.085	0.023
K	0.003	0.000	0.001	0.006
Sum	15.560	2.004	5.016	9.633
Xmg	0.811			0.198
Xan			0.917	

sample	**521101**	
wt %	Cor	Phl
SiO2	0.01	41.21
TiO2	0.00	0.91
Al2O3	100.38	20.05
Cr2O3	0.36	0.62
FeO	0.18	2.67
MnO	0.02	0.03
MgO	0.00	23.52
CaO	0.00	0.11
Na2O	0.00	0.95
K2O	0.02	7.85
Total	100.96	97.92
Oxygen	3	11
AmphBasis		
Si	0.000	2.775
Al	1.992	1.591
Ti	0.000	0.046
Cr	0.005	0.033
Fe3	0.002	0.000
Mg	0.000	2.361
Fe	0.000	0.150
Mn	0.000	0.001
Ca	0.000	0.008
Na	0.000	0.124
K	0.000	0.674
Sum	2.000	7.765
Xmg		0.940

sample		**521105**		
wt %	Ged	Crd	Chl	Phl
SiO2	43.92	48.94	35.65	39.99
TiO2	0.41	0.01	0.30	1.01
Al2O3	19.44	34.29	19.62	19.10
Cr2O3	0.41	0.02	0.62	0.38
FeO	8.95	2.03	8.79	4.87
MnO	0.25	0.02	0.15	0.02
MgO	21.70	7.61	21.01	20.46
CaO	0.57	0.04	0.54	0.16
Na2O	2.28	0.06	2.28	1.02
K2O	0.02	0.00	0.05	7.34
Total	97.96	93.02	89.01	94.36
Oxygen	23	18	14	11
AmphBasis	All Ferrous			
Si	6.078	5.131	3.354	2.817
Al	3.171	4.237	2.176	1.586
Ti	0.043	0.000	0.022	0.054
Cr	0.045	0.001	0.046	0.021
Fe3	0.000	0.000	0.000	0.000
Mg	4.477	1.189	2.947	2.149
Fe	1.036	0.178	0.692	0.287
Mn	0.029	0.001	0.012	0.001
Ca	0.085	0.005	0.054	0.012
Na	0.612	0.013	0.416	0.140
K	0.004	0.000	0.006	0.660
Sum	15.579	10.756	9.724	7.726
Xmg	0.812	0.870	0.810	0.882

sample		**521133**		
wt %	Spr	Cor	Phl	Ru
SiO2	12.32	0.16	42.00	0.03
TiO2	0.02	0.04	0.27	99.54
Al2O3	63.71	97.61	21.78	0.33
Cr2O3	0.31	0.25	0.13	0.34
FeO	4.91	0.37	5.37	0.47
MnO	0.14	0.00	0.11	0.00
MgO	17.80	0.04	19.44	0.01
CaO	0.02	0.01	0.10	0.00
Na2O	0.03	0.01	0.73	0.01
K2O	0.01	0.01	8.03	0.02
Total	99.26	98.50	97.97	100.74
Oxygen	20	3	11	2
AmphBasis				
Si	1.463	0.003	2.842	0.000
Al	8.914	1.986	1.737	0.005
Ti	0.002	0.001	0.014	0.989
Cr	0.029	0.003	0.007	0.004
Fe3	0.000	0.005	0.000	0.005
Mg	3.150	0.001	1.961	0.000
Fe	0.487	0.000	0.304	0.000
Mn	0.014	0.000	0.006	0.000
Ca	0.002	0.000	0.007	0.000
Na	0.006	0.000	0.096	0.000
K	0.002	0.000	0.693	0.000
Sum	14.069	2.000	7.667	1.004
Xmg	0.866		0.866	

sample			**521145**		
wt %	Ged	Spr	Sp	Chl	Phl
SiO2	48.90	11.32	0.00	30.08	40.68
TiO2	0.62	0.02	0.00	0.10	0.64
Al2O3	13.77	63.10	45.46	21.90	18.72
Cr2O3	1.19	6.42	27.06	1.09	0.35
FeO	1.25	1.07	7.74	0.99	1.05
MnO	0.00	0.04	0.18	0.03	0.00
MgO	18.40	18.59	20.47	31.82	24.15
CaO	12.32	0.00	0.00	0.04	0.07
Na2O	1.52	0.00	0.03	0.05	0.94
K2O	0.16	0.00	0.00	0.34	6.99
Total	98.13	100.57	100.94	86.45	93.59
Oxygen	23	20	4	14	11
AmphBasis	All Ferrous				
Si	6.705	1.327	0.000	2.828	2.829
Al	2.225	8.718	1.432	2.426	1.535
Ti	0.064	0.002	0.000	0.007	0.033
Cr	0.129	0.595	0.572	0.081	0.019
Fe3	0.000	0.031	0.000	0.000	0.000
Mg	3.761	3.249	0.816	4.459	2.504
Fe	0.143	0.074	0.173	0.078	0.061
Mn	0.000	0.004	0.004	0.002	0.000
Ca	1.810	0.000	0.000	0.004	0.006
Na	0.404	0.001	0.002	0.008	0.126
K	0.028	0.000	0.000	0.041	0.620
Sum	15.270	14.000	2.999	9.936	7.734
Xmg	0.963	0.978	0.825	0.983	0.976

sample		**521114**	
wt %	Cor	Chl	Phl
SiO2	0.03	33.45	45.80
TiO2	0.19	0.09	0.09
Al2O3	99.25	26.67	36.11
Cr2O3	0.21	0.02	0.05
FeO	0.45	4.21	0.86
MnO	0.00	0.10	0.01
MgO	0.02	22.46	1.72
CaO	0.00	0.03	0.09
Na2O	0.02	0.76	2.10
K2O	0.00	1.48	7.83
Total	100.17	89.26	94.65
Oxygen	3	14	11
AmphBasis			
Si	0.000	3.061	3.034
Al	1.987	2.876	2.820
Ti	0.002	0.006	0.004
Cr	0.003	0.001	0.002
Fe3	0.005	0.000	0.000
Mg	0.000	3.064	0.170
Fe	0.001	0.322	0.048
Mn	0.000	0.008	0.000
Ca	0.000	0.003	0.006
Na	0.001	0.134	0.270
K	0.000	0.173	0.662
Sum	2.000	9.648	7.016
Xmg		0.905	0.780

sample		**521142**		
wt %	Spr?	Cor	Chl	Phl
SiO2	9.31	0.01	46.84	40.62
TiO2	0.01	0.01	0.04	0.48
Al2O3	56.47	99.96	38.29	19.76
Cr2O3	6.81	0.29	0.05	0.98
FeO	1.29	0.11	0.20	2.67
MnO	0.12	0.00	0.02	0.01
MgO	17.22	0.00	0.29	23.48
CaO	0.03	0.02	0.04	0.04
Na2O	0.02	0.00	0.03	0.91
K2O	0.10	0.01	0.33	8.75
Total	91.37	100.41	86.12	97.69
Oxygen	20	3	14	11
AmphBasis				
Si	1.213	0.000	4.038	2.762
Al	8.672	1.994	3.891	1.583
Ti	0.000	0.000	0.002	0.024
Cr	0.702	0.004	0.003	0.053
Fe3	0.000	0.000	0.000	0.000
Mg	3.345	0.000	0.037	2.380
Fe	0.141	0.001	0.014	0.152
Mn	0.013	0.000	0.002	0.000
Ca	0.004	0.000	0.004	0.003
Na	0.005	0.000	0.005	0.120
K	0.017	0.000	0.036	0.759
Sum	14.111	2.001	8.033	7.835
Xmg	0.960		0.727	0.940

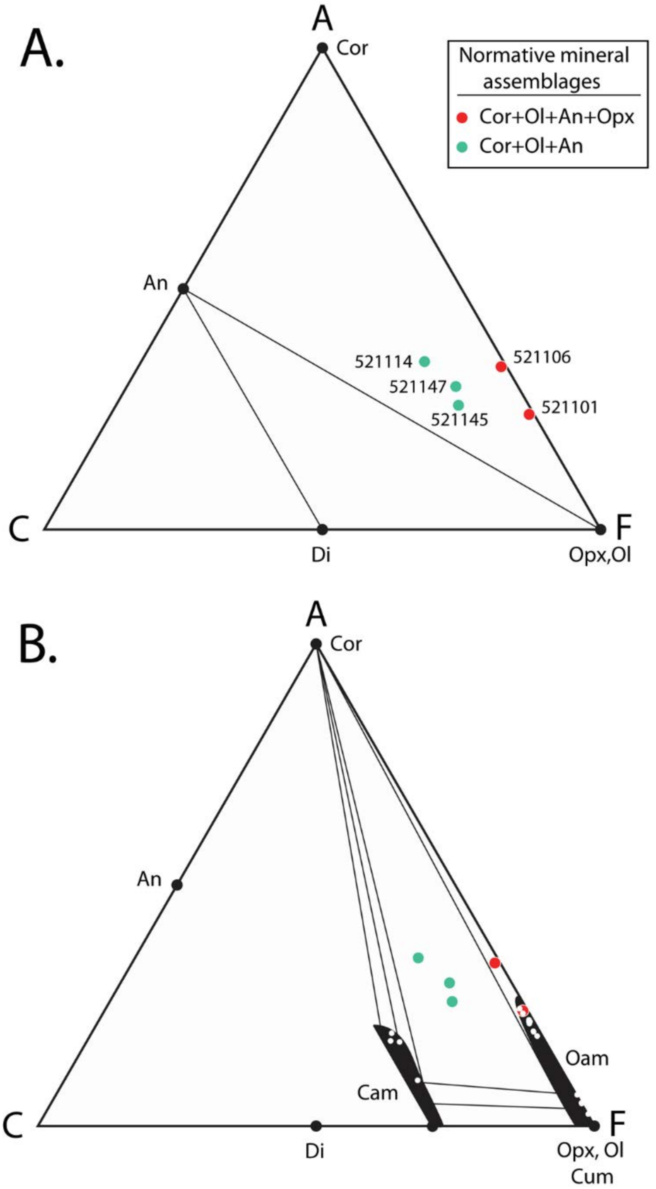

Figure 3. *ACF diagrams showing the whole-rock compositions of ruby-bearing and related rocks.* ***A***=$Al_2O_3+Fe_2O_3+Cr_2O_3+TiO_2-Na_2O$; ***C***=$CaO$; ***F***=$MgO+FeO+MnO+TiO_2$ *all in molecular proportions. A) Normative mineralogy of the whole-rock compositions straddling the Di and Cor normative boundary. B) Schematic metamorphic mineral compositions (solid-black fields) and phase relations (tie lines) superimposed on the whole-rock (bulk) compositions. Small, filled-white circles are measured ACF compositions of amphiboles from these rocks. Abbreviations:* ***An*** *= anorthite;* ***Cam*** *= Ca-amphibole;* ***Cor*** *= corundum;* ***Cum*** *= cummingtonite;* ***Di*** *= diopside;* ***Oam*** *=ortho-amphibole;* ***Ol*** *= olivine;* ***Opx*** *= orthopyroxene.*

Ruby samples from the occurrences near Maniitsoq and Storø, which also are associated with ultramafic rocks, plot well within the metamorphic rock field. Samples from the Tasiilaq area (including Nattivit) show lower Cr/Ga values than samples from the FC. Compared to the international samples included here, the Aappaluttoq-best ruby samples plot near samples from Longido, Umba and Winza, Tanzania, which all represent rubies formed in ultramafic rocks, and near the Pailin, Cambodia samples, which were collected from gabbroic xenoliths in basalts.

Table 4 (this and next page). *Average values for the LA-ICP-MS trace elements analyses. Only trace elements that yielded significant results for at least one sample are included. Values are in ppm (weight).*

Sample nr	Country	Region	Locality	Mg_m25-wt	Si_m29_wt	Ti_m49_wt	V_m51_wt	Cr_m52_wt	Fe_m57_wt	Ga_m71_wt	Nb_m93_wt	Sn_m120_wt	Ta_m181_wt	Pb_m208_wt
521101	Greenland	Fiskenæsset	Aappaluttoq	33.34	1309.66	34.90	64.82	14436.00	1932.76	31.65	0	0	0	0
521104	Greenland	Fiskenæsset	Aappaluttoq	50.88	1318.93	36.98	23.28	396.62	2210.71	23.51	0	0	0	0
521105	Greenland	Fiskenæsset	Aappaluttoq	58.87	1265.42	49.77	42.24	7702.22	3517.08	38.60	0	0	0	0
521106	Greenland	Fiskenæsset	Aappaluttoq	53.82	1246.30	27.82	61.58	10066.67	2205.56	24.07	0	0	0	0
521106	Greenland	Fiskenæsset	Aappaluttoq	44.13	598.21	57.92	71.26	9807.86	1914.89	30.53	0	0	0	0
521107	Greenland	Fiskenæsset	Aappaluttoq	51.79	540.25	58.51	56.88	6096.96	2087.86	28.26	0	0	0	0
521108	Greenland	Fiskenæsset	Aappaluttoq	36.12	1068.00	49.28	30.07	1035.75	5270.71	24.33	0	0	0	0
521109	Greenland	Fiskenæsset	Aappaluttoq	60.81	1173.67	272.27	16.73	2803.00	5307.33	23.17	0	0	0	0
521110	Greenland	Fiskenæsset	Aappaluttoq	63.22	1157.67	175.37	27.53	6731.33	3332.00	31.93	0	0	0	0
521111	Greenland	Fiskenæsset	Aappaluttoq	47.11	1146.67	59.62	67.07	6905.00	1517.37	33.96	0	0	0	0
521111	Greenland	Fiskenæsset	Aappaluttoq	32.02	559.74	46.10	46.19	9654.81	1835.67	27.26	0	0	0	0
521113	Greenland	Fiskenæsset	Aappaluttoq	109.63	610.57	76.14	44.50	8916.33	1817.66	24.15	0	0	0	0
521120	Greenland	Fiskenæsset	Aappaluttoq	59.82	510.41	78.64	34.55	3828.72	2148.41	25.21	0	0	0	0
521121	Greenland	Fiskenæsset	Aappaluttoq	0.00	1930.00	21.24	37.15	4086.72	10038.89	51.02	0	0	0	0
160098	Greenland	Fiskenæsset	QaqatAqulerit	44.69	629.17	91.44	4.75	6866.00	2938.00	22.04	0	0	0	0
459905	Greenland	Fiskenæsset	Sarfaq	39.25	559.34	52.61	25.13	3475.90	4456.55	24.34	0	0	0	0
459991	Greenland	Fiskenæsset	Kangaarsuk	82.62	586.00	176.19	36.63	2314.07	2784.48	44.91	0	0	0	0
476373	Greenland	Fiskenæsset	Tuk	51.41	855.01	80.40	99.79	1645.53	1548.60	8.93	0	0	0	0
497386	Greenland	Fiskenæsset	Pikiniq	33.04	529.40	32.00	27.22	3282.53	1837.67	16.56	0	0	0	0
497391	Greenland	Fiskenæsset	Qaqqat Akuleriit	40.49	582.47	66.73	7.78	2445.53	3692.00	12.78	0	0	0	0
508660	Greenland	Fiskenæsset	QoororsuaqEast	33.23	787.38	50.94	22.73	1144.42	541.50	20.16	0	0	0	0
160063	Greenland	Fiskenæsset	Qaqqatsiaq	28.48	659.08	29.14	11.26	3694.69	1069.00	23.54	0	0	0	0
510132	Greenland	Fiskenæsset	Qaqqatsiaq	67.67	852.11	694.76	46.62	778.48	3766.90	48.33	0	0	0	0
521123	Greenland	Fiskenæsset	U.Annertusoq	82.07	1021.33	107.96	10.27	4851.07	2569.00	16.73	0	0	0	0
521127	Greenland	Fiskenæsset	U.Annertusoq	114.58	1158.17	126.80	19.30	6239.66	7681.38	22.68	0	0	0	0
521130	Greenland	Fiskenæsset	L.Annertusoq	29.96	1119.33	20.65	28.11	1489.43	1364.73	20.42	0	0	0	0
521131	Greenland	Fiskenæsset	BjørnesundNW	24.60	1109.00	30.37	34.36	717.90	2831.33	24.71	0	0	0	0
521132	Greenland	Fiskenæsset	BjørnesundNW	26.78	1147.33	29.83	24.71	1569.30	2794.00	25.39	0	0	0	0
521134	Greenland	Fiskenæsset	BjørnesundNW	36.26	514.79	55.53	22.29	1879.43	3411.79	18.59	0	0	0	0
521135	Greenland	Fiskenæsset	BjørnesundNW	36.11	520.90	49.28	18.56	1865.61	1762.19	21.36	0	0	0	0
521138	Greenland	Fiskenæsset	Siggartatulik	69.21	1135.52	69.91	10.39	1667.94	2244.14	15.02	0	0	0	0
521140	Greenland	Fiskenæsset	Siggartatulik	0.00	1067.10	29.39	14.32	3947.00	977.90	6.42	0	0	0	0
521142	Greenland	Fiskenæsset	RubyIsland/Tarsiusarsuaq	67.85	979.91	37.03	12.86	10085.53	2541.91	19.02	0	0	0	0
521149	Greenland	Fiskenæsset	Kigutilik	46.41	1130.00	36.30	56.64	2641.34	1007.86	17.48	0	0	0	0
521163	Greenland	Fiskenæsset	Pikiniq	121.32	996.32	124.18	85.58	2001.14	1342.86	19.17	0	0	0	0
289933	Greenland	Maniitsoq	ManiitsoqNW	106.29	562.75	546.40	89.67	776.25	1670.00	51.12	0.63	0	6.18	0
289933	Greenland	Maniitsoq	ManiitsoqNW	96.31	568.83	685.29	66.27	1445.20	1765.83	46.01	0.59	0	4.57	0
289933	Greenland	Maniitsoq	ManiitsoqNW	82.50	1278.57	421.17	76.87	1049.31	1586.79	56.21	0.36	0.00	3.05	0
339590	Greenland	Maniitsoq	Kangerdluarssuk	71.58	719.21	444.21	60.69	1074.66	1417.83	29.88	0.06	0	0.39	0
339592	Greenland	Maniitsoq	Kangerdluarssuk	75.41	749.00	396.37	71.03	1382.33	1636.87	34.79	0.11	0	0.43	0
339598	Greenland	Maniitsoq	Kangerdluarssuk	54.68	641.50	137.24	25.57	3012.36	1137.96	32.09	0.04	0	0.00	0.08
339599	Greenland	Maniitsoq	Kangerdluarssuk	16.80	600.17	10.22	13.58	2223.93	810.93	20.77	0	0	0.00	0.04
339611	Greenland	Maniitsoq	Kangerdluarssuk	82.82	627.00	433.49	53.79	1368.00	1322.93	38.77	0	0	0.06	0.03
339612	Greenland	Maniitsoq	Kangerdluarssuk	101.69	625.38	442.46	89.24	2792.83	1533.03	46.19	0.22	0	0.46	0.00
339613	Greenland	Maniitsoq	Kangerdluarssuk	96.40	580.62	313.86	30.44	2774.52	1426.45	33.47	0.04	0	0.25	0.03
497396	Greenland	Nuuk	Storø	66.45	512.10	393.50	76.95	934.43	1671.53	58.56	0	0	0.00	0
545609	Greenland	Nuuk	Storø	76.44	477.04	310.82	101.89	1986.50	1623.21	47.31	0	0	0.00	0

Sample nr	Country	Region	Locality	Mg_m25-wt	Si_m29_wt	Ti_m49_wt	V_m51_wt	Cr_m52_wt	Fe_m57_wt	Ga_m71_wt	Nb_m93_wt	Sn_m120_wt	Ta_m181_wt	Pb_m208_wt
569728	Greenland	Nuuk	Storø	47.41	3579.64	60.62	71.25	1251.89	2024.21	78.71	0	0	0.00	0
224779	Greenland	Nuuk	Kapisillit	81.42	508.90	208.86	85.56	150.39	7606.03	40.54	0	0	0.00	0
545632	Greenland	Nuuk	Ujarassuit Nunaa	18.50	3810.71	15.44	1.00	1232.89	2908.86	18.11	0	0	0.00	0.21
319411	Greenland	Tasiilaq		21.36	563.44	176.41	3.11	7.49	9281.90	39.71	0.84	5.18	0.11	0.53
497397	Greenland	Tasiilaq	Nattivit	31.63	517.32	67.92	4.19	894.14	1409.57	27.20	0	0	0	0
562714	Greenland	Tasiilaq	Nattivit	14.49	828.00	81.45	6.83	44.03	1556.20	41.86	0.28	206.93	0.30	0.24
562726	Greenland	Tasiilaq	Nattivit	26.06	765.17	57.85	7.41	108.14	2085.53	40.86	0.00	88.81	0	0
562727	Greenland	Tasiilaq	Nattivit	21.56	799.21	54.93	5.69	171.97	1573.38	47.90	0.00	89.83	0.50	0
562737	Greenland	Tasiilaq	Nattivit	34.56	793.52	101.08	12.98	356.50	1770.07	37.02	0.43	74.07	2.00	2.06
545601	Sri Lanka		?Pelmadulla	108.24	380.53	423.76	98.16	1500.40	320.59	38.38	0	0	0	0
545627	India			46.33	631.83	59.67	169.55	1211.75	3334.50	130.58	0.00	0	0	0
545604	Cambodia		Pailin	512.07	626.93	450.27	23.59	4099.73	4064.67	26.47	0	0	0	0
545607	Cambodia		?Pailin	245.36	612.50	120.28	170.87	3438.21	2817.99	25.42	0	0	0	0
545608	Cambodia		?Pailin	274.71	681.93	131.15	13.69	1456.68	4132.86	19.85	0	0	0	0
545625	Myanmar	?Mong Hsu		78.49	709.13	492.24	101.42	4193.33	3157.87	49.34	0.05	0	0	0
545622	Myanmar	Mogok	Mogok West	119.49	766.17	165.91	327.43	1223.90	236.19	106.93	0	0	0	0
545624	Myanmar	Mogok	Mogok North	22.58	686.21	49.50	1.37	10.36	6110.00	79.05	0.02	0	0	0
545602	Madagascar		?Ilakaka	50.34	447.56	58.00	5.17	2446.67	3909.26	24.28	0	0	0	0
545629	Madagascar			46.68	808.70	63.15	45.64	187.61	1059.10	135.79	0	0	0	0
545630	Madagascar			51.66	764.10	74.01	17.59	141.41	2074.63	45.79	0	96.87	0	0
545631	Madagascar			51.59	814.10	73.73	25.17	324.32	3178.30	61.01	0	82.30	0	0
10	Tanzania	Longido		64.64	743.19	43.64	4.12	2535.26	2298.52	12.79	0	0	0	0
4	Tanzania	Mahenge		111.77	1248.00	101.75	34.59	2234.00	687.13	36.08	0	0	0	0
5	Tanzania	Mahenge		95.79	837.83	94.69	27.70	2066.60	633.00	56.99	0	0	0	0
2	Tanzania	Morogoro		105.18	1221.84	110.29	50.77	6698.67	427.30	54.79	0	0	0	0
3	Tanzania	Morogoro		169.57	1056.40	152.17	41.01	2525.67	0	50.96	0	0	0	0
7	Tanzania	Seza Kofi		48.67	885.35	47.25	44.77	2517.54	1447.26	47.71	0	0	0	0
8	Tanzania	Umba		78.44	704.44	78.98	17.33	940.44	1465.52	5.98	0	0	0	0
6	Tanzania	Winza		35.52	1276.77	40.35	0.00	1393.26	1699.03	19.95	0	0	0	0
545626	Ethiopia			47.13	662.67	408.55	35.32	1257.20	3241.83	74.93	0.30	0	0.83	0.79
497399	Macedonia			6.63	523.23	49.56	34.03	464.32	0	33.83	0	0	0	0

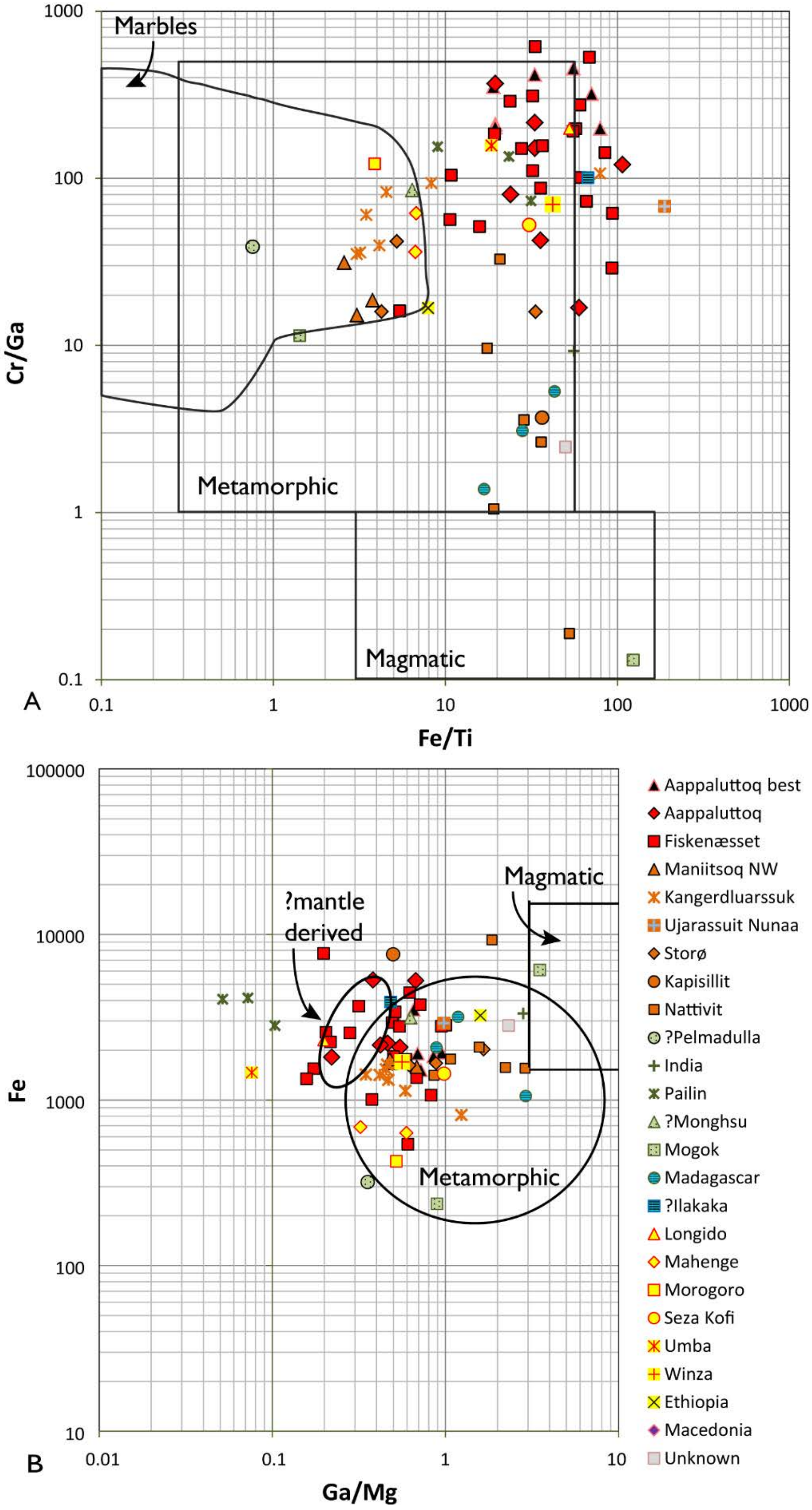

Figure 4. *Diagrams with ratios between common trace elements in rubies. Data produced in this study for Greenlandic and international deposits. A) Cr/Ga vs Fe/Ti, modified after Sutherland* et al. *(1998) and Rakontondrazafy* et al. *(2008). B) Fe vs Ga/Mg, after Peucat* et al. *(2007). The question mark for mantle-derived sapphire is part of the original figure by Peucat and co-workers.*

Figure 4B shows the data from this study in a Fe vs Ga/Mg diagram, after Peucat (2007), which was originally applied to fingerprint the country of origin and the geological background of blue sapphires. The diagram separates mafic rubies from metamorphic rubies and has a tentative small area for mantle-derived rubies. Not all samples yielded data of sufficient quality to allow for Mg to be displayed; therefore, this diagram contains fewer samples than Figure 4A. Again, the rubies from the FC plot away from the magmatic rocks field, straddling the outer boundary of the metamorphic rock field. Some of the FC samples plot in the potentially mantle-derived field (see Figure 4B). Samples from other localities in Greenland all plot in the metamorphic rocks field. Ruby samples from Greenland, including Aappaluttoq, overlap with many other localities in this diagram, mainly because all investigated ruby samples have relatively similar Fe values.

Triangular diagrams may be used to compare relative abundances of trace elements in rubies in order to establish a grouping of samples per country of origin or per deposit type (Guilong and Günther 2001). In Figure 5, we show our data for Greenland, including Aappaluttoq-best and high quality samples from two other localities in the FC (Bjørnesund NW and Siggartatulik) and for international samples, which all are compared to data from literature. The six triangular plots are combined in Figure 5, showing different combinations of the trace elements Fe, Ga, V, Cr and Ti. Data for Aappaluttoq-best is compared to literature data (*Aappaluttoq av.*) from Smith *et al.* (2016) and Thirangoon (2008). These triangular diagrams demonstrate that Aappaluttoq-best commonly plots near the other two FC localities of high quality and near the literature data for Aappaluttoq. A high degree of overlap is observed with samples from Umba, Seza Kofi and Longido (mainly ultramafic setting, Tanzania) and with the basaltic samples from Cambodia and Australia.

Figure 6 shows the trace element distribution for the highest quality Aappaluttoq ruby samples (this study, in black), and the average for the other Aappaluttoq samples from this study, from Thirangoon (2008) and from Smith *et al.* (2016) (all three in red), compared to international ruby deposits, where our own data is supplemented with literature data. Samples are grouped per country and per deposit, where known. Areas in Greenland outside the FC are not included here, as they do not contain large amounts of gem-quality rubies. The results shown in these diagrams are assessed in Chapter 4 Discussion.

3.3 Oxygen isotope composition

Oxygen isotope composition for rubies separated from ten selected samples from Greenland are listed in Table 5 and an overview of $\delta^{18}O$ values for previously described ruby deposits and the new data for the Greenland samples is given in Figure 7. $\delta^{18}O$ values vary between 1.62 and 4.20‰ for the FC area and are generally low for the other areas in Greenland with the exception of the sample from Maniitsoq (10.03‰).

Low values for $\delta^{18}O$ in ruby (4‰ and under) generally fit with rubies found in rock types like ultramafic rocks, mafic gneisses, basalts, and desilicated pegmatite in mafic rocks (Giuliani *et al.* 2005). Values in the range of about 4-7‰ are typical for rubies found in association with basalts, mafic rocks, lamprophyre, syenite, pegmatites, and desilicated pegmatite in mafic rocks; those around 10‰ are typical for rubies in skarns and biotitite in gneiss, while higher values of ca. 17-24‰ are typically for rubies formed in marbles (Giuliani *et al.* 2005). The FC rubies have oxygen isotope ratios that largely overlap with the values for mafic-ultramafic rocks reported by Giuliani *et al.* (2007). The sample from Nattivit has oxygen isotope values overlapping with those for the FC. The Nattivit sample was collected from ruby formed by a plumasite-type metasomatism caused by the intrusion of a pegmatite into an ultramafic rock (Van Hinsberg *et al.* 2017). The samples from Kapisillit and Storø also yield δ^{18}O values that lie within the mafic-ultramafic field defined by Giuliani (2007, see Figure 7), whereas the sample from Maniitsoq NW with a δ^{18}O value of 10.03‰ yielded the highest value obtained for the studied Greenland ruby samples.

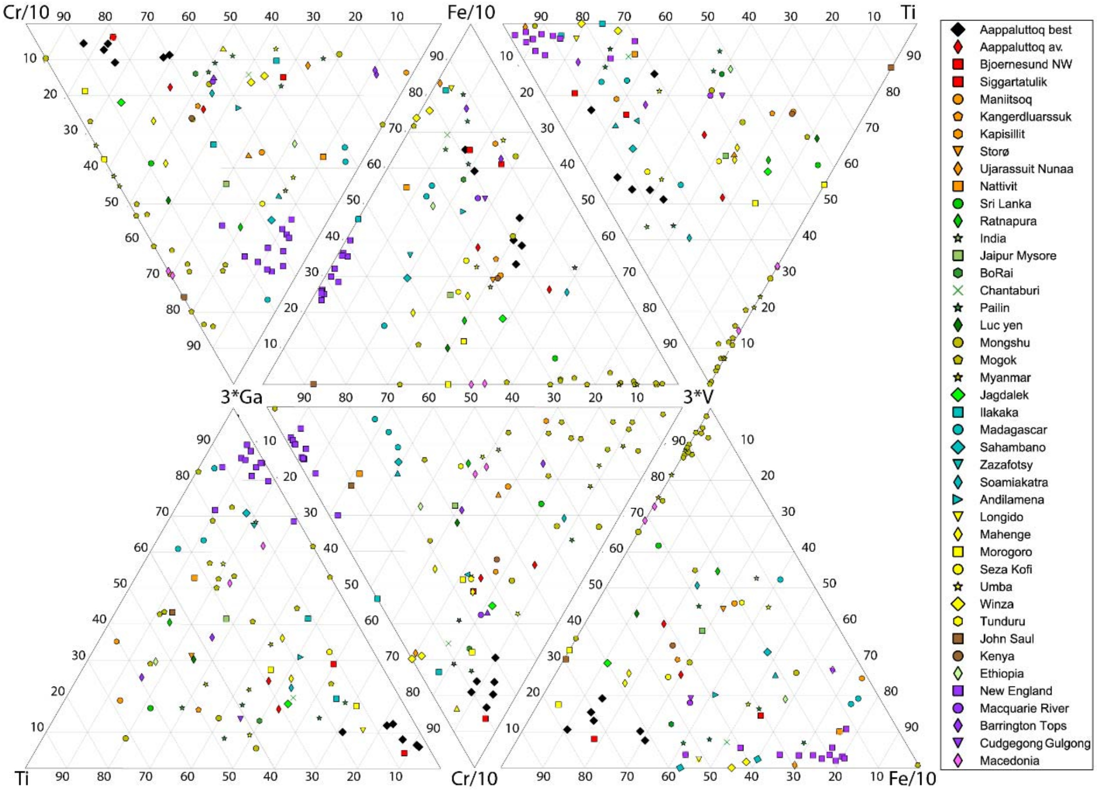

Figure 5. *Triangular diagrams with relative distributions of trace elements in rubies showing data produced in this study for Greenlandic and international deposits as well as literature data from Calligaro (1999), Calvo del Castillo* et al. *(2009), Harlow and Bender (2013), Pornwilard* et al. *(2011) Rakontondrazafy* et al. *(2008), Schwarz* et al. *(2008), Sutherland* et al. *(2015, 2017), and Zaw* et al. *(2014). Aappaluttoq av. shows average values for Aappaluttoq after Smith* et al. *(2016) and Thirangoon (2008). Bjoernesund NW and Siggartatulik show data for two ruby samples of high quality from the FC. From left to right, top and bottom: Cr-Fe-Ga, Fe-Ga-V, Fe-Ti-V, Ga-Ti-Cr, Ga-V-Cr, and V-Cr-Fe. Figures plotted after Guilong and Günther (2001).*

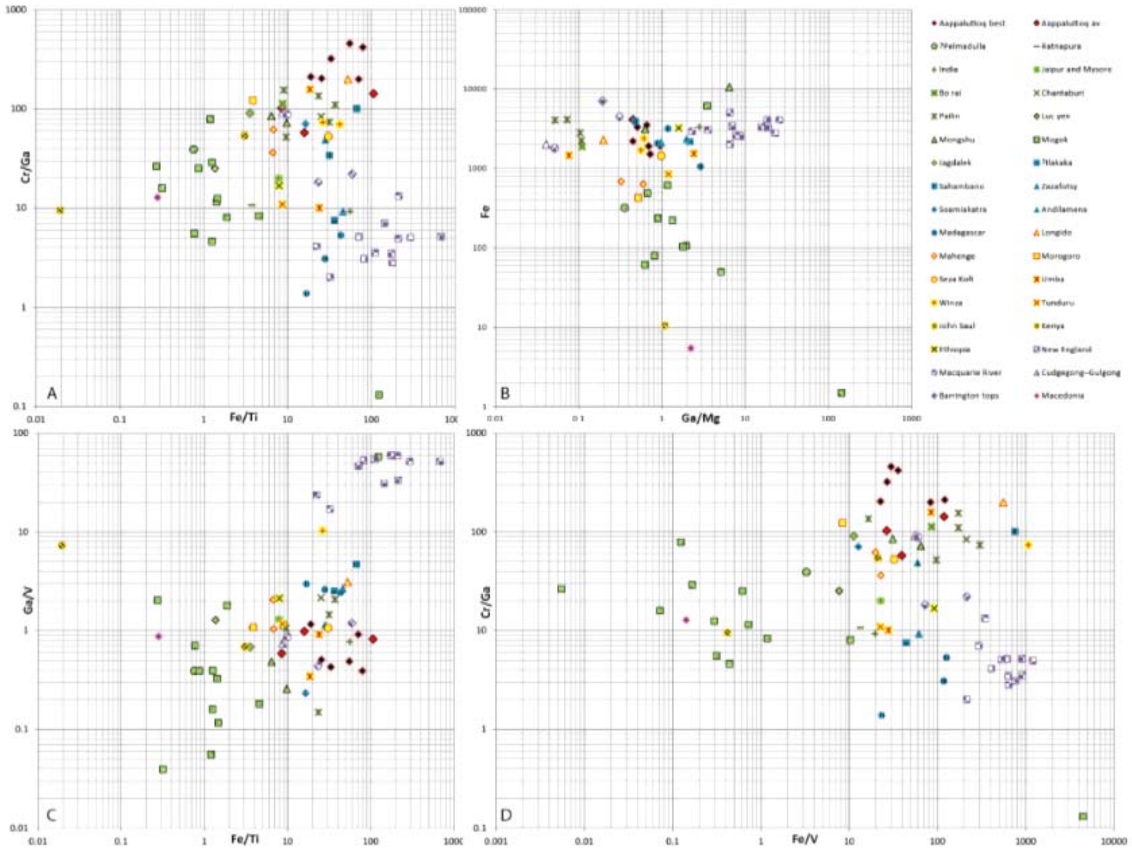

Figure 6. *Diagrams with ratios between common trace elements in rubies. Data produced in this study for Greenlandic and international deposits plus comparison of own data to literature data from Calligaro (1999), Calvo del Castillo* et al. *(2009), Harlow and Bender(2013), Kalvig and Frei (2010), Pornwilard* et al. *(2011) Rakontondrazafy* et al. *(2008), Schwarz* et al. *(2008), Smith* et al. *(2016), Sutherland* et al. *(2014, 2017), Thirangoon (2008), Zaw* et al. *(2014). A) Cr/Ga vs Fe/Ti. B) Fe vs Ga/Mg. C) Ga/V vs Fe/Ti. D) Cr/Ga vs Fe/V, lines for basalts are marked with S (based on Sutherland* et al. *(1998)) and Z (based on Zaw* et al. *(2014)). Dashed line in C) and D) indicates rubies derived from metamorphic rocks. Figures modified from Sutherland* et al. *(1998), Peucat* et al. *(2007), Rakontondrazafy* et al. *(2008), and Zaw* et al. *(2014), see chapter 4 Discussion for further explanation.*

Table 5. *Corrected $\delta^{18}O$-values in ‰ V-SMOW for ruby samples from Greenland.*

Sample no.	**Region**	**Locality**	**corr. $\delta^{18}O$**
497397	Tasiilaq	Nattivit	**2.41**
497395	Fiskenæsset	Aappaluttoq	**4.2**
78667	Fiskenæsset	Annertussoq	**3.39**
513743	Fiskenæsset	BjørnesundNW	**3.93**
497393	Fiskenæsset	Ruby Island/Tarsiusarsuaq	**2.56**
497392	Fiskenæsset	Siggartartulik	**1.62**
497383	Fiskenæsset	Pikiniq	**3.28**
289933	Maniitsoq	Maniitsoq	**10.03**
224779	Nuuk	Kapisillit	**4.52**
497396	Nuuk	Storø	**6**

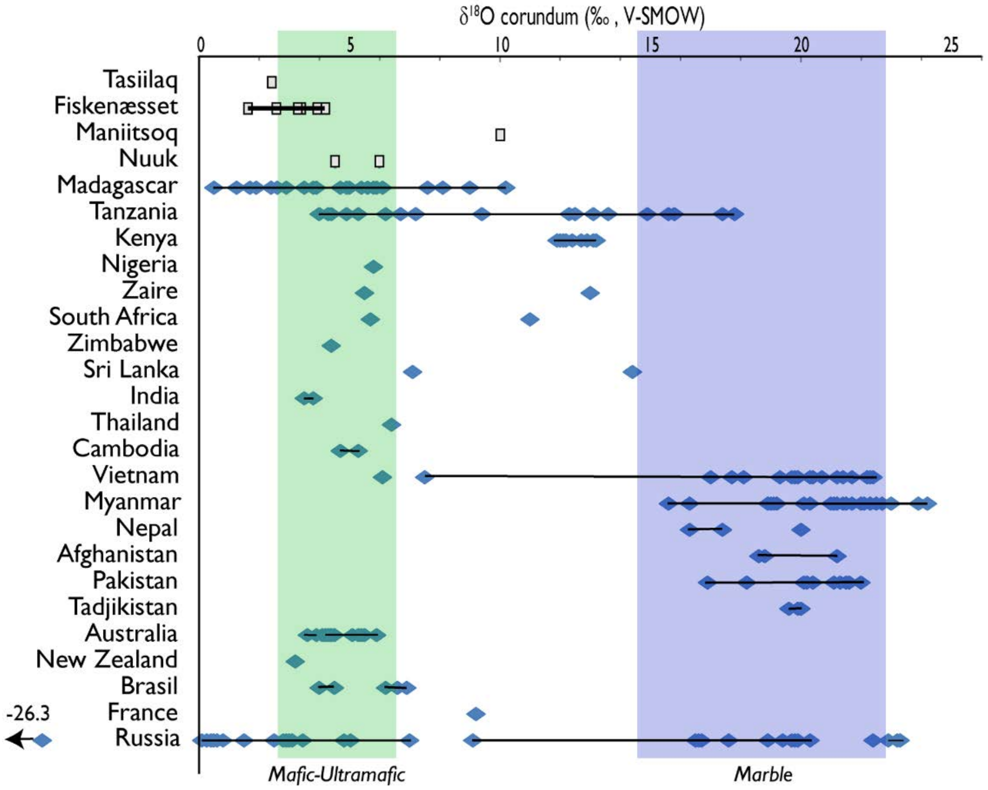

Figure 7. *Oxygen isotope values of ruby from deposits in Greenland (squares) compared to $\delta^{18}O$ values for ruby from other world-wide deposits after Giuliani* et al. *(2005, 2007), Sutherland* et al. *(2009, 2017), Vyotskiy* et al. *(2015), Zaw* et al. *(2014) and references herein (diamonds). Lines indicate the range of values within single localities, where different localities may overlap. Colour bands for mafic-ultramafic rocks and marbles after Giuliani* et al. *(2007). Vyotski* et al. *(2015) show negative $\delta^{18}O$ values for ruby down to -26.3‰ (arrow), which not all are shown.*

3.4 Inclusions and growth features

Optical and scanning electron microscopy demonstrate that mineral inclusions and internal features like growth zoning are very typical for the FC samples (Figure 8 and Figure 9). The samples show a series of common mineral inclusions like phlogopite (Figure 8A, Figure 9A), amphibole (anthophyllite; Figure 8B and pargasite, Figure 9B), spinel and chromite (Figure 8C, Figure 9C), and rutile (Figure 8A). Zircon (Figure 9D) and possible apatite occur less frequently, but are visible in several samples, as is anorthite (Figure 9D). Other less common minerals include: cordierite, muscovite, sapphirine, and pyrite (Table 6).

Table 6. *Mineral inclusions observed with SEM in rubies from Aappaluttoq and the rest of the Fiskenæsset complex.*

Mineral\Locality	Qoororsuaq East	Qaqqatsiaq	Aappaluttoq	U. Annertusoq	L. Annertusoq	Bjørnesund NW	Siggartartulik	Rubin Ø	Kigutilik
anorthite	x		x	x	x	x	x		
zircon/baddeleyite	x		x			x			x
ilmenite/rutile	x	x	x	x	x	x	x		x
phlogopite/biotite/stilpnomelane		x	x		x		x	x	
muscovite			x						x
pargasite			x						
anthophyllite/gedrite/amphibole	x	x	x	x					
cordierite		x	x	x					
spinel/chromite/gahnite			x	x				x	x
sapphirine/alumnosilicate			x	x				x	x
calcite/dolomite			x						
FexSy/pyrite		x							x
brucite/periclase		x	x						
kaolinite/Ca-Na-clay/clinochlore	x	x	x		x		x		x

A special type of growth pattern, referred to as growth zoning, is a common feature in the FC rubies (Figure 8D). The feature originates from small variations in concentrations of trace elements during mineral growth and is commonly taken as an indication that the ruby is naturally-occurring (GIA 2003). Another common feature in the FC rubies are finely-dispersed rutile needles (e.g. Figure 8D). Parallel to these rutile needles arrays of small inclusion and milky zones of finely dispersed fluid or solid material can be observed (Figure 8D). Negative crystals (cavities in the crystal structure with the same shape and habit as the host crystal during its cooling), often with trapped fluids inside, commonly appear in the FC ruby. A combination of these features, included crystals, milky zones and negative crystals in a healed fracture can produce a so-called fingerprint inclusion (Figure 8E) (GIA 2003). Zonal clouds, which are a type of milky zone with finely dispersed material, occur rarely. Fluid inclusions and combined fluid-solid inclusions trapping two or three phases are rather common in FC samples (Figure 8F). Two less common phenomena are shown in the last two photographs: the first is a series of irregularly oriented tubules that are filled with solid material (Figure 8G); the second is small secondary material that have a feathered appearance and grow away from needles or healed fractures in the crystal structure (Figure 8H). In both cases, the included material is most likely either boehmite or rutile.

The colour of the FC rubies is shown in Table 7, applying the GIA colour grade and Munsell colour system. Ruby colours vary between light reddish purple and medium dark strongly purplish red. In the same table also provides an average impression of the transparency – given as a relative five-step scale.

Figure 8 (next page). *Typical optical features in Fiskenæsset complex rubies; stereomicroscope photographs. A: Reddish brown, tabular, hexagonal, partially translucent phlogopite minerals and stubby dark red rutile minerals; sample 521159. B: Elongated brownish amphibole, most likely anthophyllite, sample 521131. C: Dark-red mineral, presumably spinel, sample 521159. D: Growth pat-terns (parallel to black arrows) and crosscutting rutile needles (white arrows), sample 521152. E: Healed fracture, also called fingerprint inclusion consisting of tiny included crystals, negative crystals and milky zone, sample 521151. F: Multiphase inclusions (fluid and solid inclusion in two or three phases), sample 521132. G: Irregularly oriented tubules filled with an unknown phase (?rutile or boehmite), sample 521108. H: Secondary feathers growing away from needles or former fractures, sample 521120.*

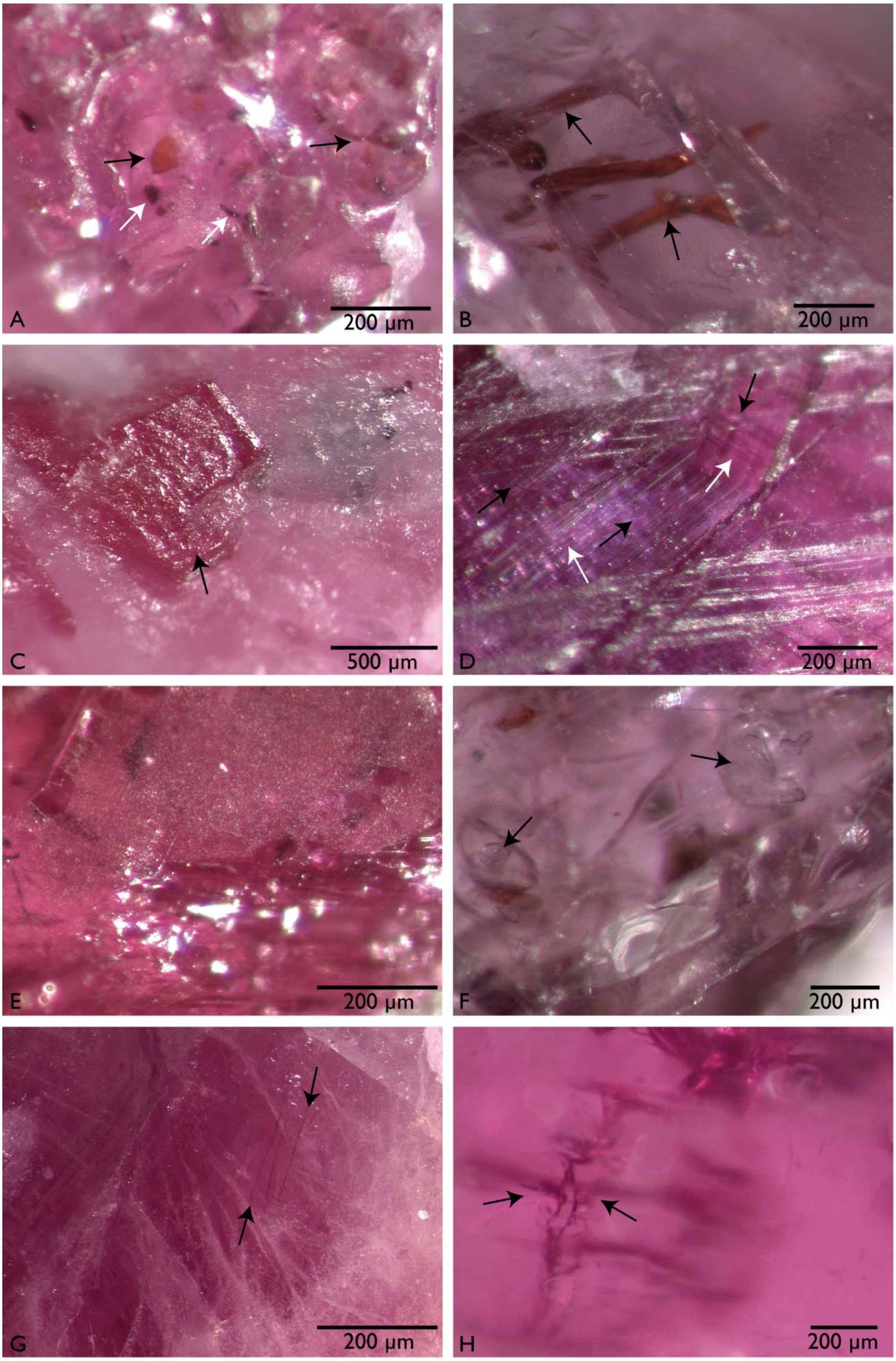
A
200 µm
B
200 µm
C
500 µm
D
200 µm
E
200 µm
F
200 µm
G
200 µm
H
200 µm

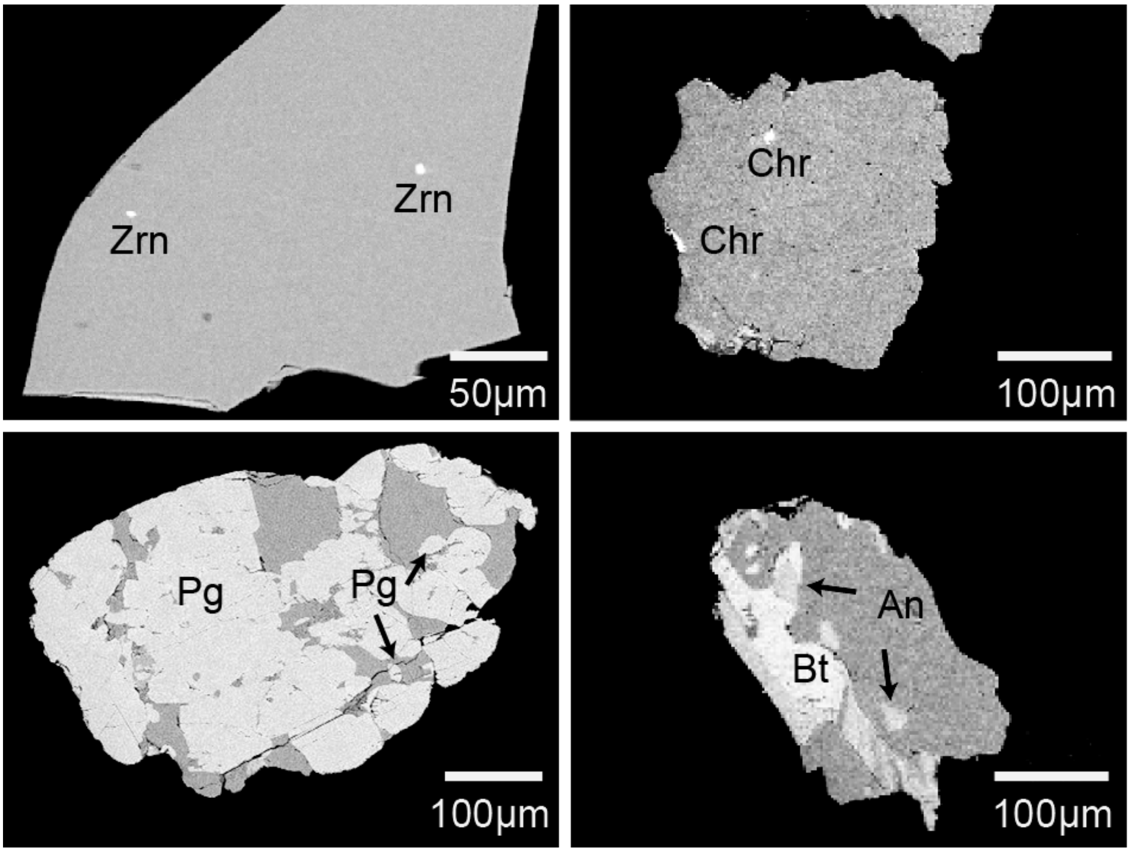

Figure 9. *Typical mineral inclusions in Fiskenæsset complex rubies, observed with a Scanning Electron Microscope in Back-Scatter contrast mode. A: Anorthite (An) and biotite (Bt) inclusions in ruby, sample 521138.B: Pargasite (Pg) inclusions in ruby and ruby in pargasite, sample 521104. C: Chromite or Chrome-spinel (Chr) inclusions, sample 521101. D: Zircon (Zrn) inclusions, sample 521131.*

Table 7. *Colour and transparency description for samples from the Fiskenæsset complex and the other Greenlandic ruby localities. Colour description apply the Munsell classification and GIA colour grade system of Gemval (2014). Transparency is ranked by a relative scale: Transparent-Semitransparent-Translucent-Milky-Opaque.*

Sample nr.	Region	Locality	Colour description	GIA colour grade	Munsell	Transparency
521101	Fiskenæsset	Aappaluttoq	Medium-dark, strongly purplish Red; strong	214	7.5RP 2/8 - 2.5RP 4/6	Transparent
521104	Fiskenæsset	Aappaluttoq	Light reddish Purple; strong	199	5RP 5/8 - 2.5RP 7/4	Milky
521105	Fiskenæsset	Aappaluttoq	Medium-dark, strongly purplish Red; strong	214	5RP 5/8 - 7.5RP 2/6	Transparent
521106	Fiskenæsset	Aappaluttoq	Medium-dark, strongly purplish Red; strong	214	7.5RP 6/4 - 5RP 6/6	Some Transparent
521107	Fiskenæsset	Aappaluttoq	Medium-dark, strongly purplish Red; very slightly brownish	215	7.5RP 5/4 - 7.5RP 2/8	Some Transparent
521108	Fiskenæsset	Aappaluttoq	Light Red; very slightly brownish	003	2.5RP 7/4 - 7.5RP 4/6	Milky
521109	Fiskenæsset	Aappaluttoq	Medium-dark, slightly purplish Red; strong	222	5RP 6/6 - 10RP 2/8	Milky
521110	Fiskenæsset	Aappaluttoq	Medium-dark Red; very slightly brownish	011	7.5RP 3/10 - 7.5RP 2/8	Semitransparent
521111	Fiskenæsset	Aappaluttoq	Medium-dark, strongly purplish Red; strong	214	2.5RP 5/12 - 7.5RP 2/8	Transparent
521113	Fiskenæsset	Aappaluttoq	Medium-dark, strongly purplish Red; very slightly brownish	215	7.5RP 4/8 - 7.5RP 2/4	Semitransparent
521120	Fiskenæsset	Aappaluttoq	Medium-dark, strongly purplish Red; strong	214	7.5RP 5/4 - 7.5RP 2/8	Translucent
521121	Fiskenæsset	Aappaluttoq	Medium strongly purplish Red; slightly brownish	213	2.5RP 8/4 - 10RP 2/6	Semitransparent
521123	Fiskenæsset	U.Annertussaq	Medium-dark, strongly purplish Red; very slightly brownish	215	7.5RP 4/8 - 10RP 2/8	Milky
521127	Fiskenæsset	U.Annertussaq	Medium-dark, strongly purplish Red; strong	214	10RP 2/8 - 7.5RP 6/4	Milky
521130	Fiskenæsset	L.Annertussaq	Light strongly purplish Red; very slightly brownish	207	7.5RP 6/4 - 7.5RP 2/8	Translucent-Semitranspa
521131	Fiskenæsset	BjørnesundNW	Medium-light strongly purplish Red; very slightly brownish	209	7.5RP 6/4 - 7.5RP 5/6	Translucent-Semitranspa
521132	Fiskenæsset	BjørnesundNW	Medium-dark, slightly purplish Red; strong	222	7.5RP 5/6 - 7.5RP 3/10	Transparent
521134	Fiskenæsset	BjørnesundNW	Medium-light, slightly purplish Red; strong	219	5RP 5/10 - 7.5RP 3/6	Translucent-Semitranspa
521135	Fiskenæsset	BjørnesundNW	Medium-dark, strongly purplish Red; strong	214	2.5RP 6/6 - 5RP 2/10	Semitransparent
521163	Fiskenæsset	Pikiniq	Medium strongly purplish Red; very slightly brownish	212	2.5RP 6/4 - 7.5RP 2/6	Semitransparent
521149	Fiskenæsset	Kigutilik	Medium strongly purplish Red; slightly brownish	213	5RP 4/6 - 7.5RP 2/8	Translucent
508660	Fiskenæsset	QoororsuaqEast	Greyish Purplish Pink	0	10P 7/4 - 10P 5/4	Translucent
521142	Fiskenæsset	RubyIsland/Tarsiu	Medium-dark, reddish Purple; strong	204	7.5RP 2/8 - 7.5RP 3/6	(Semi-)Transparent
521138	Fiskenæsset	Siggartatulik	Light reddish Purple; strong	199	7.5RP 8/4 - 5RP 6/4	Opaque-Milky
521140	Fiskenæsset	Siggartatulik	Medium-dark, strongly purplish Red; strong	214	7.5RP 4/8 - 7.5RP 2/8	(Semi-)Transparent
521159	Fiskenæsset	Siggartatulik	Medium slightly purplish Red; very slightly brownish	221	5RP 5/8 - 7.5RP 3/6	Translucent-Semitranspa
521160	Fiskenæsset	Siggartatulik	Medium-dark, strongly purplish Red; strong	214	2.5RP 7/4 - 10RP 2/8	Translucent

3.5 Micro-XRF investigations

The average of the elemental concentration for the samples from µXRF and LA-ICP-MS analysis were compared, and plotted on diagrams for the elements Mg, Si, Ti, V, Fe, Cr, and Ga (Figure 10 to Figure 16). The LA-ICP-MS can measure very small concentrations of elements in the range ppb to ppm. The spot size for analysis is much smaller for the LA-ICP-MS than for the µXRF, from about 30 µm to 100 µm. The LA-ICP-MS measures fairly fast, but leaves a tiny hole in the sample after measurements. The LA-ICP-MS has a small spot size and measures the elemental concentration in the rubies more precisely than µXRF. The method is also better suited for measuring inclusions in the corundum, because the smaller spot size will give a smaller uncertainty for the elemental concentrations.

The difference in concentrations for the elements Mg, Si, Ti, V, Cr, Fe and Ga are listed as intervals in Table 8.

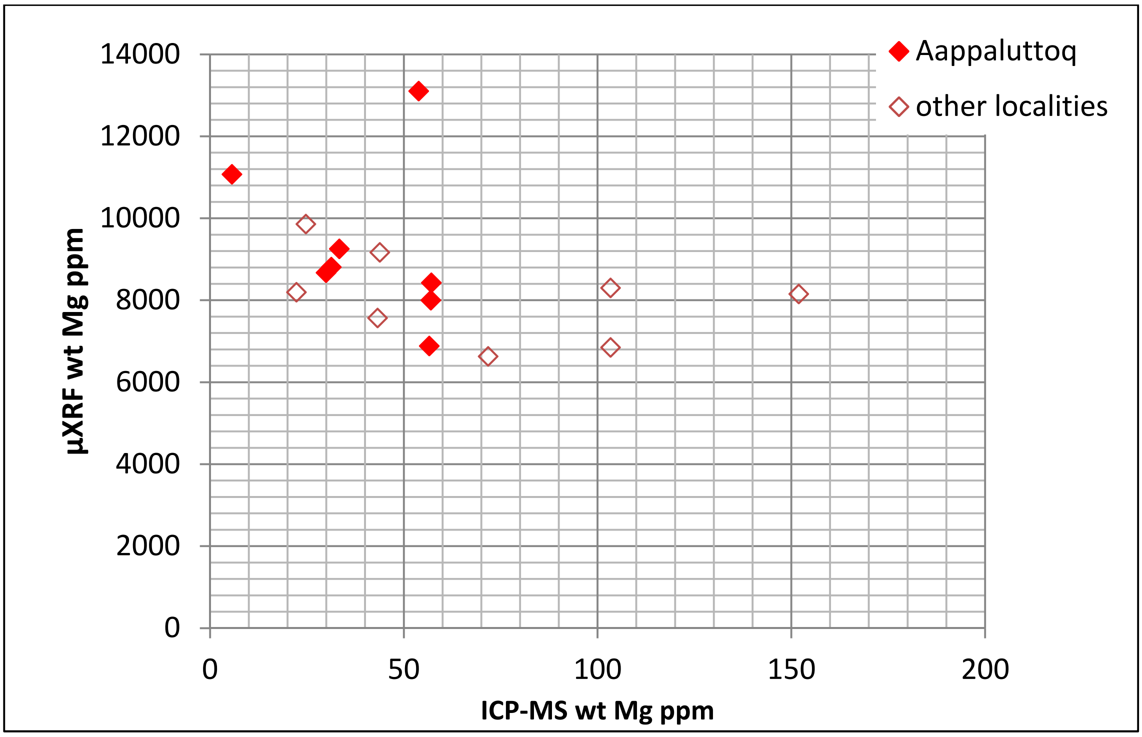

Figure 10. *The average of the results for Mg in ppm for the two methods µXRF and LA-ICP-MS. The red diamonds are corundum samples from Aappaluttoq, and the unfilled diamonds are from the other corundum localities in Greenland. The Aappaluttoq samples plot with less scatter.*

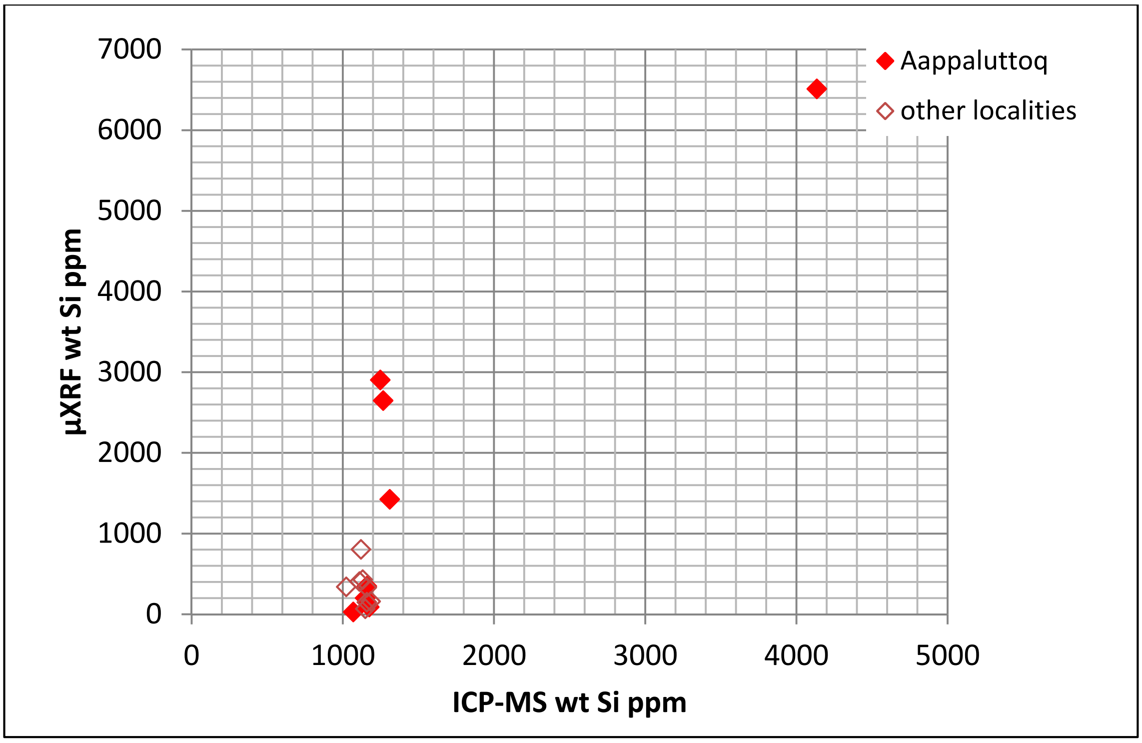

Figure 11. *The average of the results for Si in ppm for the two methods µXRF and LA-ICP-MS. The red diamonds are corundum samples from Aappaluttoq, and the unfilled diamonds are from the other corundum localities in Greenland. The Aappaluttoq samples plot with less scatter.*

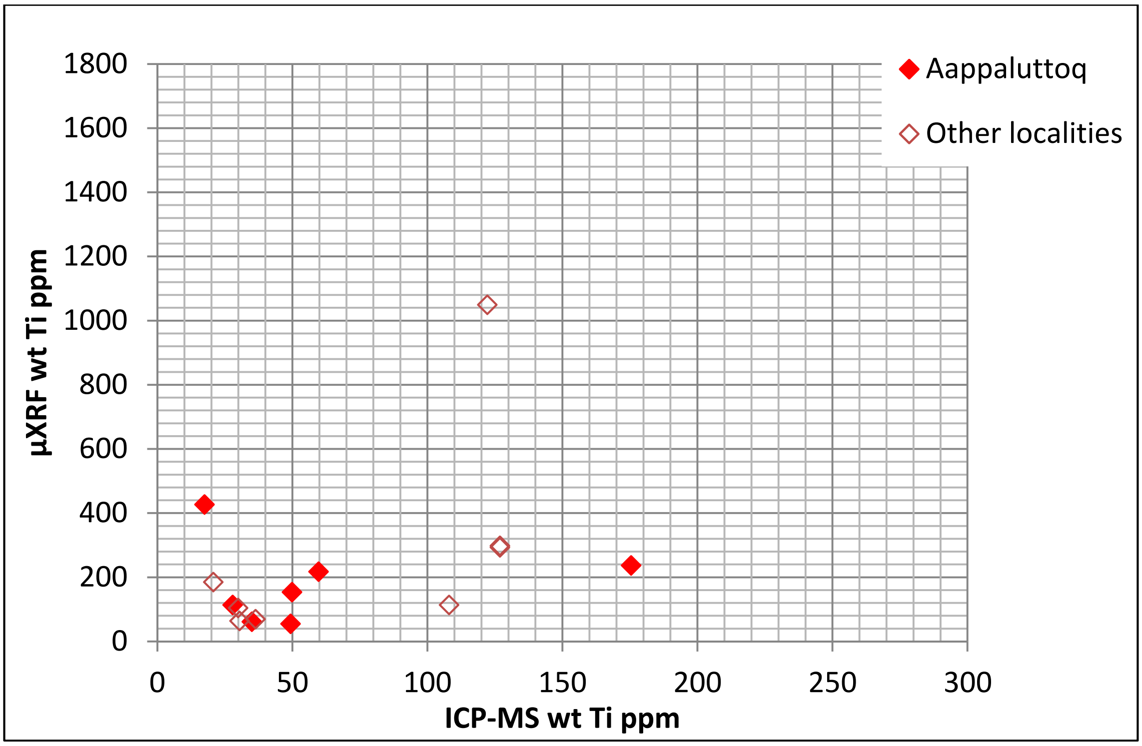

Figure 12. *The average of the results for Ti in ppm for the two methods µXRF and LA-ICP-MS. The red diamonds are corundum samples from Aappaluttoq, and the unfilled diamonds are from the other corundum localities in Greenland.*

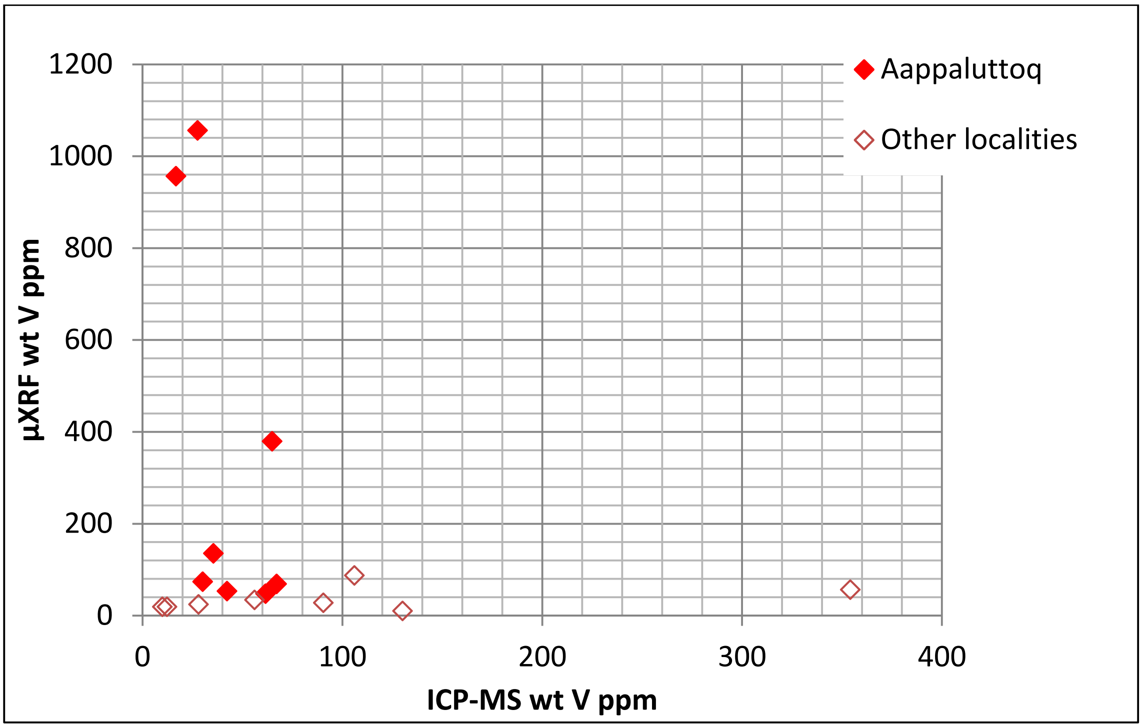

Figure 13. *The average of the results for V in ppm for the two methods µXRF and LA-ICP-MS. The red diamonds are corundum samples from Aappaluttoq, and the unfilled diamonds are from the other corundum localities in Greenland.*

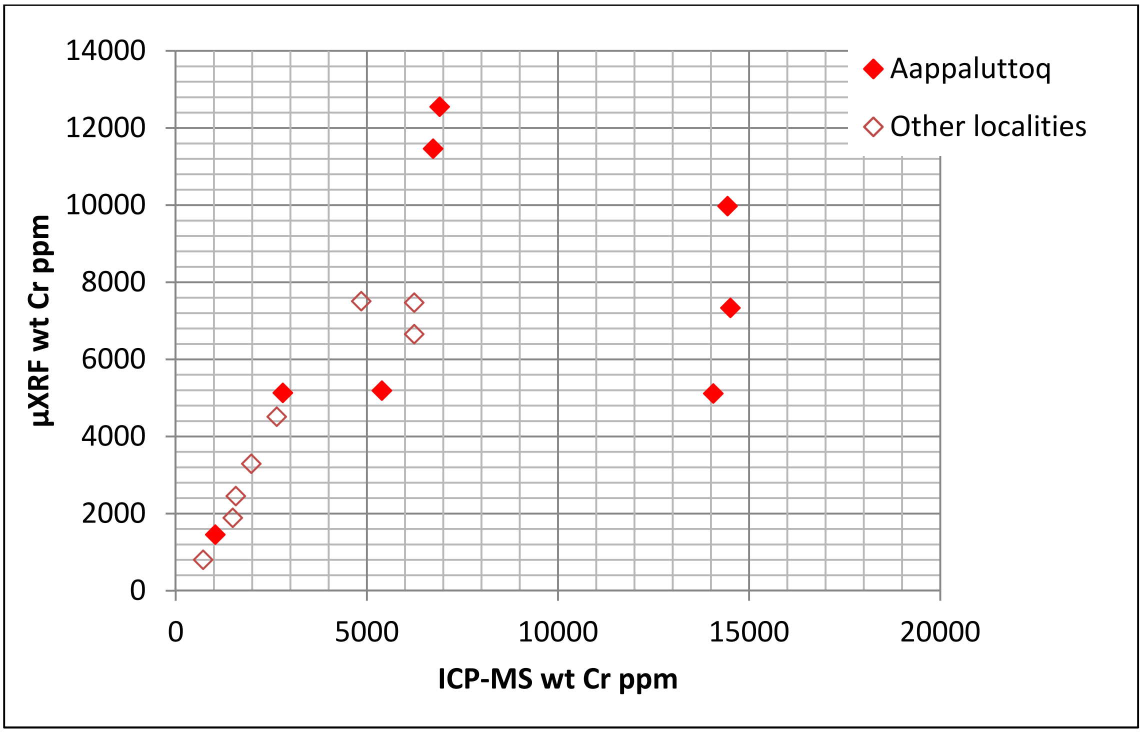

Figure 14. *The average of the results for Cr in ppm for the two methods µXRF and LA-ICP-MS. The red diamonds are corundum samples from Aappaluttoq, and the unfilled diamonds are from the other corundum localities in Greenland.*

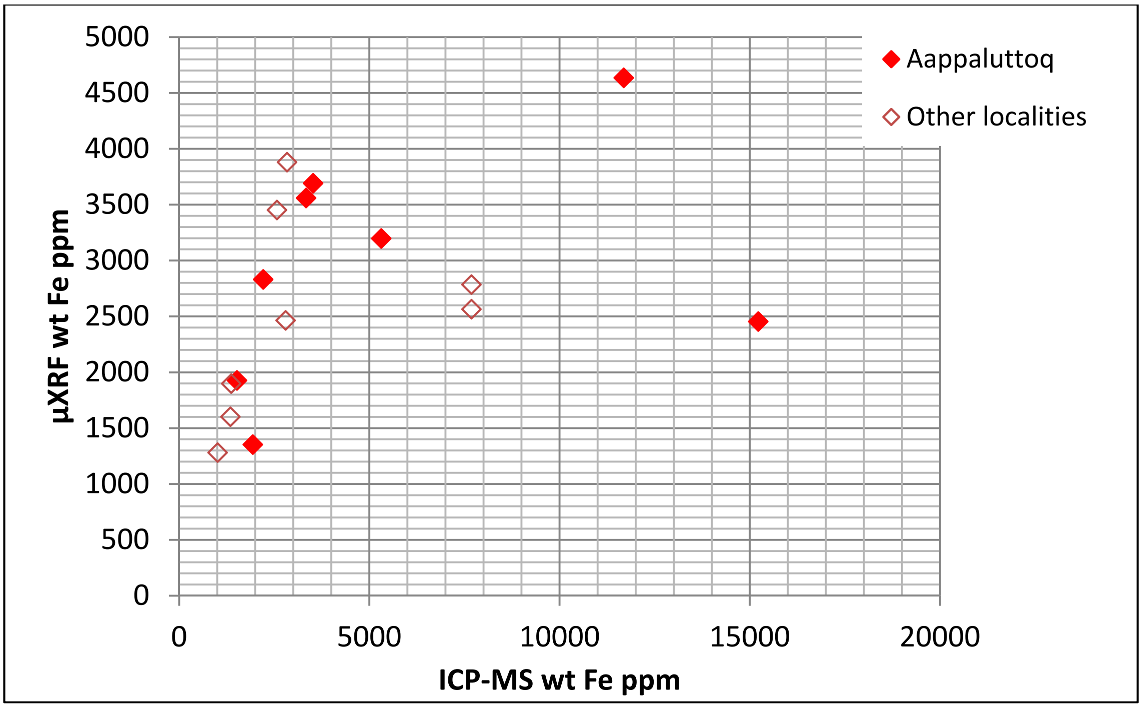

Figure 15. *The average of the results for Fe in ppm for the two methods µXRF and LA-ICP-MS. The red diamonds are corundum samples from Aappaluttoq, and the unfilled diamonds are from the other corundum localities in Greenland.*

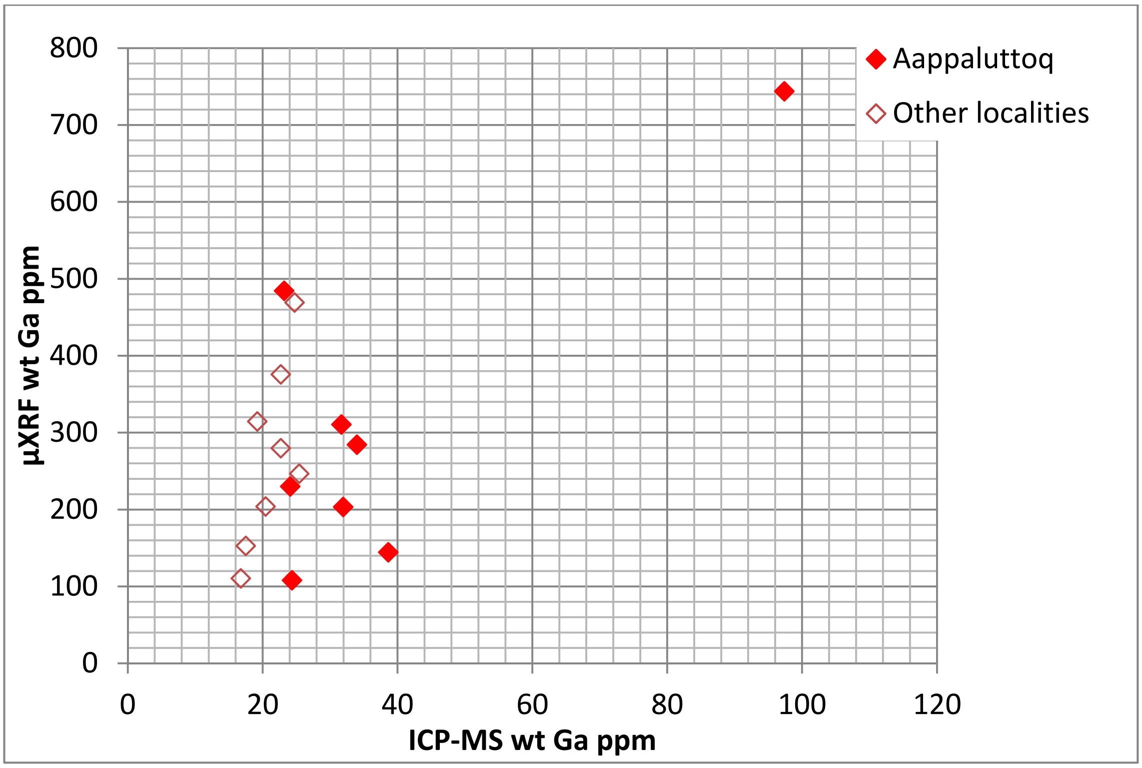

Figure 16. *The average of the results for Ga in ppm for the two methods µXRF and LA-ICP-MS. The red diamonds are corundum samples from Aappaluttoq, and the unfilled diamonds are from the other corundum localities in Greenland.*

Table 8. *Comparison between the range in concentration (ppm) for the methods µXRF and LA-ICP-MS. The table shows actual values measured on the same corundum samples from the Fiskenæsset complex.*

Element	Micro-XRF	LA-ICP-MS
Mg	6000 to 12000	10 to 150
Si	100 to 300	1000 to 1200
Ti	40 to 1600	20 to 270
V	10 to 350	20 to 1100
Cr	800 to 14000	800 to 12000
Fe	1200 to 4600	1000 to 5000
Ga	100 to 150	20 to 40

For Mg the concentration between the two methods is more than 100 times higher for the µXRF method, which could indicate that at least one of the methods is not precise enough for the lightest elements (Figure 10). For Si the concentrations measured with µXRF analysis are approximately 1/4 for most of the samples for µXRF compared to the LA-ICP-MS analysis (Figure 11). For Ti the concentration measured with µXRF is about 4 times larger than with the LA-ICP-MS (Figure 12. For V the concentration for µXRF is about 2 times smaller than for the LA-ICP-MS method (Figure 13). The concentration for Cr lies in the same intervals for both methods (Figure 14). The concentrations measured for Fe with the two methods lies within the same intervals, but two samples have higher Fe concentration measured with the LA-ICP-MS method, while most other samples show concentrations that are lower in µXRF than in LA-ICP-MS (Figure 15). For Ga the concentration range measured with the µXRF is about 1/5 of the LA-ICP-MS analysis (Figure 16). Table 9 and Table 10 compare the results for both methods.

Table 9. *Samples of corundum analysed with LA-ICP-MS. The values are the average of 25-30 measurements. The localities are A =Aappaluttoq, B = U. Annertusoq, C = L. Annertusoq, D= Bjørnesund, E=Kigutilik, F=Piqinik.*

Sample /ICP-MS average	Locality	Mg_ppm_m25	Si_ppm_m29	Ti_ppm_m49	V_ppm_m51	Cr_ppm_m52	Fe_ppm_m57	Ga_ppm_m71
521108	**A**	29.92	1068.00	49.28	30.07	1035.75	15219.33	24.33
521109	**A**	56.97	1173.67	272.27	16.73	2803.00	5307.33	23.17
521110	**A**	57.10	1157.67	175.37	27.53	6731.33	3332.00	31.93
521111	**A**	31.30	1146.67	59.62	67.07	6905.00	1517.37	33.96
521121	**A**	5.64	4134.00	17.36	35.47	5392.70	11685.00	97.34
521101	**A**	33.34	1309.66	34.90	64.82	14436.00	1932.76	31.65
521105	**A**	56.58	1265.42	49.77	42.24	14511.43	3517.08	38.60
521106	**A**	53.82	1246.30	27.82	61.58	14064.00	2205.56	24.07
521123	**B**	71.75	1021.33	107.96	10.27	4851.07	2569.00	16.73
521127	**B**	103.34	1158.17	126.80	19.30	6239.66	7681.38	22.68
521127	**B**	103.34	1158.17	126.80	19.30	6239.66	7681.38	22.68
521130	**C**	43.80	1119.33	20.65	28.11	1489.43	1364.73	20.42
521131	**D**	22.29	1109.00	30.37	34.36	717.90	2831.33	24.71
521132	**D**	24.70	1147.33	29.83	24.71	1569.30	2794.00	25.39
521149	**E**	43.21	1130.00	36.30	56.64	2641.34	1007.86	17.48
521163	**F**	151.93	1183.69	122.10	87.69	1979.03	1343.79	19.17

Table 10. *Samples of corundum with the analytical method micro-XRF. The values are the average of 5 or 6 measurements and are given in ppm. The localities are A =Aappaluttoq, B = U. Annertusoq, C = L. Annertusoq, D= Bjørnesund, E=Kigutilik, F=Piqinik.*

Sample micro-XRF average	Locality	O	Mg	Al	Si	Ti	V	Cr	Fe	Ga	Zr
521108	**A**	464574.38	8676.06	522308.43	27.70	54.98	74.16	1459.38	2453.68	108.06	263.18
521109	**A**	461405.64	8002.93	518745.89	89.66	1673.55	956.79	5135.33	3197.10	484.37	308.74
521110	**A**	458683.71	8430.61	515685.70	347.97	237.17	1056.15	11468.59	3559.39	203.42	327.29
521111	**A**	459265.80	8812.83	516340.13	201.85	217.77	69.07	12556.76	1927.64	284.30	323.86
521121	**A**	456599.92	11075.20	513342.96	6511.23	426.74	135.53	5194.53	4634.81	743.78	1335.31
521101	**A**	459845.22	9257.70	516991.56	1425.54	61.58	379.55	9977.99	1352.78	310.48	397.62
521105	**A**	460725.46	6887.83	517981.18	2647.70	154.00	53.60	7338.26	3690.80	144.35	376.84
521106	**A**	459136.58	13105.82	516194.85	2904.88	114.09	47.84	5117.79	2830.24	230.05	317.85
521123	**B**	461865.18	6632.88	519262.55	339.99	298.10	130.13	7513.59	3452.65	110.58	394.35
521127	**B**	461522.53	8304.04	518877.32	149.75	293.14	12.23	7476.80	2784.48	279.84	299.86
521127	**B**	462603.92	6851.48	520093.10	331.21	185.26	9.92	6658.84	2563.92	375.72	326.60
521130	**C**	463971.72	9170.69	521630.87	804.53	64.22	90.42	1892.20	1898.12	203.97	273.25
521131	**D**	464033.12	8199.23	521699.91	405.61	104.43	56.04	807.78	3880.31	469.23	344.33
521132	**D**	463460.96	9861.53	521056.62	67.20	69.56	27.98	2457.21	2464.39	246.76	287.81
521149	**E**	463359.82	7569.40	520942.94	429.45	1049.33	354.11	4515.68	1280.84	152.80	345.64
521163	**F**	464071.25	8156.57	521742.77	160.08	241.37	106.01	3297.61	1602.52	314.52	307.31

The second µXRF technique that can be applied on rubies for characterisation is the creation of element maps, especially for zones grains and grains with large inclusions (Figure 17). Where tiny inclusions are present in the corundum the spot size is too large to detect these as separate phases. In corundum grains with small inclusions, this will give a high uncertainty for the elemental concentrations of the corundum and the inclusions, as the measurements will be a combination of the elemental concentration of the inclusions and the corundum surrounding the inclusion.

The corundum from the Aappaluttoq area has little chemical zonation in the grains (Figure 17A and Figure 17B), which eliminates the possibility for fingerprinting or crystal characterisation by element mapping. The sample from Maniitsoq shows an irregular banding of Cr and Fe in the corundum fragment (Figure 17C). Other samples also showed zonation in V. If the grains from Aappaluttoq would have been similar to those from Maniitsoq, element mapping as a way to characterise individual stones might have been possible.

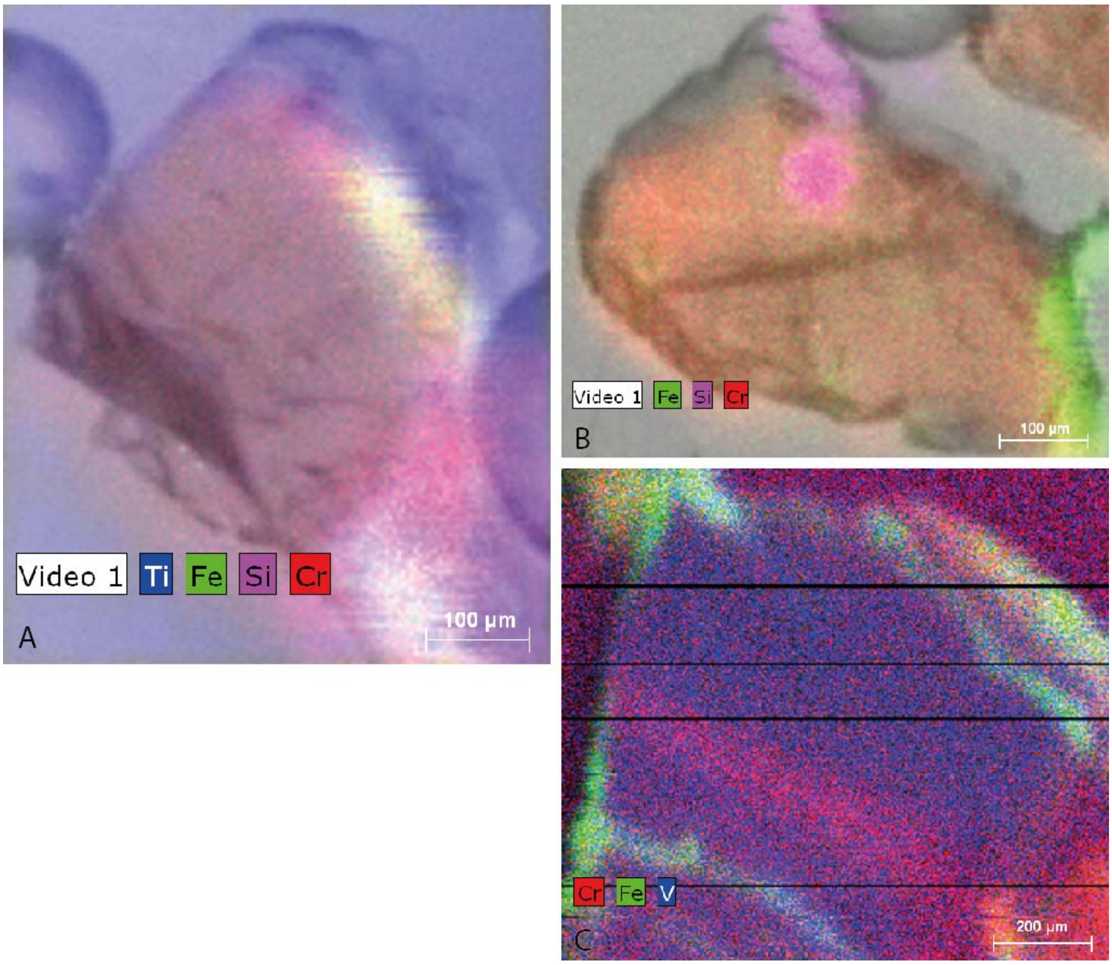

Figure 17. *Element mapping with µXRF. A) Corundum grain from Aappaluttoq. B) Corundum grain from Aappaluttoq with an inclusion, possible anorthite. C) Corundum grain from Maniitsoq.*

3.6 Results of the Laser-Induced Breakdown Spectroscopy analyses

The results of the LIBS analyses are shown in Table 11. Elements that were detected with LIBS, but not with LA-ICP-MS are Na, Ca, Zr, Ba, Tm, Lu, and Tb. Elements that were not detected with LIBS, but are observed with LA-ICP-MS are given in the rightmost column. Figure 18 shows the strongest peaks of the Aappaluttoq samples, compared to NIST standard glasses, which were used for calibration of the signal.

Table 11. *LIBS information on samples from the Fiskenæsset complex. 1) Elements contained with more than one characteristic peak in the LIBS spectrum. 2) Elements of which only one characteristic peak was observed. 3) Elements that were not observed with LIBS, even though present in higher concentrations in LA-ICP-MS analyses (concentration in brackets).*

Sample no.	[1]Contains	[2]Maybe contains (only 1 peak)	[3]Failed to identify
521104	Al, Cr, Mg, Ti, Fe, Si, Ca, K, Na	Ba, Tm, Li, Lu	
521105	Al, Cr, Mg, Tia, Fe, Si, Ba, Zr, Ca, K, Na	Ba, Mn, Li, Lu	
521105	Al, Cr, Mg, Fe, Ca, K, Na	Ti, Si	
521108	Al, Mg, Ti, Ca, Na	Cr	Fe (2253 ppm), Si (1068 ppm)
521110	Al, Cr, Mg, Ti, Fe, Si, Ca, K, Na	Tb	
521123	Al, Mg, Fe, Ca, Na	Cr, Si, Sr	Ti (108 ppm)
521132	Al, Mg, fe, Si, Ca, K, Na	Ti, Ba, Li	Cr (1570 ppm)
521149	Al, Cr, Mg, Fe, Si, Ba, Ca, K, Na	Sr, Li	Ti (36.3 ppm)
521160	Al, Cr, Mg, Fe, Ca, Na	Si	
545622	Al, Mg, Fe, Si, Ca, K, Na	Cr, Ti, Tb	
545625	Al, Mg, Ca, K, Na	Tm	Cr (10.4 ppm), Ti (492 ppm), Fe (3158 ppm), Si (109 ppm)
545626	Al, Mg, Ti, fe, Si, Zr, Ca, K, Y, Na	Tm, Ba, Sr, Li	Cr. (1257 ppm)
545627	Al, Mg, Ti, Fe, Si, Ba, Sr, Ca, K, Na	Tm	Cr (1212 ppm)
545630	Al, Mg, Ti, Fe, Si, Ba, Sr, Ca, K, Na	Zr, Mn, Tb, Li	Cr (141.4 ppm)

3.7 Results of the Raman spectroscopy and fluorescence analyses

Figure 19 shows the results of the Raman spectroscopy analyses on corundum. Two synthetic sapphires were used to calibrate and verify the system. Several of the theoretical Raman bands were observed in these synthetic sapphires.

A ruby crystal from Aappaluttoq (FC) was tested with Raman (GGU sample 521104). The sample was very fluorescent, causing a large noise peak on the right site of the spectrum. This fluorescence suppressed the Raman bands that are nearly invisible in the spectrum. The high fluorescence is caused by the presence of chromium (Cr) in the sample. Sample 521104 has a moderate amount of Cr, compared to other Aappaluttoq samples, thus even more fluorescence is expected of gem-quality rubies.

To demonstrate the applicability of Raman on natural corundum, a pale blue sapphire crystal from Tanzania has been analysed. The sapphire shows several of the typical Raman bands that indicate corundum, but also gave some extra peaks, which are caused by impurities in the crystal. Further analyses would have been necessary to attribute these extra peaks to specific trace elements or tiny mineral inclusions.

Raman spectroscopy is not suitable to fingerprint the rubies from the FC, because of the high Cr content. For corundum in general, Raman spectroscopy is very difficult, because the obtained peaks and their relative intensity depend on the crystallographic orientation of the crystal. Hence, it is impossible to obtain a unique spectrum for a crystal. Raman could be used though, to characterise the nature of inclusions in ruby in cases where other techniques are not applicable, and to detect glass and lead fillings.

Figure 18. *Strongest lines in LIBS spectra for samples from Aappaluttoq, compared to NIST standards.*

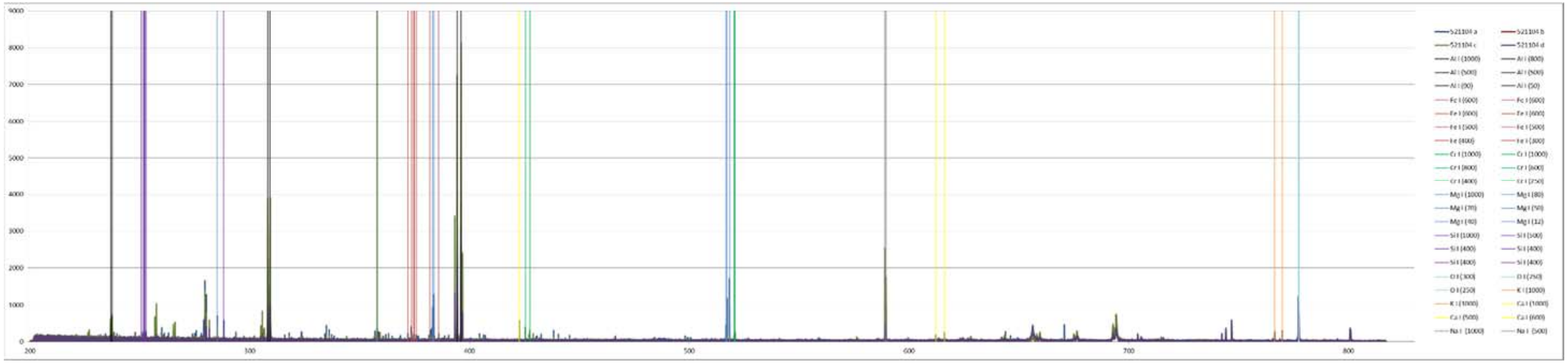

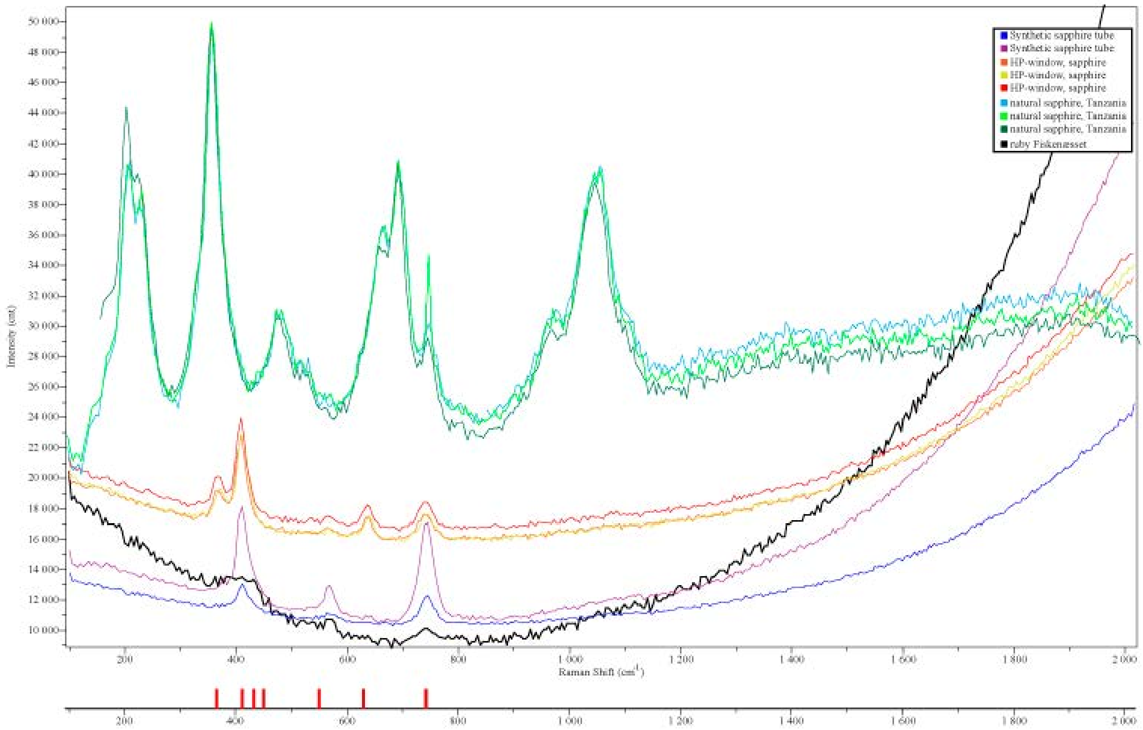

Figure 19. *The Raman effect of corundum. Raman shift of two synthetic sapphires, natural (faint blue) sapphire from Tanzania, and Fiskenæsset (Aappaluttoq) rubies in the upper part of the figure and known Raman bands for corundum in the bottom of the figure. The intensity of the Raman spectrum on the vertical axis is at a relative scale, spectra have been shifted upward to enable comparison.*

The Aappaluttoq rubies show the characteristic R1 and R2 fluorescence peaks that have been described in literature (Figure 14). Due to the high amount of Cr and low amount of Fe, the samples show a well-developed fluorescence. No special peaks or other features were observed, thus this technique is not suitable for fingerprinting.

3.8 Multivariate statistics – results for ruby/sapphire samples

The results for the Self Organising Maps (SOM; Kohonen 2001) and cluster analysis of all investigated samples are shown in Figure 21. Warm colours indicate a high amount of clustering. The results for all samples (Figure 21A) are compared with the SOMs for Aappaluttoq (Figure 21B) and for Cr (Figure 21C). The clustering based on all samples is shown in the cluster map (Figure 21D). The four maps show that the samples from Aappaluttoq, Upper Annertussaq, and Ruby Island together form the light blue cluster (Figure 21D) and this cluster is strongly influenced by the Cr-concentration of the samples (Figure 21C). Samples from the other FC outcrops mainly plot in the adjacent brown, purple, dark yellow, dark blue and orange cluster, together with a number of international occurrences.

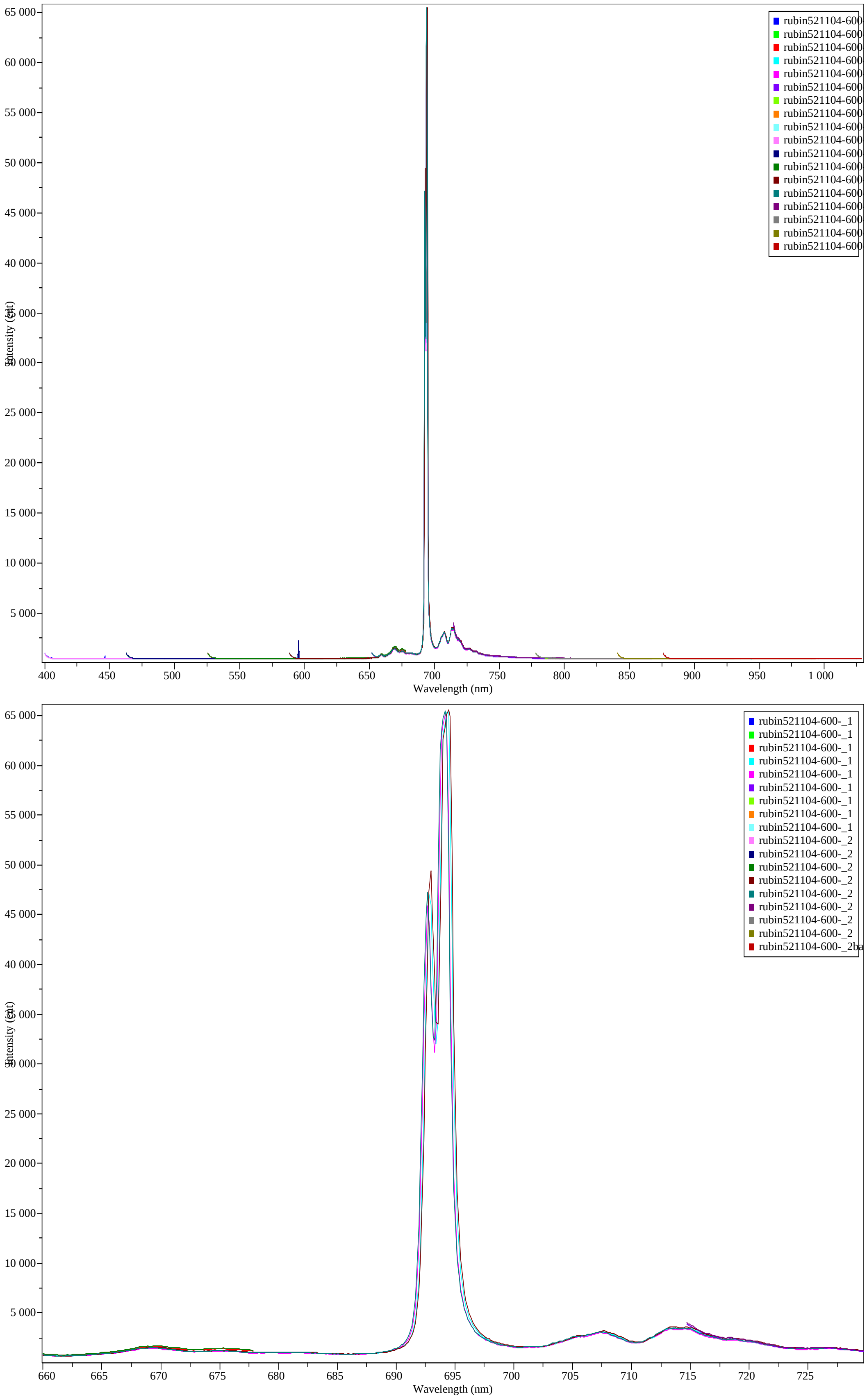

Figure 20. *Fluorescence effect of Aappaluttoq ruby (sample 521104). The ruby shows its characteristic peaks at wavelengths 692.6 and 694.2 nm. The figure at the bottom is a blow-up of the large peak in the upper figure.*

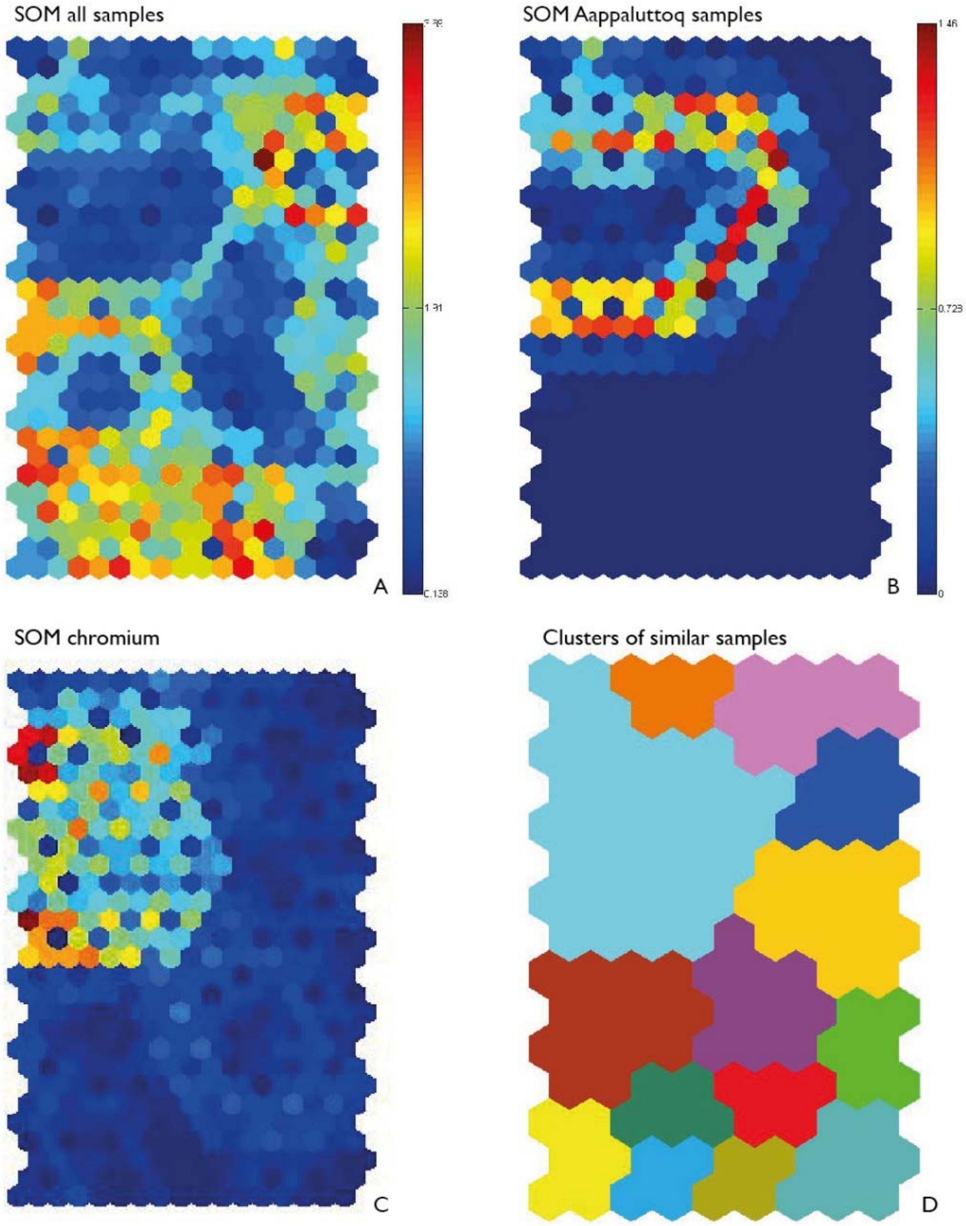

Figure 21. *Self Organising Maps for all (A) analysed samples and (B) for all Aappaluttoq samples, taking into account their trace elements Mg, Si, Ti, V, Cr, Fe, Ga concentrations and δ^{18}O values, (C) SOM for Cr concentration, and (D) cluster analyses in which similar samples are grouped into one cluster. Aappaluttoq, Ruby Island, and Upper Annertussaq samples are grouped in the light blue cluster.*

Figure 22 shows the variation in the data between the Aappaluttoq samples and the other samples. The R^2-value is indicated, which is a statistical measure of how well the data fit to the modelled average data. The samples from Aappaluttoq plot in three different R^2-value levels. The samples from Aappaluttoq that are the most typical for Aappaluttoq and the least similar to samples from other areas are 521101, 521105, 521106, 521107, 521110, and 521113 (Figure 22; sample numbers in Table 12). Samples 521108, 521109 and 521121 form a second group of Aappaluttoq samples, with many similarities to the previous samples, but also to the samples from Upper Annertussaq. Samples 521104, 521111 and 521120 from Aappaluttoq resemble the sample from Ruby Island.

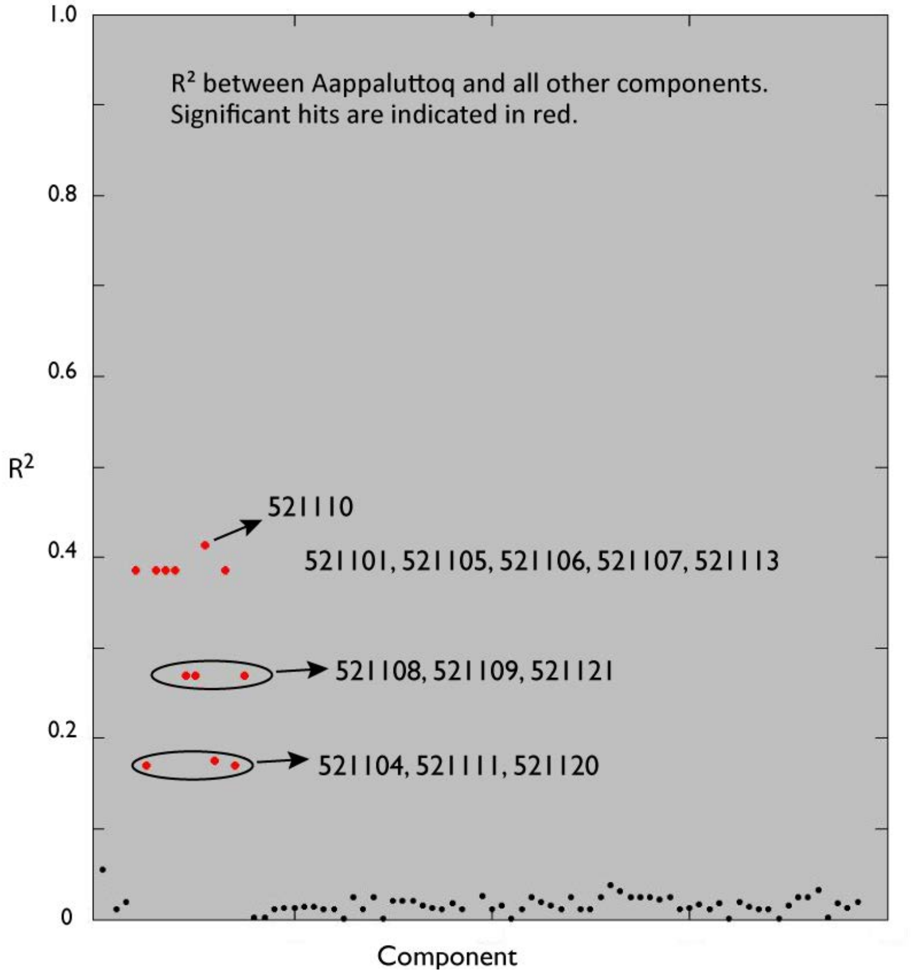

Figure 22. *R^2-values for a component correlation (horizontal axis) between Aappaluttoq and other investigated components. All indicated sample numbers are from Aappaluttoq samples. Significant hits have an R^2 value larger than 0.16.*

Figure 23 shows the principle component analysis for the two main principal components (PC1 vs PC2). The software defines the positions of the individual points in the figure. The analysed variable Fe, Cr, Ti, V, Ga, Si, Mg and $\delta^{18}O$ values are plotted in the figure together with the average results for the individual areas. Variables that plot far away from the origin are important for separation of the individual components (e.g. Fe, $\delta^{18}O$ or Si), while variables closer to the origin (like Mg) are relatively unimportant to separate individual areas. Variables that plot in the same quadrant correlate with the individual area (Aappaluttoq has a high Fe, Cr, and Si concentration compared to other areas), variables that plot in opposite quadrants anticorrelate (Aappaluttoq has very low $\delta^{18}O$ values). Individual areas that show up close to Aappaluttoq in the PCA diagram (Figure 23) are similar in fingerprint to Aappaluttoq.

The cluster analysis and PCA show that the Aappaluttoq samples as a singular group resemble the samples from other parts of the FC, most notably Kangarssuk, Qororssuaq, Upper Annertussaq, Ruby Island, and the samples from international occurrences in Longido (Tanzania), Winza (Tanzania), Chanthaburi (Thailand), Ilalaka (Madagascar), Bo Rai (Thailand), Pailin (Cambodia), Andilamena (Madagascar) and Umba (Tanzania). All show geochemical signatures that overlap or closely resemble the samples from the FC and those that have oxygen isotope data generally show low values, like the FC (compare to Figure 7).

Table 12. *Investigated samples from the Fiskenæsset complex for the multivariate statistics analysis.*

sample #	Outcrop	sample #	Outcrop
521101	Aappaluttoq	459905	Sarfaq
521104	Aappaluttoq	459991	Kangarssuk
521105	Aappaluttoq	476373	Tuk
521106	Aappaluttoq	497386	Top 670
521107	Aappaluttoq	508660	Qaqqatsiaq
521108	Aappaluttoq	521123	U. Annertussaq
521109	Aappaluttoq	521127	U. Annertussaq
521110	Aappaluttoq	521130	L. Annertussaq
521111	Aappaluttoq	521131	Bjørnesund 2008
521111	Aappaluttoq	521132	Bjørnesund 2008
521113	Aappaluttoq	521134	Bjørnesund 2008
521120	Aappaluttoq	521135	Bjørnesund 2008
521121	Aappaluttoq	521138	Siggartartulik
160063	Qaqqatsiaq	521140	Siggartartulik
510132	Qororssuaq East	521142	Rubin Ø
160098	Beer Mountain	521149	Kigutilik
497391	Beer Mountain	521163	Intex

For the Aappaluttoq samples, typical concentrations are: Mg ≈ 40 ppm, Si ≈ 1000 ppm, Ti ≈ 80 ppm, V ≈ 60 ppm, Cr >4000 ppm, Fe ≈ 2500 ppm, Ga ≈ 30 ppm, and $\delta^{18}O \approx 4‰_{(SMOW)}$. Of these values, Cr and Fe have the highest significance, while Ti, Ga, V and $\delta^{18}O$ values in combination can be used to separate Aappaluttoq from other occurrences.

3.9 Blind test: Interpretation of the origin of the samples

The following text is taken from the report made by Asta F. Jørgensen (2014):
In the ternary diagrams the samples are classified by locations and the unknown samples are tried to be tied to a location. Table 13 gives a summary of the information in the ternary diagrams. In the table, the overlapping samples are listed and from that it is tried to give an estimate of where the unknown sample originate from.

Unknown-1 overlaps with Pailin in all four ternary diagrams and with Kangarssuk in Fe-Cr-Ti and in Cr-Ti-Ga, with Aappaluttoq and Bjørnesund in Fe-Cr-Ga and in Si-Fe-Ga, and with Beer Mountain in Si-Fe-Ga. Unknown-1 does have most in common with the corundum from Pailin.

Unknown-2 overlaps with Kangarssuk and Cambodia in all four ternary diagrams, in Fe-Cr-Ti there is an overlap with Maniitsoq, in Fe-Cr-Ga Unknown2 overlaps with Top670, and in the Si-Fe-Ga diagram is an overlap with Aappaluttoq. Unknown-2 is most likely derived from Kangarssuk.

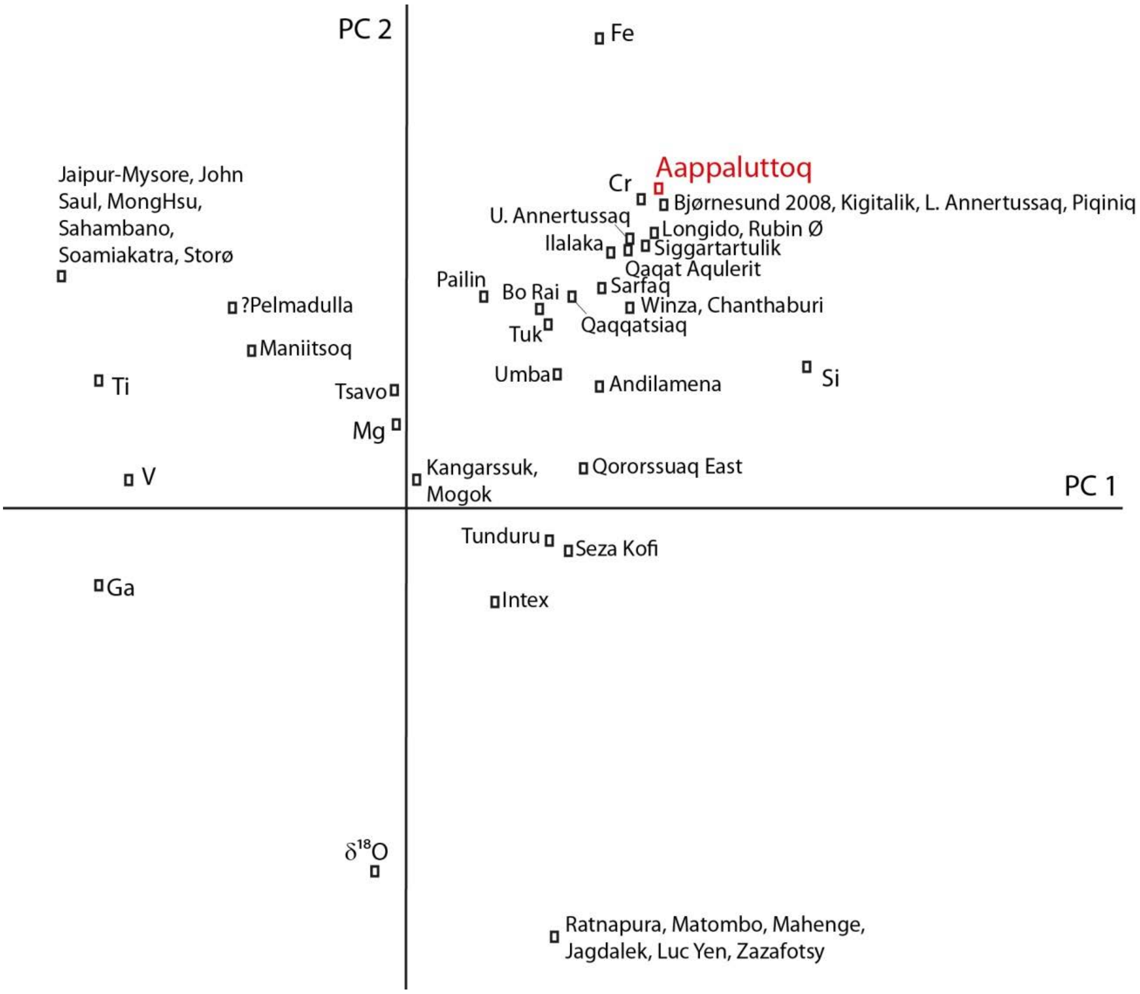

Figure 23. *Principle component analysis (PC1 vs PC2) for the trace element and stable oxygen isotope compositions from all investigated regions. The PCA is based on a dataset including Mg, Si, Ti, V, Fe, Cr, Ga and $\delta^{18}O$.*

Table 13. *Areas, in which the trace element chemistry overlaps with the unknown samples.*

Name	FeCrTi	FeCrGa	CrTiGa	SiFeGa
Unknown-1	Pailin Kangarssuk	Pailin Bjørnsund Aappaluttoq	Pailin Kangarssuk	Pailin Bjørnesund Aappaluttoq Beer Mountain
Unknown-2	Kangarssuk Pailin Maniitsoq	Kangarssuk Pailin Top 670	Kangarssuk Pailin	Kangarssuk Pailin Aappaluttoq
Unknown-3	Aappaluttoq Rubin Ø Top 670	Aappaluttoq Pailin Top 670	Aappaluttoq Top 670 Rubin Ø	Aappaluttoq Nattivit Madagascar Pailin
Unknown-4	Aappaluttoq Top670	Aappaluttoq Qororssuaq East Sri Lanka	Aappaluttoq Sarfaq	Sri Lanka Tuk Madagascar

Unknown-3 overlaps with Aappaluttoq in all four diagrams, with Top 670 in all the diagrams except Si-Fe-Ga, with Ruby Island in Fe-Cr-Ti and Cr-Ti-Ga, with Cambodia in Si-Fe-Ga and Fe-Cr-Ga. An overlap with Nattivit and Madagascar is present in the Si-Fe-Ga diagram. Unknown-3 fits best with Aappaluttoq.

Unknown-4 overlaps with Aappalutoq in Fe-Cr-Ti, Fe-Cr-Ga and Cr-Ti-Ga, with Sri Lanka in Fe-Cr-Ga and Si-Fe-Ga, and with Top 670, Qororssuaq East, Sarfaq, Tuk, and Madagascar in one diagram each. Unknown-4 is hard to fingerprint, but contains the best correlation with Aappaluttoq.

3.10 Effect of ICP-MS analyses on polished stones

Three polished sapphire stones bought at the market in Pailin, Cambodia and claimed to derive from the local area, have been analysed with LA-ICP-MS. The stones are not very well polished, but the images below illustrate the effect of the LA-ICP-MS analyses on the polished stones (Figure 24 to Figure 27).

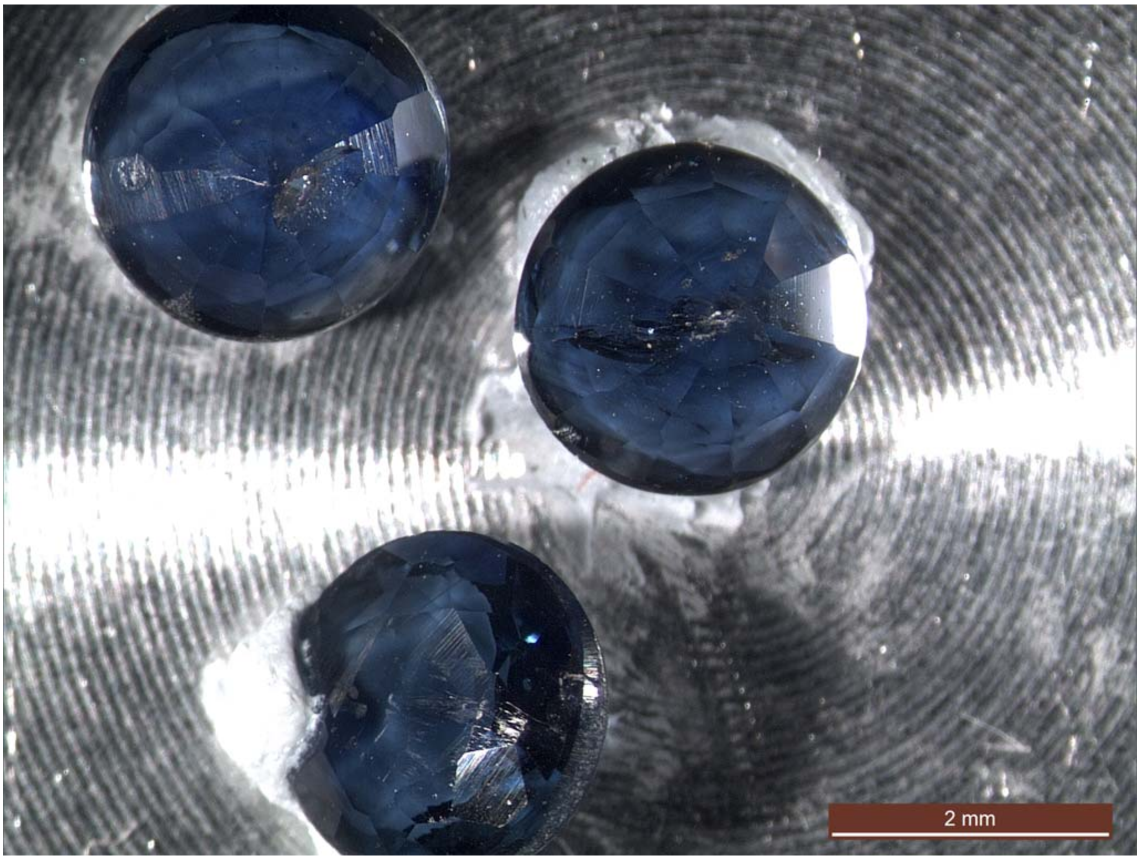

Figure 24. *Three analysed polished sapphires seen in an optical microscope. LA-ICP-MS spots in the upper sample were mainly placed in the facets of the culet. In the sample on the right the spots were placed in edges of the facets in the culet, and in the sample at the bottom the spots were place in the girdle.*

Typical LA-ICP-MS analyses would not be placed on the facets (Figure 25), and certainly not on the facets of the table, as this would influence the way the light is transmitted through the sample, but would be placed on the edges of the facets in the culet or in the girdle (Figure 26 and Figure 27). In these samples at least, the marks on the sample left after polishing are larger than the spots burned with the LA-ICP-MS.

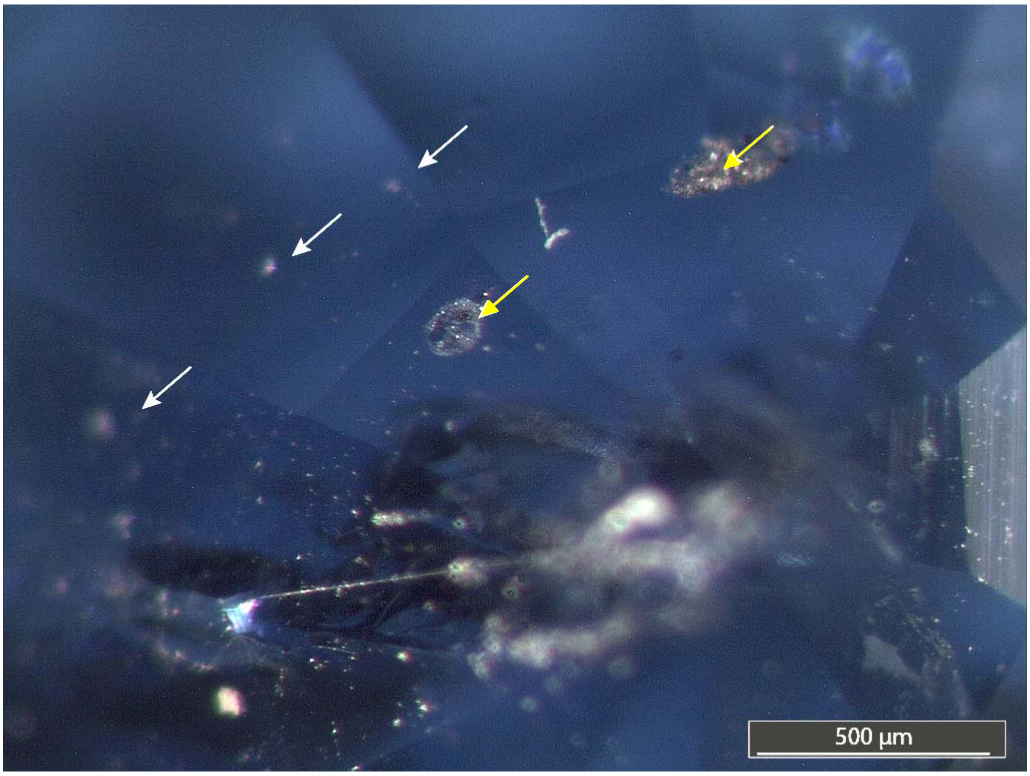

Figure 25. *Detail of the upper sample in Figure 24, in which LA-ICP-MS spots mainly were placed in the facets of the culet (white arrows). Damage of the sample inflicted during polishing is shown with yellow arrows.*

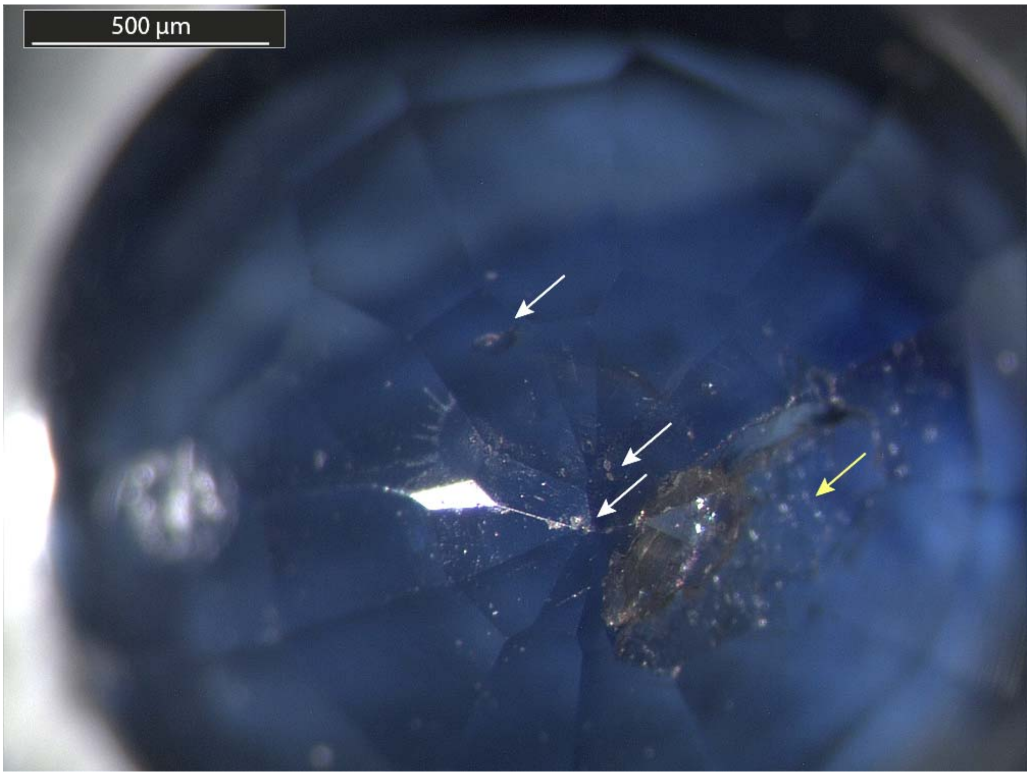

Figure 26. *Detail of the sample on the right in Figure 24, in which LA-ICP-MS spots mainly were placed in the edges of the facets of the culet (white arrows). Damage of the sample inflicted during polishing is shown with a yellow arrow.*

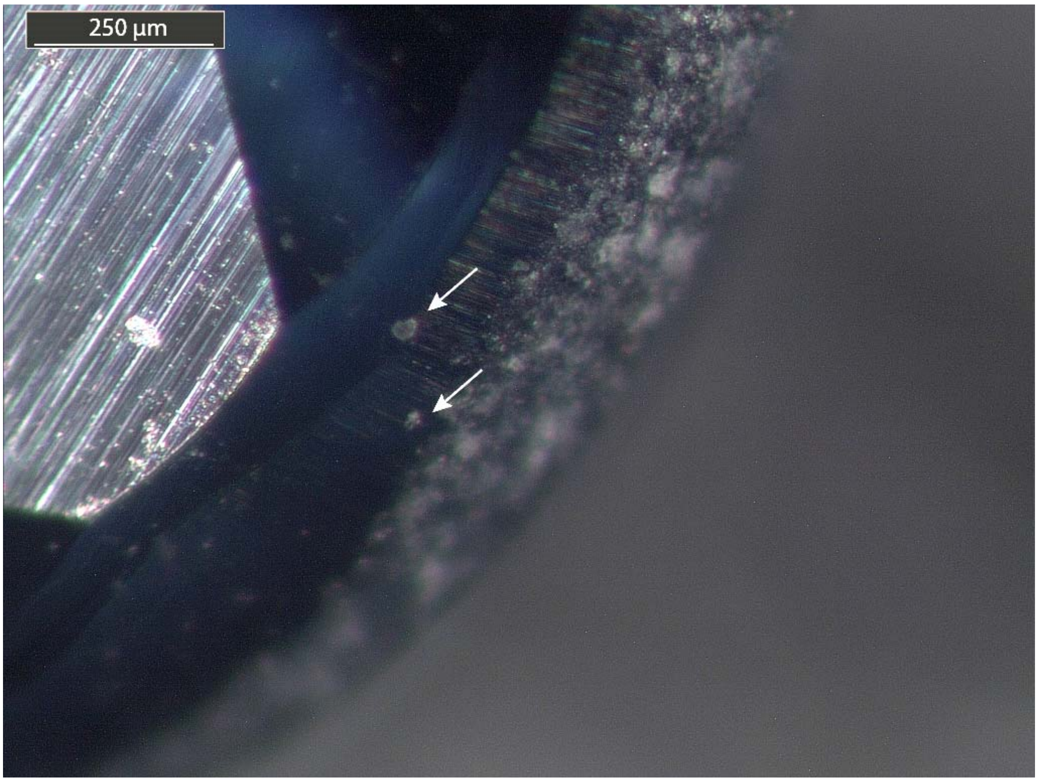

Figure 27. *Detail of the lower sample in Figure 24, in which LA-ICP-MS spots mainly were placed in the girdle (white arrows).*

4. Discussion

4.1 Metamorphic history of the Fiskenæsset complex focused on ruby formation

Ruby in the FC is formed in a setting associated with ultramafic rocks, as is the case for all other known ruby occurrences in Greenland: Maniitsoq, Storø, Kapisillit, Ujarassuit Nunaa, and Nattivit. However, the ruby-forming reactions in all of these localities are not identical: Ruby in Maniitsoq and on Storø formed by a metamorphic reaction between an ultramafic rock (metaperidotite) and an alumnosilicate-rich schist at amphibolite-facies conditions (Garde and Marker 1988; van Gool 2006; Yakymchuk and Szilas 2017). The rocks near Kapisillit are not described in detail, but their mineral assemblage sapphirine, gedrite, corundum, black spinel and phlogopite. Bøggild (1953) suggests an ultramafic-rock or possibly hydrothermally altered mafic rocks affinity. At Ujarassuit Nunaa rubies are found in amphibolite-facies metamorphosed gabbro-anorthosite associated with dunite (Appel *et al.* 2002). At Nattivit, the ruby forms in ultramafic rocks, which are cut by felsic sheets, all metamorphosed at amphibolite-facies metamorphic conditions (Poulsen *et al.* 2016).

The localities mentioned above, with a possible exception of Kapisillit, are examples of metasomatic reactions with or within ultramafic rocks in the classification system of Simonet *et al.* (2008), however, not all of the localities are of the same subtype. The Maniitsoq occurrence is an example of a desilicated gneiss sub-type (Simonet *et al.* 2008; own field observations); here a felsic rock, e.g. a gneiss, is brought tectonically into contact with an ultramafic rock. The occurrence on Storø is probably formed by a comparable mechanism (K. Szilas, pers. comm 2017; own field observations), while the outcrops in Nattivit are of the plumasite *s.l.* -type metasomatism (own field observations; see Simonet *et al.* 2008 for details on the mechanism).

For the FC, a different model has been proposed. Schumacher *et al.* (2011) and Keulen *et al.* (2014b) proposed that ruby was formed in a reaction between anorthite-rich plagioclase in leucogabbro or anorthosite and serpentinite/forsterite in an ultramafic rock, triggered by the intrusion of a granitic sheet that is low in Si, but enriched in B or F. For the southernmost part of the FC, the ruby-formation occurred immediately after peak-metamorphism, which was calculated to 580-630◦C and 4-6 kbar (Keulen *et al.* 2014b). Guiliani *et al.* (2014) describe the FC outcrops at Aappaluttoq as gabbroic rocks subjected to “metamorphic metasomatism”, where the ruby mineralisation is connected with specific stratigraphic horizon, which probably has a high Al, low Si content and a high fluid flux. Smith *et al.* (2016) describe the same outcrops as a metasomatised reaction zone between a peridotite and a leucogabbro, in which fluid interaction during regional metamorphism produced ruby and pink sapphire. The latter two models for Aappaluttoq are based on Herd *et al.’s* (1969) work, in which they describes local K-enriched metasomatism, confined to certain structural positions in the FC near boudinaged spinel-bearing ultramafic rock at the contact between anorthosite and pyribolite/amphibolite horizons.

Here, we present the first detailed isochemical modelling of the rocks in the FC around Aappaluttoq, to establish the precise metamorphic reactions to determine the pT-conditions for the ruby-formation. The results are used to discuss the classification of the ruby-forming reaction and to establish the connection between typical fingerprint for these rubies and their geological history.

4.1.1 Source of the Al_2O_3

Field observations in the FC suggest that the ruby-bearing and related assemblages (reaction zones, RZ) result from the interaction of three components: pegmatite fluids (PEG) with ultramafic bodies (UM) that are interlayered with calcic plagioclase-rich rocks like anorthosite (AN) or quartz-poor, plagioclase-rich gneisses (Herd *et al.* 1969; Schumacher *et al.* 2011; Keulen *et al.* 2014b; Smith *et al.* 2016). Fluids clearly played a crucial role in the development of the RZ rocks, facilitating mineral growth and acting as a medium for rapid material transport between rocks and minerals. The key to understand the paragenesis of ruby is to know the source of the Al_2O_3.

The rocks of the PEG-AN-UM association limit the sources of the Al_2O_3 to two possibilities: (1) the Al is derived from minerals present prior to mineralisation or (2) excess Al is introduced with the PEG and associated fluids, e.g. via muscovite component or saturation of an Al-rich pegmatite mineral.

For possibility (1), the most Al-rich and abundant minerals occurring in the rocks prior to mineralisation were feldspars. Both the albite component of plagioclase and K-feldspar are not suitable sources for Al_2O_3 because compositional variation in K- and Na-bearing minerals of the RZ (mainly amphiboles and micas) are coupled substitutions that pair K or Na with Al in these minerals. As a consequence, Al from albite and K-feldspar cannot be used to produce ruby. However, extraction of Al from the anorthite component of plagioclase is possible. Ca from anorthite that forms Ca-amphibole is not coupled with Al, and most of the Al_2O_3 from anorthite is potentially available for ruby or other Al-rich minerals.

If the primary PEG were peraluminous (i.e. muscovite-, aluminosilicate-, garnet-, or cordierite-bearing), possibility (2) could also explain Al mineralisation, as such Al-rich compositions could react with UM rocks to form RZ mineral assemblages. While Al-rich minerals occur rarely in some of the PEG in RZ rocks, these are interpreted to be a result of the modification of PEG and PEG fluids during mineralisation, rather than indication of the primary PEG composition.

There is no evidence of a widespread, strongly peraluminous pegmatitic intrusive event in the FC, or elsewhere in southern West Greenland and South-West Greenland. Muscovite is a rare mineral in pegmatites and where present, only occurs as a minor pegmatite component. The anorthite component of plagioclase from the K-enriched PEG could serve as the source of Al for the ruby; however, K-enriched pegmatites are extremely fractionated and fluid-rich products of crystallisation, thus they contain albite- rather than anorthite-rich plagioclase (Schumacher *et al.* 2011). As a result, PEG is not considered a good source for the Al_2O_3, but the associated fluids are a necessary component of the mineralisation (see below). The ruby-forming reaction in the FC is therefore not a plumasite *s.l.*-type metasomatism reaction.

4.1.2 Ruby formation

The important stages leading to ruby (corundum) formation are summarised in Figure 28. The key event is the introduction of fluid-rich pegmatites proximate to the interlayered anorthosite and leucogabbro with ultramafic rocks slightly past conditions of peak metamorphism. The initial, pre-mineralisation state (stage 1 in Figure 28) is given by the interlayering of anorthositic and ultramafic rocks before the introduction of pegmatitic fluids.

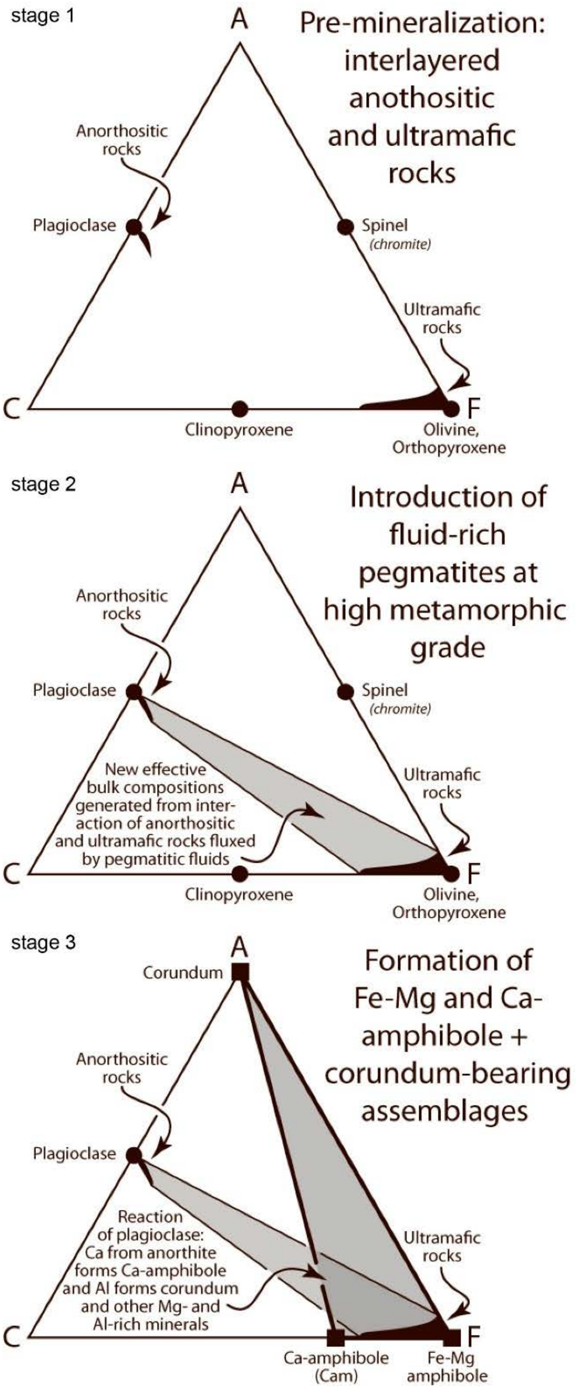

Figure 28. *Schematic ACF showing the major stages leading to the formation of ruby (corundum) and other Al-rich minerals. A=Al_2O_3+ Fe_2O_3+Cr_2O_3+TiO_2-Na_2O; C=CaO; F=MgO+FeO+MnO-TiO_2 all in molecular proportions. Fe-Mg amphibole = anthophyllite, cummingtonite, or gedrite.*

Fluid enhances the transport of material and, as a result, expands the reactive volume of the rocks. At the locations of the ruby-bearing and related rocks, the influx of these fluids at or near peak metamorphic temperatures (Keulen *et al.* 2014b) allowed extensive chemical reaction between the UM and AN rock units. However, modification of the pegmatite and fluid by the host rocks is also important to the eventual formation of the ruby-bearing and associated mineral assemblages (stage 2 in Figure 28). K is depleted from the fluid by the reaction of olivine (UM) + K-feldspar (PEG) + H_2O (PEG) => phlogopite (RZ) + anthophyllite (RZ). Reducing silica activity is essential to stabilizing ruby in the RZ, which can be achieved by the reaction: olivine/serpentine (UM) + aqueous SiO_2 (PEG) + H_2O (PEG) => anthophyllite (RZ). Manifestation of both these reactions on the outcrop is the presence of biotite or phlogopite in close association with the pegmatites and monomineralic zones of anthophyllite separating the ultramafic rocks from the pegmatite (Schumacher *et al.* 2011).

The source of the Al that forms the ruby and other Al-rich minerals of the RZ is the anorthite component of plagioclase. The Al in the plagioclase is liberated by the reaction: olivine/serpentine (UM) + plagioclase (AN) + H_2O (PEG) => Ca-amphibole (RZ) + ruby (RZ). Sapphirine (RZ) and cordierite (RZ) could form by analogous reactions at slightly different local bulk rock compositions (stage 3 in Figure 28).

The reaction scenario suggested above could plausibly explain at least part of the variation in the rock composition in Figure 3. The reactions imply mobility of Mg and Ca within the RZ. Locations where Ca-amphibole nucleated and grew are places where the Ca/Al ratio increased relative to the pre-mineralisation rocks (UM and AN). This change in Ca/Al results from the transport of Ca to the location of Ca-amphibole growth. Locations where Ca/Al has markedly decreased (e.g. the corundum normative rocks, Figure 3) are likely places where breakdown of the anorthite component of the plagioclase is more extensive and more Ca is removed (Schumacher *et al.* 2011).

4.1.3 Source of the Cr

The red colour in ruby requires that some Cr is incorporated in the crystal structure. Cr is an element that under most geologic conditions is essentially immobile. However, the extensive occurrence of pargasite (Cr-bearing calcic amphibole) and ruby suggests Cr was mobile during ruby-formation in the FC. The source of this Cr is likely the chromite from the ultramafic rocks, but trivalent Cr (its valence in chromite) is considered immobile under most conditions. Here, we propose that Cr was mobile resulting from an unusual local environment that could lead to chrome mobility. The temperature during the metasomatic reaction that formed ruby and pargasite was close to 600°C, based on isochemical modelling (Figure 29) and field observations on outcrops in the FC, which contain supersolvus orthoamphibole. Some insight in to the high-temperature behaviour of Cr may be gained from the Eh-pH relations of chrome species at 600°C. Figure 30 shows that hexavalent Cr, which is highly soluble (and hence mobile) in oxidizing and alkaline solutions. If this is also true at high temperature, then oxidizing and/or high-pH pegmatitic fluids may play a role in the mobilizing Cr at the time of ruby formation. Another possibility is that boron in the fluid associated with the pegmatites could complex with Cr. Boron must have been present, because both kornerupine and tourmaline formed in some of the reaction zones between the anorthite-rich rocks and the ultramafic rocks (Herd *et al.* 1969; Schumacher *et al.* 2011).

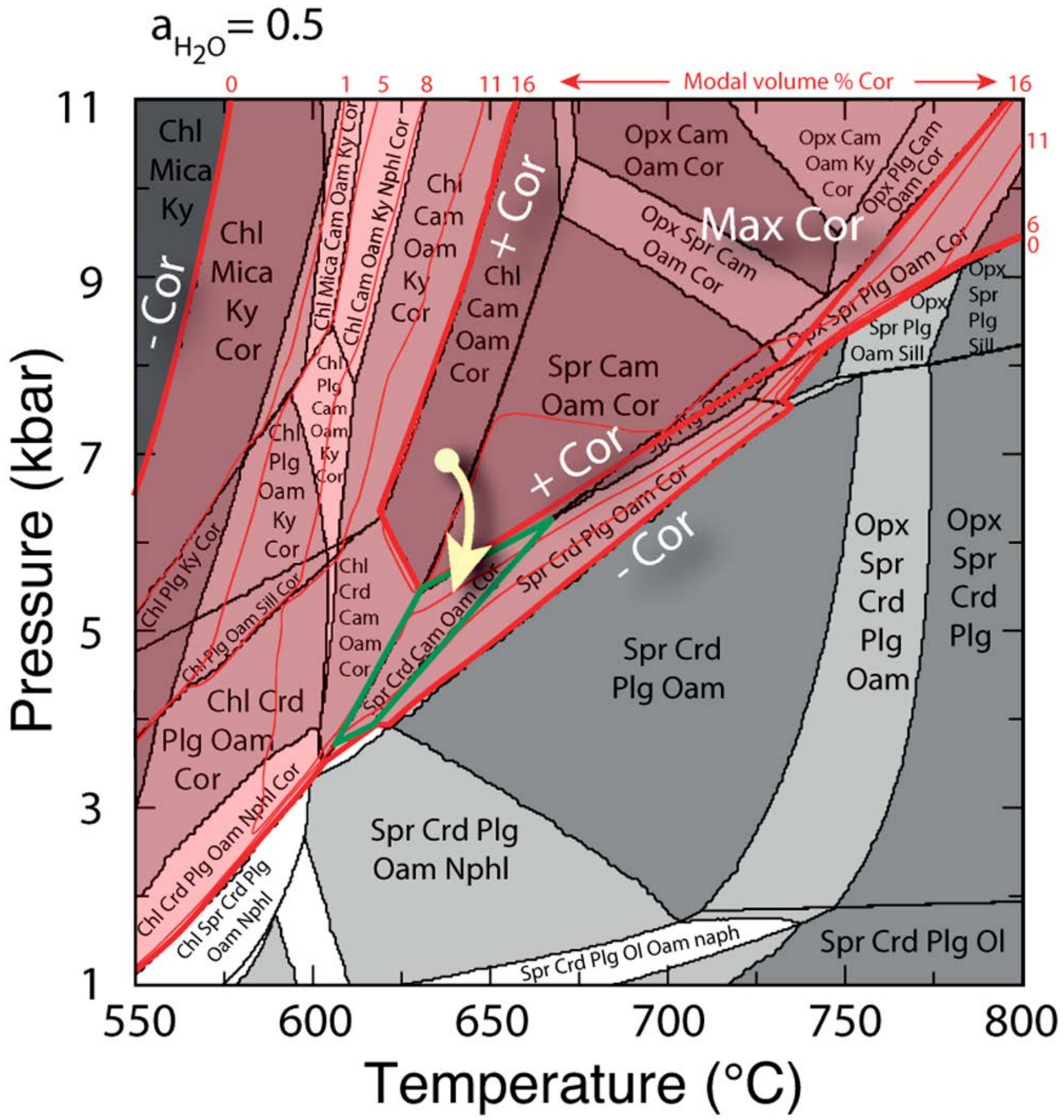

Figure 29. *Isochemical P-T section for analysis sample 521106, Aappaluttoq, Fiskenæsset complex. Note that, since the rock composition was created by the interaction pegmatite fluids and host rocks, only the part of the P-T path that postdates the pegmatites can be shown. Filled yel-low circle = hypothetical P-T of pegmatite fluid introduction; heavy yellow arrow = partial P-T path. Diagram parameters: Abbreviations: Cam = Ca-amphibole; Chl = chlorite; Cor = corundum; Crd = cordierite; Cum= cummingtonite; Ky = kyanite; Mica = white mica; Nphl = Na-phlogopite; Oam = ortho-amphibole; Ol = olivine; Opx = orthopyroxene; Plg = plagioclase; Sill = sillimanite; Spr = sapphirine. Model parameters–Simplified composition: Na2O (1.33); MgO (19.50); Al2O3 (35.93); SiO2 (36.86); CaO (0.71); FeO (5.40). Solution models (Perple_X): oAmph(DP2), cAmph(DP2), hCrd, Pl(h), Opx(HP), Chl(HP), Sapp(HP), O(HP), Mica(CHA1).*

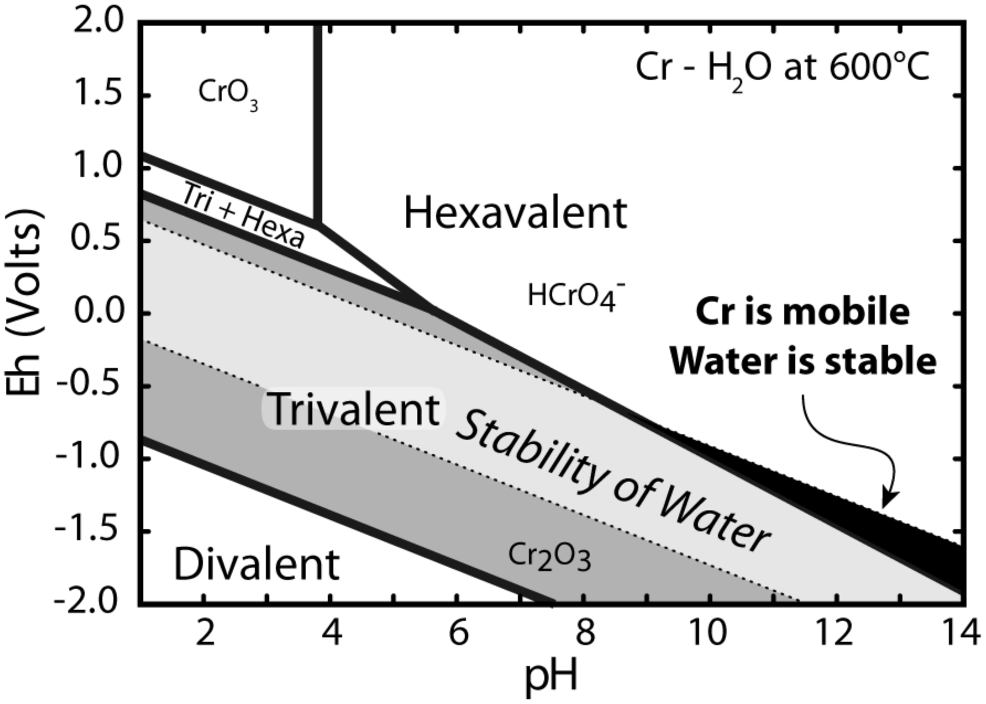

Figure 30. *Eh-pH diagram showing the valance and species of Cr along with the stability of water, modelled for T = 600°C. Reproduced with permission of GEUS.*

4.1.4 Metamorphic conditions

Metamorphic p-T conditions are commonly determined through the construction of isochemical p-T sections (pseudosections) from bulk rock compositions. However, the origin of these ruby-bearing and related rocks complicates the application of these diagrams. Since the reaction zone rocks did not exist until the pegmatite fluids intruded, only the part of the p-T history after their formation can be shown on an isochemical p-T section constructed for the composition of a reaction zone rock. This is illustrated in Figure 29, which shows calculated phase relations for sample 521106 from Aappaluttoq, with the onset conditions for the ruby-forming reaction at ca. 640°C and 7 kbar. Figure 29 has three general p-T regions that are relevant for ruby stability: one, existing of two fields, where ruby is unstable (-Cor), one where reactions cause large changes in modal amounts of ruby (red fields contoured for modal corundum), and one with abundant ruby and little change in modal volume (+Cor/Max Cor). Because the same reaction is also plausible for other types of corundum the abbreviation, Cor is used rather than ruby. For sample 521106, the important near-peak metamorphic mineral phases are ortho-amphibole, Ca-amphibole, and ruby along with texturally later sapphirine followed by cordierite (see also Figure 2). This sequence of minerals can be explained, if the pegmatite fluids were introduced at the conditions of the Chl-Cam-Oam-Cor field (filled yellow circle, Figure 29); this would represent the main phase of ruby formation. If the rocks followed a trajectory (heavy yellow arrow, Figure 29) of decreasing pressure *en route* to the surface, they would encounter the stability field of Spr-Cam-Oam-Cor that would result in the formation of the observed sapphirine rims on ruby. Further pressure decrease would move the rocks into the p-T region indicated by the heavy green line (Figure 29), where cordierite formation could occur.

Guiliani *et al.* (2014) describe the FC rubies as a metasomatically formed deposit, but classify the outcrops as metamorphic deposits in amphibolite and gabbro, together with anyolite (intergrown ruby and green zoisite) outcrops in e.g. Winza or Longido, Tanzania (Simonet *et al.* 2008, Guiliani *et al.* 2014). In this type of reactions, ruby-bearing amphibolite is associated with ultramafic complexes like dunites and typically forms at granulite-facies conditions, commonly with sapphirine as a precursor mineral (sapphirine is stable at both higher temperatures together with corundum and lower pressures without corundum, see Figure 29). Simonet *et al.* (2008) describes these types of ruby deposits as anorthosites, norites or troctolites associated with ultramafic complexes that were hydrated at granulite-facies conditions. Even though we agree with this classification for the FC rocks, there are two important things to point out: First, within the FC complex, there is a variation in metamorphic grade between lower granulite-facies conditions (e.g. near Aappaluttoq) and amphibolite facies in the eastern and southern parts of the complex (Schumacher *et al.* 2011, Keulen *et al.* 2014b). As described above (see Figure 29), the ruby-forming reaction might – even in Aappaluttoq – have occurred at upper amphibolite-facies conditions (see Figure 29); and sapphirine can form at upper amphibolite-facies metamorphic conditions. Thus, this classification (Simonet *et al.* 2008) of ruby deposits should be extended to include the upper amphibolite-facies rocks, and, as Herd *et al.* (1969) already pointed out: sapphirine in the FC can be observed both as a pre-cursor mineral to and as a rim growing around ruby – it is therefore not always a precursor mineral.

Secondly, it should be noted that these granulite-facies ruby-bearing amphibolites or mafic granulites, as they are called by Giuliani *et al.* (2014) and Simonet *et al.* (2008), ought not to be confused with common amphibolites (i.e. plagioclase-hornblende-bearing rocks), or mafic granulites; at least not in the FC. The ruby-bearing rocks of the FC, and those from e.g. Winza or Longido, Tanzania, are phlogopitites or anthophyllitites, or other rocks very rich in amphiboles like pargasite or hornblende and including gedrite and cummingtonite, and lack or contain only little plagioclase. They are products of metasomatic reactions, and did not form through regional metamorphism of basalts or similar rocks. A more suitable name for these kinds of deposits might thus be ruby-bearing ultramafic complexes.

However, we do not concur with Giuliani *et al.* (2014) or Herd *et al.* (1969), who connect the ruby-forming reaction to a specific stratigraphic horizon with a high Al, low Si content and a high fluid flux. Our work shows that the ruby-forming reaction can occur anywhere in the FC where an anorthite-rich rock (e.g. an anorthosite or leucogabbro) is positioned adjacent to an ultramafic rock. Whether a reaction occurs or not, is dependent on the presence of a cross-cutting B- or F-enriched pegmatite sheet to provide the necessary fluids to trigger the reaction (see also Keulen *et al.* 2014b). The ultramafic rocks are an essential component of the reaction too. Also of importance is that the metasomatising fluids are not enriched in K, but that K is derived from the pegmatite.

4.2 Tools for origin determination of ruby from Greenland

4.2.1 Trace elements

Trace elements in rubies are not only the cause for the colour nuances in ruby and sapphire (e.g. Nassau 1983, Emmett et al. 2003), but also a good means to trace their geographical or geological origin. The most commonly used trace elements are Cr, Ga, Fe, Ti, V, Mg and Si, as they occur in varying proportions in most rubies (Guilong and Günther 2001; Pornwilard et al. 2011). Mg is a light element, which can be challenging to analyse on a trace element level with LA-ICP-MS. Therefore, we present our data here, but did not use this element in the comparison with literature data, where the amount of data for Mg is low too. However, Mg is relatively enriched in the FC rubies compared to other international deposits. Kochelek *et al.* (2015) apply the enrichment in Mg, together with Ca, as distinguishing elements to separate the FC rubies from international deposits, using laser-induced breakdown spectroscopy (LIBS). Si is commonly found in rubies and can occur both in the crystal lattice, and as element in sub-micron scale mineral inclusions. Most samples analysed in this study, i.e. from both the FC and elsewhere yielded relatively constant Si levels between 500-1200 ppm (weight). Hence, Si is less suitable as a fingerprinting tool. Consequently, we focused our investigations on the remaining five elements: V, Fe, Ga, Cr and Ti (Figure 4 to Figure 6).

Of those five elements V, Fe and Ga are considered the most independent variables to determine the fingerprint of the rock, as only these are common and usually incorporated in the crystal lattice, and only rarely in sub-micron scale inclusions in the rubies (V. Pardieu pers. Comm. 2017). An example of the latter is Ti, which can be found both in the crystal lattice and as tiny rutile inclusions in the ruby grains. However, as long as the rutile needles are small and evenly distributed within the rubies from the same deposit, e.g. as silk (finely dispersed tiny rutile needles); it makes no difference for the fingerprinting, whether Ti occurs in the crystal lattice or as tiny inclusions. Cr is the most important element for the colour of the rubies, and its concentration is highly dependent on the Cr concentration in the host rock and the conditions that favour its mobility. Variations in Cr contents cause a range of pink to red shades in rubies from the same deposit that else have roughly the same trace element distribution. However, Cr is widely available to grow rubies in the FC, but also in the other Greenlandic occurrences, all of which are associated with Archaean ultramafic rocks, which contain very high Cr levels. The Cr concentration in nearly all Greenland rubies is significantly higher than nearly all other localities worldwide (Table 4). Thus, even though Cr levels correlate with desirable colour ranges, we include this element in our analyses, as the Cr levels in the FC are characteristically very high compared to other source areas for rubies, even when compared to rubies from other deposits with similar colours. High values for Cr and Fe for samples from Aappaluttoq agree with previous studies (e.g. Thirangoon 2008; Kochelek *et al.* 2015; Smith *et al.* 2016), demonstrating Cr concentrations of up to 13266 ppm (weight) (Thirangoon 2008), and 8387 ppm (weight) (Smith *et al.* (2016). Thus, V, Fe and Ga form the core of the relative trace element concentration diagram in Table 4), but the data are compared with plots for Ti and Cr as well. Although Figure 5 is a very helpful tool to separate different ruby deposits, the diagrams nevertheless only show relative concentrations, whereas absolute values may prove more conclusive when evaluating rubies from unknown localities. This is because the location of the each individual point in the triangular diagrams not only depends on a high concentration for one element, but also the concentration of the three elements together. Excess of one trace element, e.g. high V contents in some Mogok, Myanmar samples, will thus shift the relative amount of Fe and Ga to apparently lower levels, whereas in absolute numbers, the Fe and Ga concentrations are comparable to other Mogok samples. Therefore, below we discuss two novel diagrams (Figure 6C and Figure 6D) that plot absolute ratios between ruby trace elements.

Figure 6A shows the commonly applied trace element ratios Cr/Ga vs Fe/Ti, also plotted in Figure 4A (Saminpanya *et al.* 2003, Rakontondrazafy *et al.* 2008). The Fe/Ti ratio in this plot is capable to separate marbles from other metamorphic rock, while the effect of the Cr/Ga ratio is mainly to separate ruby samples from ultramafic rocks-related deposits from the former two, as magmatic ruby deposits are rare. High Cr/Ga ratios are characteristic for most rubies associated with ultramafic rocks (Aappaluttoq, Longido, Umba, Winza, ?Ilakaka). Cr concentrations are usually elevated in rubies associated with ultramafic rocks, while Ga is a good indicator for the depth of formation of the ruby – a low Ga/Al is attributed to mantle-derived rocks (Hutchison *et al.* 2004). The magmatic rubies box (with Cr/Ga<1) in Figure 6A, only contains one pale ruby sample, which is actually derived from a marble-hosted ruby deposit. Rubies depend on the presence of a relatively large amount of Cr to define the red colour, and ratios of Cr/Ga<1 are highly unusual. The Cr/Ga ratio is therefore a good tracer for ultramafic-mafic rocks.

Figure 6B shows the second, commonly applied diagram for geological – and even geographical – typing, displaying Fe vs Ga/Mg. Peucat *et al.* (2007) defined the diagram for blue sapphires, which strongly depend on the amount of iron for their blue colour. Most data for ruby shows iron-values between 1000 and 10000 ppm (weight), except for the marble-hosted rubies, which contain an order of magnitude less Fe. The former group is further separated by varying Ga/Mg levels into high Ti-high Mg basalt rubies, potentially mantle derived rubies, metamorphic rubies (including part of the marble-hosted ruby samples), and mafic rubies. For rubies, the fields defined by Peucat *et al.* (2007) could include lower Fe-values than blue sapphire, such that marble-hosted rubies are included in the metamorphic field.

Figure 6C shows a new type of diagram combining the previous two diagrams (Figure 6A and Figure 6B). Here Fe/Ti (Figure 6A) is plotted against Ga/V. The latter ratio is a variation on Ga/Mg, as was used in Figure 6B. Applying the Ga/V ratio has a large advantage over the Ga/Mg ratio, namely that V is easier to measure and has a lower detection limit for the ICP-MS than Mg. This results in data of a higher quality and more samples can thus be included in the diagram. The Ga/Mg and Ga/V ratios give very similar results for most samples, except for the high-Ti and high-Mg rubies from xenoliths in basalts, which plot near the other basalt samples in Ga/V plots (see Figure 6C), but at very low Ga/Mg ratios as opposed to the other basalts (see Figure 6B). The resulting plot (as shown in Figure 6C) can now be divided into fields defining rubies hosted by marbles, mantle derived rocks, mafic rocks and metamorphic rocks. Boundaries between the fields were taken from Peucat *et al.* (2007) for the vertical axes, and adjusted to Ga/V values (by including the same samples in the same fields) and from Rakontondrazafy *et al.* (2008) for the horizontal axis. Another advantage of this type of diagram is that the three trace elements Fe, V, and Ga, that are the most reliable trace elements to use for origin determination, are applied here – together with Ti.

The Cr/Ga ratio is the most effective tool to separate ultramafic rock-related rubies from rubies from other host rocks. The Cr/Ga ratio is a very proficient parameter to separate Aappaluttoq rubies from rubies from other localities, therefore this ratio is employed in Figure 6D. A low Cr/Al ratio has a similar effect as a low Ga/Mg ratio (used by Peucat *et al.* 2007), and is used to separate mantle-derived material from crustal affinity sapphires. Figure 6D shows trace elements in different combinations of trace element pairs compared to Figure 6C. Figure 6D separates marbles, UM and basalts well, but the field for metamorphic samples overlaps with all other fields. On the horizontal axis, Fe/V has been used rather than Fe/Ti, to exclude Ti in favour of V, such that also in this diagram the trace element combination Fe, Ga and V is applied. This diminishes the effect of potential unevenly distributed sub-microscopic rutile inclusions in the crystal on the typing of the origin. Fe in rubies derived from marbles is usually low, whereas the content of V in these rocks is intermediate to high, yielding an effective separation of the marbles.

Basalt-derived samples can be separated by Cr/Ga vs Fe/Ti ratio, as defined by Sutherland and co-workers (1998) and discussed above. In the same publication, the authors also used the Fe/Cr vs Ga/Ti ratio to obtain the same separation. Samples with Fe/Cr > ≈ 25 were classified as metamorphically derived, while the Ga/Ti ratio did not have any influence. In many samples, the Ga/V ratio is approximately 5, with only slightly lower values for basalts (i.e. ca. 2). Therefore, a line can be drawn to separate basalts from metamorphic rocks (see line S in Figure 6D). The same can be done based on the work of Zaw *et al.* (2014), in which they plot (V+Cr)/Ga vs Fe/Ti ratios. V is low in most samples, except for some from Mogok, and the Ti/V ratio is ca. 2 for most samples, leading to a separate, slightly less steep line to separate basaltic from metamorphic rock samples (line Z in Figure 6D). The latter line (Z) however, is based on blue sapphires rather than rubies and thus might need some adjustment to slightly higher Cr/Ga ratios to be valid for rubies too. Therefore, the basalt-derived rubies can be separated from the metamorphic rubies by these lines; a tentative boundary for the formation of those rubies was drawn in the lower right corner of Figure 6D.

Even with the most optimal diagrams to show the trace element signature for the Aappaluttoq rubies (Figure 5, Figure 6C and Figure 6D), overlap between Aappaluttoq and other occurrences is observed, mainly with other samples that formed in a similar setting. These include Umba, Seza Kofi and Longido (all from Tanzania), the placer deposit of Andilamena (Madagascar), and to a lesser degree the metamorphic basaltic samples from Vietnam-Cambodia (Bo Rai, Pailin) and Australia (Cudgegong-Gulgong, Macquarie River). Of those, Bo Rai rubies contain trace amounts of Ni (C. Hauzenberger, pers. comm. 2013) and can therefore be separated from the FC rubies.

Many ruby deposits contain additional trace elements like e.g. Na, Ca, Mn, Ni, Sr, Zr, Nb, Sn, Ba, La, Ce, Ta, Pb. Apart from trace amounts of Mn in 2 out of 35 FC ruby samples, these trace elements were not observed in the FC samples. (It should be noticed, though, that Ca and Ni could not be analysed by the LA-ICP-MS system due to an increased Ca background and the usage of Ni cones during analysis, respectively.) Preliminary LIBS investigations on the FC rubies at the University of Copenhagen, Department of Plant and Environmental Sciences/GEUS indicate the likely presence of Ca, Na, Ba, Zr, K and Sr, apart from Cr, Mg, Fe, Ti, and Si (S.H. Serre, pers. comm. 2017), which is in good correspondence with LIBS observations by Kochelek *et al.* (2015), who found Ca, Mg, Fe, Ba, Zr, Cr and Na as enriched elements suitable to fingerprint the FC rubies. Equally, our preliminary investigations of rubies at the µXRF at Roskilde University showed the presence of Zr in the FC rubies.

The rubies from NW Maniitsoq are characterised by up to 6.2 ppm (weight) of Ta and trace amounts of Nb. Both elements are also observed in small concentrations in the samples from Kangerdluarssuk, Maniitsoq, together with trace amounts of Pb. The samples from Nattivit show a clear enrichment in Sn, and trace amounts of Sr, Nb, Ta and Pb. The single sample from Ujarassuit Nunaa contains 0.2 ppm (weight) Pb. These observations, but mainly the data on the most common trace elements (Table 4 and Figure 4) shows that individual Greenlandic ruby occurrences can be distinguished from each other, thus even though all deposits are related to ultramafic rocks, their trace element signatures are not identical.

4.2.2 Oxygen isotopes

Oxygen isotope ratios are a helpful parameter to characterise rubies, even though the method applied in this study is destructive for the ruby sample and therefore not readily can be applied on cut and polished gemstones. The $\delta^{18}O$ values for the FC vary between 1.62 and 4.20‰, which is on the lower side of the previously reported range of $\delta^{18}O$ values for mafic-ultramafic rocks (3-7‰, Giuliani *et al.* (2007), Figure 7). This is in good agreement with the geological setting of the FC rubies – as they are derived from a metasomatic reaction between a leucogabbro-anorthosite and an ultramafic rock. Low $\delta^{18}O$ values for the FC also fit with the proposed metamorphic scenario, where Al is derived from mafic rocks (leucogabbro-anorthosite), rather than from the felsic pegmatites, which generally gives higher $\delta^{18}O$ values (above 9‰; Guiliani *et al.* 2005, 2007).

The measured values for $\delta^{18}O$ values (1.62-4.20‰) for the FC and Nattivit (2.41‰) are low compared to most other investigated deposits (see Figure 7), with the exception of the negative isotope values found in Karelian, Russia deposits affected by glacial melting water (Vyotskiy *et al.* 2015). Apart from the Karelian deposits metamorphosed with glacial meltwater, very low values ($\delta^{18}O \leq 3$‰) are nearly diagnostic for the FC rubies – worldwide only rubies from Madagascar (Andilamena, Ilakaka, Soamiakatra, Iankaroka, Ambatomena) have lower or similar reported $\delta^{18}O$ ratios. Those deposits in Madagascar are partly related to rocks with a similar history to the FC: cordieritites and pyroxenites; the other deposits are placer deposits of unknown primary origin (Giuliani *et al.* 2007). Rubies from Tanzania with trace elements overlapping the FC (Winza, Umba, Seza Kofi and Longido) all have $\delta^{18}O >$ 5‰ (Table 6; Keulen *et al.* 2014a). Rubies from Pailin and Macquarie River have a $\delta^{18}O$ of around 5‰ (Giuliani *et al.* 2005, Sutherland *et al.* 2009).

Herd *et al.* (1969) described the sample from Maniitsoq NW as sapphirine-bearing hornblendite. Hornblendites are a rock type that fall in the category mafic-ultramafic rocks. However, this sample from Maniitsoq has a $\delta^{18}O$ value of 10‰, indicative of a high fluid activity, possibly caused by desilicification of a pegmatite in contact with the ultramafic rock.

4.2.3 Optical features and inclusions

One of the most notable features observed with the optical microscope is the presence of brown amphibole inclusions in the samples (Figure 8B). Even though no Raman analyses have been performed on inclusions, it is most probably that this brown amphibole is anthophyllite. Anthophyllite has been observed as mineral inclusion in the FC rubies with the SEM and in hand specimen collected in complex. Apart from brown amphibole, the green and black amphiboles pargasite and gedrite have been observed in rubies from Aappaluttoq; paragasite was also reported as a mineral inclusion in ruby by Smith *et al.* (2016). Amphiboles, and especially the reddish brown anthophyllite in the FC samples, are relatively rare mineral inclusions in international ruby deposits. Green or black amphibole inclusions are known from mafic-ultramafic host-rock derived deposits in, among others, Montepuez, Mozambique, Longido, Msinji & Winza, Tanzania and several places in Madagascar (Gübelin and Koivula 2008). Green-black pargasite is noted rarely as well in the marble-hosted rubies from Mogok, Myanmar and the Hunza Valley, Pakistan, but anthophyllite inclusions are not described in the very comprehensive atlas of Gübelin and Koivula (2008).

Similarly, phlogopite occurred as inclusions in many FC samples (Figure 8A). It is usually tabular-shaped and reddish brown in colour; but, near-black phlogopite was also observed. Similar reddish brown phlogopite inclusions were e.g. observed in samples collected in Luc Yen, Vietnam, Mogok, Myanmar, Tanzania, (Gübelin and Koivula 2008); Chimwadzulu, Malawi (Smith 2014); and the Hunza Valley, Pakistan (Gübelin 1982).

Rutile is the most common mineral inclusion in natural rubies and it is common in the FC samples as well, as individual grains (Figure 8C), in needles, as silk (compare also to Smith *et al.* 2016) and possibly in tubules. Cross-hatching of rutile was described from rubies derived from other areas; however, it was not observed in the investigated FC rubies.
Optical investigations show small aggregates of minerals, most likely zircon, but possibly anorthite, in several rubies from the FC. The presence of both minerals as inclusions in rubies was confirmed by SEM investigations (Figure 9). Similar clouds of fine-grained zircon have been described for rubies from Mangari, Kenya (Smith 2014), but anorthite has only been described as an inclusion mineral for rubies from Ruyil, Nepal (Gübelin and Koivula, 2008). Smith *et al.* (2016) additionally indicate inclusions of talc.

Straight growth zones with angular intersections, slight colour variations due to minor trace element ratio variations and crosscutting net-shaped rutile needles are all features that are indicative of a naturally grown ruby. Growth patterns like those shown in Figure 8D are known from a small range of deposits like Monghsu, Myanmar (Smith 2014), Umba Valley, Tanzania and Vatomandry, Madagascar (Gübelin and Koivula, 2008). The growth zonations are not visible in the colour or trace element distribution; both are relatively constant within one ruby grain. Similarly, negative crystals are commonly observed in e.g. Mangari, Kenya (Smith 2014), in Mogok, in various magmatic rubies like Bo Rai and Chantaburi, Thailand, and in Sri Lankan rubies (Gübelin and Koivula, 2008) and Smith *et al.* (2016) also mention them for the FC. Streams, flakes, milky zones (Figure 8E) and zonal clouds consisting of finely dispersed material were observed in those rubies. Zonal clouds are reported for rubies from Mangari, Kenya, while milky zones more commonly occur in, e.g. Vietnamese ruby deposits (Smith

2014). Fluid inclusions and fluid-solid multi-phase inclusions (Figure 8F) are interesting features that allow studying the geological conditions during the entrapment of the fluids and/or solids. Secondary tubing, and feathering from boehmite needles (Figure 8G and Figure 8H) were also observed in samples from Mogok, Myanmar (GRS 2015), but is only rarely seen in FC rubies (see also Smith *et al.* 2016).

Mineral inclusions and other internal features of rubies are helpful in characterising their origin. However, for a reliable geographic ‘fingerprinting’, a range of features needs to be examined. Especially larger mineral inclusions, will, however, commonly be missing in the case of gem-quality samples. Mineral inclusions of reddish-brown anthophyllite are – on a worldwide scale – fairly uncommon in gem-quality ruby, as only a few amphibole-bearing localities globally are producing gem-quality stones, and the amphiboles from these localities frequently are a greenish or black variety. Similarly, phlogopite is globally not a very common mineral inclusion in rubies, although the former mineral occurs more abundantly than anthophyllite. As both anthophyllite and phlogopite are rather common inclusions in the FC rubies, they are important indicators for a FC origin. Additionally, growth patterns, dispersed clouds of small zircon grains, zonal clouds and milky zones are distinguishing features for the FC rubies.

Optical features and inclusions from the FC most strongly overlap with Mogok (Myanmar), Hunza (Pakistan) and Mangari (Kenya). In the latter deposits, rubies are found associated with small ultramafic bodies enclosed by graphite-bearing aluminous metasediments (Mercier *et al.* 1999), while the other two are hosted by marbles.

4.3 Fingerprint of Greenlandic rubies

The distinguishing features for the Greenlandic rubies are summarised in Table 14. Trace element ratios vary considerably among the individual deposits; however, all investigated ruby samples are rich in Fe and poor in Ga and V. Aappaluttoq, FC and Kangerdluarssuk, Maniitsoq, have more Cr than Fe; and Kangerdluarssuk, Maniitsoq NW and Kapisillit have a considerable concentration of the trace element Ti. Aappaluttoq has an average Cr concentration of 9275 ppm (weight); such high values are fairly unique. Only one of the samples from Mogok, Myanmar, one from Mongshu, Myanmar and one from Morogoro, Tanzania reached similar concentrations. These three areas all contain rubies in a marble setting, which, in combination with trace elements, easily can be separated from Aappaluttoq or the FC. Where applying combinations of trace elements in relative or absolute diagrams (Figure 4 and Figure 6) Aappaluttoq shows an overlap with especially Umba, Seza Kofi, Longido, Andilamena, Pailin, Cudgegong-Gulgong, Macquarie River. However, all these deposits have $\delta^{18}O$ values slightly higher (5‰ or more) than Aappaluttoq and the FC (4‰ and 3‰, respectively). As long as enough distinguishing optical features can be found in gem-quality stones, Aappaluttoq and rubies from the FC are well-separable from other deposits by their optical characteristics and typical mineral inclusions. Especially calcium-amphiboles, zircons, sapphirine and anorthite are uncommon mineral inclusions in other deposits, which combined with the presence of e.g. growth zonation, negative crystals, milky zones, zonal clouds or rutile and boehmite needles would be indicative for an origin from Aappaluttoq and the FC.

Rubies from Aappaluttoq and the FC are most strongly overlapping with other ultramafic-mafic ruby deposits. In these, the same trace elements are available during the metasomatism, the same minerals are available during metamorphism and the resulting rubies are likely to have low $\delta^{18}O$ values. However, the FC, including Aappaluttoq, is one of the few deposits where anorthosite or leucogabbro form the mafic component in the reaction, or where the ultramafic rock is Archaean, and therefore enriched in Mg and Cr. Also the pegmatite triggering the metamorphic reaction is Archaean (Keulen *et al.* 2014b), however, this is mainly of value for geological purposes rather than gemmological studies – probably only non-gem “rubies” will include zircons large enough to be dated by U/Pb isotopes. However, this age for the ruby-formation is, to our knowledge, not described outside Greenland.

Although we compare with a large number of international samples in this study, both by own analyses and literature data, still a considerable number of ruby deposits are not included in this study. Thus, as long as not all deposits are studied, our fingerprinting results are not ultimately conclusive.

Smith *et al.* (2016) wrote in their paper that we (Keulen and Kalvig 2013) analysed opaque material in our preliminary origin study. This remark is incorrect. Since raw material rather than polished grains were used for the analyses – both in that study and in this work – the gemmological quality of the individual grains is hard to assess. Therefore, we cannot guarantee that all investigated grains were of top gem-quality. Nevertheless, we concentrated our investigations on the best samples, which were transparent or in cases translucent, and covered the colour range between pale pink and fine red. To analyse opaque, hence heavily included, samples in a trace element study does not, in our opinion, make sense.

In Figure 31 we compare the results of our work to literature data on Aappaluttoq (Kalvig and Frei 2010; Smith *et al.* 2016) and on the entire FC. There is a good overlap in the analytical results for the three studies, therefore Smith *et al.* (2016)’s concern that our (Keulen and Kalvig 2013) geographical origin study results would not compare well to high-quality stones is unjustified. As samples are separated in “best” samples for expectedly high-quality gem-material and a second group of good quality material, our results are also useful for more geologically oriented studies in which a large focus rests on the entire range of possible values (see Figure 4 and Figure 31).

Table 14. *Overview of the distinctive features for Greenlandic rubies. Mineral abbreviations after Kretz (1983). * = None observed with LA-ICP-MS; apart from minor Mn in very few samples. n.i. = not investigated.*

Area	Ti	V	Cr	Fe	Ga	Less common trace elements	$\delta^{18}O$	common inclusion minrls.	optical features
Aappaluttoq	67.57	55.75	9275	2403	31.79	None*	4.2	bt, Cam, rt, zrc,sp, spr, an	growth zonation, negative crystals, rutile & boehmite needles, milky zones, zonal clouds
Fiskenæsset	89.96	35.15	4343	2619	23.88	None*	3.0	bt, Cam, rt, zrc,sp, als, an	growth zonation, negative crystals, rutile & boehmite needles, milky zones, zonal clouds
Maniitsoq NW	551	77.6	1090	1674	51.11	Nb = 0.5; Ta = 5	10.03	rutile; n.i.	not investigated
Kangerdluarssuk	311.1	49.19	2090	1327	33.71	Nb = 0.07, Ta = 0.2; Pb = 0.03	n.i	rutile; n.i.	not investigated
Kapisilit	208.9	85.56	150.4	7606	40.54	None	4.52	not investigated	not investigated
Storø	255	83.36	1391	1773	61.53	None	6.0	not investigated	not investigated
Ujarassuit Nunaa	15.44	0.999	1233	2909	18.11	Pb=0.2	n.i	not investigated	not investigated
Tasiiliaq	176.4	3.107	7.49	9282	39.71	Mn=10; Nb=0.8;Sn=5; Ce=0.4; Ta=0.1; Pb=0.5	n.i	not investigated	not investigated
Nattivit	72.65	7.421	315	1679	38.97	Sr=0.1; Nb=0.1;Sn=91; Ta=0.6; Pb=0.5	2.41	not investigated	not investigated

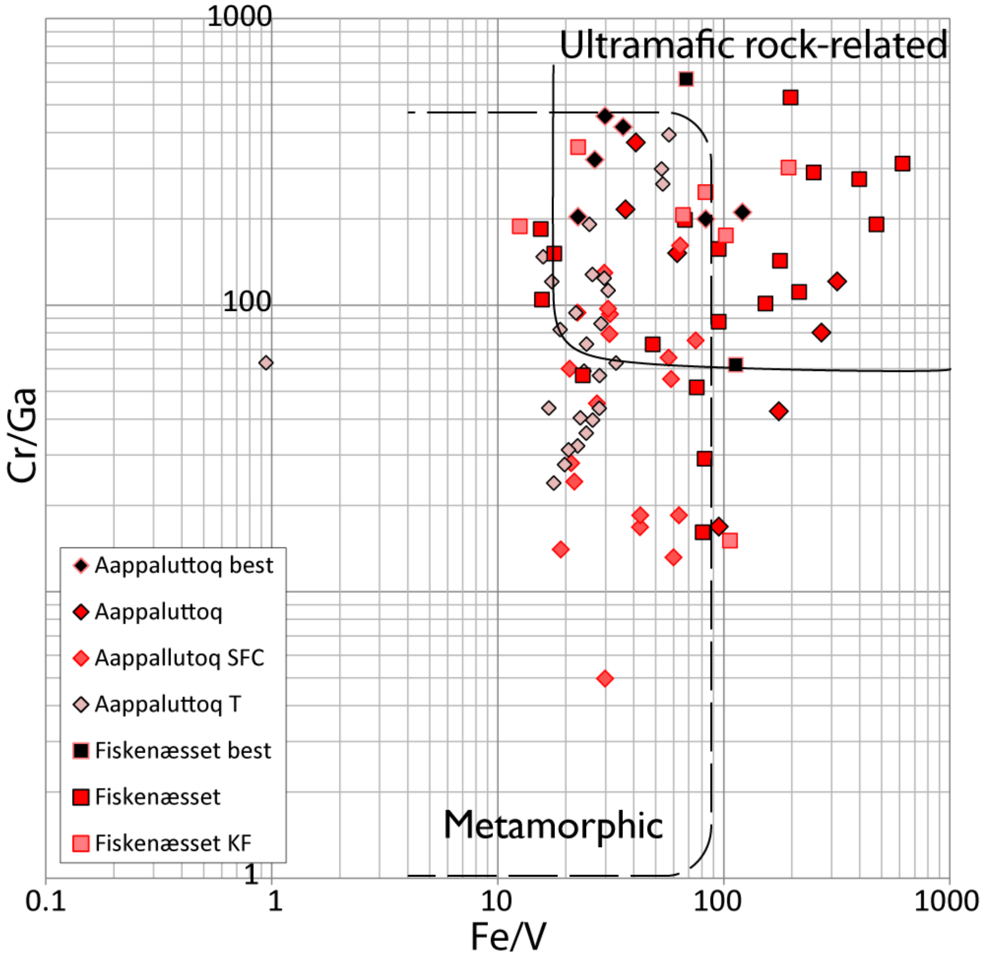

Figure 31. *Cr/Ga vs Fe/v plot for the trace element geochemical data of the Fiskenæsset complex collected in this study compared to earlier observations. The data is compared to typical data ranges for ultramafic rock-related rubies (solid line) and metamorphic-rock hosted rubies (dashed line). SFC = Smith* et al. *(2016), T = Thirangoon (2008), KF = Kalvig and Frei (2010).*

4.4 Other fingerprinting methods

4.4.1 µXRF compared to LA-ICP-MS

The LA-ICP-MS method has some difficulty, when measuring the light elements such as Mg and Si, which can influence the accuracy for the concentrations. However, the difference between the standards and the ICP-MS analyses is small compared to the differences between µXRF and LA-ICP-MS for these elements. When plotting the elements for the methods µXRF and LA-ICP-MS there are some differences in the measured concentration of the elements. The differences could be real, if the points analysed by the two methods are not entirely overlapping, but most likely the differences are due to a too low accuracy of the elemental concentrations for each measurements for at least one of the methods applied.

The difference in results between the two methods is large (see *Table 9* and *Table 10*). As the results for the LA-ICP-MS can be compared to the standards and known unknowns that were measured together with the samples, we know that the LA-ICP-MS analyses only have a small error in accuracy and are rather precise. Therefore, the quality of the µXRF analyses is too low to be able to use as a fingerprinting tool. It has been investigated whether a correction factor could be applied to correct the µXRF data. However, the scatter in the µXRF data is too large to be able to do this reliably.

4.4.2 LIBS compared to LA-ICP-MS

After the pilot study, the quality of the LIBS data was not good enough to measure concentrations of the individual trace elements. Therefore, the method does, at the moment, not form a substitution for LA-ICP-MS. The method is however interesting as a supplement to LA-ICP-MS analyses, as elements that cannot be detected easily with LA-ICP-MS were detected with LIBS; e.g. Na, Ca, Zr. Especially the presence of the latter element in the FC samples is interesting to note. A positive signal for Zr was also detected with µXRF, but it was uncertain whether the Zr came from the sample or was an artefact created by a signal from within the µXRF-instrument.

4.4.3 Raman and fluorescence

Raman and fluorescence spectrometry are only able to record that the rubies from FC are rubies and no other types of minerals. Due to the high contents of Cr and low concentrations of other trace elements, no special spectrum lines were detected that could help to fingerprint the rubies. The methods are suitable to characterise mineral inclusions in the rubies, but have not been used to this goal during this study.

4.4.4 Multivariate statistics investigations

Samples 521101, 521105, 521106, and 521110 are the four samples mentioned in Keulen & Kalvig (2013) as the four most transparent and most intensively red-coloured samples from Aappaluttoq in the FC. Samples 521107 and 521113 were analysed subsequently in 2014, and especially sample 521107 is characterised by high chromium values (Keulen & Poulsen 2014). Therefore, it seems like the samples that are most significant and typical for Aappaluttoq (Figure 22) are the samples with the highest quality, and the samples that are most distinct from corundum from other localities. This fact will help in the fingerprinting of Aappaluttoq samples, as it shows that the high quality samples from Aappaluttoq have a specific geochemical signature.

However, the fact that these samples from Aappaluttoq overlap more strongly with samples from Longido (Tanzania), Winza (Tanzania), Chanthaburi (Thailand) and Ilalaka (Madagascar) than with other samples from some areas in the FC, and even with some of the samples from Aappaluttoq, indicates the need for further study of international samples from mafic-ultramafic occurrences. It might be possible that other localities exist, with a fingerprinting signature that is very similar to Aappaluttoq.

The best chance for separating the samples from Aappaluttoq versus the overlapping and similar international occurrences is, apart from this principle component analysis, a ternary diagram of Cr/Fe vs Si vs Ti/V/Ga or of Fe vs Cr/Si vs Ti/V/Ga (see Figure 5). These three groups define the axes of the principle component diagram (Figure 23).

It needs to be emphasized that the analysis of many samples, especially from the international occurrences, often is based on one or two values only and that limited literature with geochemical results exists. To obtain better and more certain results, the dataset needs to be extended with more analyses.

Ruby/sapphire samples from Storø show a strong overlap in their geochemical signature with samples from Jaipur-Mysore (India), John Saul mine (Kenya), Mong Hsu (Myanmar), Sahambano (Madagascar), and Soamiakatra (Madagascar). With a further investigation of the higher order components (PC3, PC4 etc.) these samples can possibly be separated out. Mong Hsu and John Saul mine have for example much higher $\delta^{18}O$ values than the other samples, Sambano has low Ti concentrations, while Soamiakatra is much richer in iron than the other samples. The ruby/sapphire samples from Maniitsoq have a unique position in the principal component plot. Their most significant neighbours are the sample from Tsavo, and the sample from Sri Lanka that might originate from Pelmadulla.

4.4.5 Discussion of the blind test

The main aim of the test was to see, whether a sample from Aappaluttoq could be recognised by its geochemical characteristics. The test is skewed, as the student Asta F. Jørgensen could reasonably expect that at least one of the samples was from Aappaluttoq, as she was briefly informed about the aim of the ruby project. Furthermore, the GEUS database contains a large set of samples from Aappaluttoq, thus this location is better defined than all other localities. The student only used ternary diagrams for the fingerprinting of the rubies and concentrated her work on only four different ternary diagrams.

Nevertheless, she was able to recognise a sample from Aappaluttoq as being derived from Aappaluttoq, and a second sample from the FC, was also attributed to Aappaluttoq, but with a lesser certainty, and her other options for this sample include many localities within the FC. She also recognised the sample from Pailin correctly, even though only a few ruby and pink sapphire samples from this area are contained in the data set.

Unknown-2 was not fingerprinted correctly. This ruby sample from Storø has a large overlap with the sapphire sample from Storø, a fact that was not recognised by the student. This overlap is hard to detect from ternary diagrams that include Fe and Cr, as these two trace elements are not the same for the ruby and sapphire samples. The unknown-2 sample overlapped as well with samples from the FC in the Fe-Cr-Ga and Fe-Ga-Si diagrams, but not in Ti-Ga-Cr, Fe-Cr-Ti- and Ti-Cr-V diagrams, and should therefore not be confused with the FC.

5. Summary and conclusions

Ruby formation in the FC, including Aappaluttoq results from a metasomatic reaction of anorthite-rich rocks (anorthosite and leucogabbro) and ultramafic rocks, triggered by the intrusion of pegmatites shortly after peak metamorphic conditions (ca. 640°C and 7 kbar; 2.72-2.70 Ga). The anorthite component of the plagioclase is the source for the aluminium and oxygen in the rubies, while important trace elements, including Cr, are derived from the Archaean ultramafic rocks. Cr is mobile at high pH-levels (hexavalent) at roughly 600°C. The pegmatites, which react with the ultramafic rock, cause the formation of Ca-rich amphiboles (anthophyllite, pargasite, gedrite) and biotite in the reaction zone; they are however, not the source of the Al in the ruby. The presence of pegmatite with a special composition (halide anion- and/or K-enriched), ultramafic rocks and anorthosite-rich rocks define, together with the correct pressure and temperature conditions, whether the ruby-forming reaction will take place in ruby-bearing ultramafic complexes.

The most suitable trace elements to define the origin of the FC rubies (including Aappaluttoq) are Cr, Ga, V, Fe, and Ti. Rubies from the FC yield high Cr, intermediate Fe, rather low V, and low Ga and Ti concentrations compared to abundances in rubies from international deposits. In addition, Mg, Si, Ca, Na, Ba, Zr, K and Sr are common trace element in FC rubies. Values for Aappaluttoq agree well with previous studies and compare well to other high-quality localities in the FC. There is an overlap in trace element composition with some other samples derived from similar outcrops with ruby-bearing ultramafic complexes such as Umba, Seza Kofi and Longido, and with the placer deposit derived of possibly the same primary rocks like Andilamena (Madagascar), and also to a lesser degree with the several metamorphic basaltic samples of Bo Rai, Pailin, Cudgegong-Gulgong and Macquarie River. Here, we developed two novel plots to separate different groups of geological environments with ruby-formation: Ga/V vs Fe/Ti and Cr/Ga vs Fe/V diagrams. These diagrams focus on the most abundant, most commonly applied, and mutually independent trace elements Ga, V, Fe, Cr and Ti, and add to the tools to be better able to separate individual deposits. Rubies from other Greenland localities near Maniitsoq are slightly enriched in Ta, Nb and locally Pb, while those from the Tasiilaq area are relatively enriched in Sn, Sr, Nb, Ta and Pb, but show lower Cr/Ga values than FC ruby samples.

The obtained $\delta^{18}O$ values (1.62-4.20‰) for the FC and Nattivit area are low compared to most other analysed deposits outside Karelia (NW Russia) and Madagascar. While glacial melt water during metamorphism creates uniquely low $\delta^{18}O$ values in Russia, the Madagascan rubies are expected to share a similar geological history. Rubies from other ultramafic rock complexes including Tanzania (Winza, Tunduru, and Songea), and Kapisillit, Greenland, as well as samples derived from xenoliths in basalts display slightly higher $\delta^{18}O$ values.

The investigation of optical features and inclusions was limited to the FC, including Aappaluttoq. For these rubies typical features include growth zonation, negative crystals, rutile and boehmite needles, milky zones, and zonal clouds combined with the typical mineral inclusions biotite, Ca-rich amphiboles (anthophyllite, pargasite), rutile, zircon, spinel, sapphirine, and anorthite. While rutile is a very common inclusion mineral, and biotite and spinel occur frequently, the other minerals are rarer. The combined presence of several inclusion minerals and other optical features is required for a successful fingerprinting.

For the most beneficial fingerprinting, the three described fingerprinting techniques (trace elements, oxygen isotopes, optical features) should be combined. The three methods are – up to a certain degree – independent of each other, which enhance the chance of a unique fingerprint, when compared to applying only one of the methods. However, as all methods are to a varying degree dependent on the geological setting of the ruby-forming mineral reaction, overlap is mainly expected with rubies from similar geological settings. As the geological history of the FC is relatively unique – only few other anorthosite-ultramafic rock complexes metamorphosed at granulite-upper amphibolite facies yield high-quality rubies – fingerprinting of these Greenlandic rubies is possible with only few possibilities for overlapping localities. For rubies from the other Greenlandic localities, more investigations are needed, especially with a focus on their optical features. However, also for these localities less-typical trace element compositions and oxygen isotope values are observed.

µXRF and LIBS cannot be used as independent fingerprinting methods, as the quality of their trace element data is not sufficient. However, both methods are interesting as a supplement to the LA-ICP-MS methods, as they can reveal the presence of elements that else are not or hard to measure precisely with LA-ICP-MS. For rubies derived from areas with zoned rubies, µXRF mapping of rubies might serve as a valid fingerprinting tool.

Traditionally, fingerprinting efforts are mainly directed at investigating the country of origin for a deposit, as the country to a higher degree than the locality of the individual deposit, defines the value of their rubies. However, within a single country, including Greenland, due to differences in the geological history of the rocks, large differences in fingerprinting characteristics between different deposits may exist, even when the deposits have a similar generic history. This is exemplified by the Greenlandic ruby occurrences where all ruby occurrences in Greenland are associated with ultramafic rocks; however, each has its own trace element signature and shows variation in $\delta^{18}O$-values. This is not an atypical feature, as differences are even larger among deposits in other countries like Madagascar, Tanzania or Vietnam.

Overview of the appendices

A. Field report on collection of samples in the FC in 2011 (in Danish).
B. Article published in the Review of the Surveys Activities, 2013.
C. Whole-rock geochemistry data for samples from the FC.
D. Chondrite-normalized plot of rare-earth element analyses from ruby-bearing and related rocks.

Acknowledgements

This project has been financed by the Ministry of Mineral Resources (now: the Ministry of Mineral Resources, Labour and the Interior) of the Government of Greenland, the Geological Survey of Denmark and Greenland and Geocenter Danmark (Bevilling SASMIN 01/2010). The authors wish to thank K. Bauer for help with the oxygen isotope analyses and M. Smit for assistance in setting up the electron microprobe analyses. F.F. Aguilera, M. Alaei, O. Nielsen, T. Hvenegaard, and M. Nielsen helped with the sample preparation. A.F. Jørgensen, and S.H. Serre performed part of the LA-ICP-MS analyses. The authors would like to thank I.T. Olsen, S.Wennick, and J.Blomsterberg for sharing samples with us. J.B. Jønsson is kindly thanked for assistance during the sample collection in Tanzania. H. Stendal and A. Juul-Nielsen participated in part of the sample collection in the FC, other samples were borrowed from the GEUS archive.

References

Appel CC, Appel PWU, Rollinson HR (2002) Complex chromite textures reveal the history of an early Archaean layered ultramafic body in West Greenland. Mineral Mag 66:1029–1041

Appel PWU, Ghisler M (2014) Ruby- and sapphirine-bearing mineral occurrences in the Fiskenæsset, Nuuk and Maniitsoq Regions, West Greenland. Danmarks og Grønlands Geologiske Undersøgelse Rapport 2014/72, 71pp

Beckhoff, B., Kanngießer, B., Langhoff, N., Wedell, R. (eds.) 2006 Handbook of practical X-Ray Fluorenscence Analysis. 44p.

Bøggild OB (1953) The mineralogy of Greenland. Meddelelser om Grønland 149(3), 442 pp

Calligaro T, Poirot J-P, Querré G (1999) Trace element fingerprinting of jewellery rubies by external beam PIXE. Nuclear Instruments Methods in Physics Res B 150:628-634.

Connolly J. (2005) Computation of phase equilibria by linear programming: a tool for geodynamic modeling and its application to subduction zone decarbonation. Earth Planet Sci Lett, 236: 524–541

Calvo del Castillo H, Deprez N, Dupuis T, Mathis F, Deneckere A, Vandenabeele P, Calderón T, and Strivay D (2009) Towards the differentiation of non-treated and treated corundum minerals by ion-beam-induced luminescence and other complementary techniques. Anal Bioanal Chem 394:1043–1058

Emmett JL, Scarratt K, McClure SF, Moses T, Douthit TR, Hughes R, Novak S, Shigley JE, Wang W, Bordelon O, Kane RE (2003) Beryllium diffusion of ruby and sapphire. Gems & Gemology 39: 84-135

Evans BW, Frost BR (1975) Chrome-spinel in progressive metamorphism—a preliminary analysis. Geochim Cosmochim Acta 39:959–972

Friend CRL, Nutman AP (2001) U–Pb zircon study of tectonically-bounded blocks of 2940–2840 Ma crust with different metamorphic histories, Paamiut region, South-West Greenland: implications for the tectonic assembly of the North Atlantic craton. Precamb Res 105:143–164

Garde AA, Marker M (1988) Corundum crystals with blue-red colour zoning near Kangerdluarssuk, Sukkertoppen district, West Greenland. Rapport Grønlands Geologiske Undersøgelser 140:46—49

Gemval 2014: GEMVAL reference values of gemstones. www.gemval.com/color_grade.html, Retrieved 25th April 2017

Giuliani G, Fallick AE, Garnier V, France-Lanord C, Ohnenstetter D, Schwarz D (2005) Oxygen isotope composition as a tracer for the origins of rubies and sapphires. Geology 33: 249-252

Giuliani G, Fallick AE, Rakotondrazafy M, Ohnenstetter D, Andriamamonjy A, Ralantoarison T, Rakotosamizanany S, Razanatseheno M, Offant Y, Garnier V, Dunaigre C, Schwarz D, Mercier A, Ratrimo V, Ralison B (2007) Oxygen isotope systematics of gem corundum deposits in Madagascar: relevance for their geological origin. Mineral Dep 42:251-270

GRS (2015) Gemresearch Swisslab Inclusion Gallery. http://gemresearch.ch/inclusion-gallery/. Retrieved October 2015.

Gübelin EJ (1982) Gemstone of Pakistan, emerald, ruby and spinel. Gems & Gemology 18:123-139

Gübelin EJ, Koivula JI (2008) Photoatlas of Inclusions in gemstone, V3. Opinio Publishers, Basel, Switzerland, 672pp.

Guilong M, Günther D (2001) Quasi 'non-destructive' laser ablation-inductively coupled plasma-mass spectrometry fingerprinting of sapphires. Spectrochim Acta B 56:1219-1231

Harlow GE, Bender W (2013) A study of ruby (corundum) compositions from the Mogok Belt, Myanmar: Searching for chemical fingerprints. Am Mineral 98:1120–1132

Hellstrom J, Paton C, Woodhead J, Hergt J (2008) Iolite: Software for spatially resolved LA-(quad and MC) ICPMS analysis. In: Sylvester P (ed) Laser Ablation ICP–MS in the Earth Sciences: Current Practices and Outstanding Issues, Mineral. Assoc. of Canada, Quebec, Canada, 343–348

Herd RK, Windley BF, Ghisler M (1969) The mode of occurrence and petrogenisesis of the sapphirine-bearing and associated rocks of West Greenland. Rapport Grønlands Geologiske Undersøgelse 24, 44pp.

Hutchison MT, Nixon PH, Harley SL (2004) Corundum inclusions in diamonds—discriminatory criteria and a corundum compositional dataset. Lithos 77:273 – 286, doi:10.1016/j.lithos.2004.04.006

Jørgensen, A.F., 2014: Fingerprinting of red corundum from the Fiskenæsset complex. Report for GEUS as part of an MSc Thesis, unpublished, 18 pp.

Kalvig P, Frei D (2010) Testing the use of geochemical characteristics of corundum from Greenland as a tool for geographical typing. Danmarks og Grønlands Geologiske Undersøgelse Rapport 2010/68, 36pp

Kasemann S, Meixner A, Rocholl A, Vennemann T, Schmitt A, Wiedenbeck M (2001) Boron and oxygen isotope composition of certified reference materials NIST SRM 610/612, and reference materials JB-2G and JR-2G. Geostandards Newsletter 25:405-416

Keulen N, Kalvig P (2013) Fingerprinting of corundum (ruby) from Fiskenæsset, West Greenland. Geol. Surv. Den. Greenl. Bull. 28:57–60, Open access:www.geus.dk/publications/bull

Keulen N, Kalvig P, Thomsen TB, Kokfelt TF, Vennemann T, Jønsson JB (2014a) Determination of the origin of corundum (ruby and sapphire) from Tanzania by geochemical fingerprinting. 31st Nordic Geol Winter Meet Lund, Sweden p9

Keulen N, Næraa T, Kokfelt TF, Schumacher JC, Scherstén A (2010) Zircon record of the igneous and metamorphic history of the Fiskenæsset anorthosite complex in southern West Greenland. In: Bennike O, Garde AA, Watt WS (eds) Review of Survey Activities 2009. Geol Surv Den Greenl Bull 20:67–70. Open access:www.geus.dk/publications/bull

Keulen N, Schumacher JC, Næraa T, Kokfelt TF, Scherstén A, Szilas K, van Hinsberg VJ, Schlatter DM, Windley BF (2014b) Meso- and Neoarchaean geological history of the Bjørnesund and Ravns Storø Supracrustal Belts, southern West Greenland: settings for gold enrichment and corundum formation. Precamb Res 254:36-58

Kochelek KA, McMillan NJ, McManus CE, Daniel DL (2015) Provenance determination of sapphires and rubies using laser-induced breakdown spectroscopy and multivariate analysis. Am Mineral 100:1921-1931; DOI: 10.2138/am-2015-5185

Kohonen, T., 2001: Self-Organizing Maps. Springer, Heidelberg, 371pp.

Kokfelt TF, Keulen N, Næraa T, Scherstén A, Heijboer T (2011) New zircon U/Pb-age data from the Archaean craton, South-West and southern West Greenland(61◦30’N–64◦00’N). Geophys Res Abstr 13 (EGU2011-14038), 2 pp

Kretz R (1983) Symbols for rock-forming minerals. Am Mineral 68:277-279

Ludwig KR (2003) Isoplot/Ex 3.00. A Geochronological Toolkit for Microsoft Excel, Berkeley Geochronological Center Spec Publ 4, Berkely

McGregor VM, Friend CRL (1992) Late Archean prograde amphibolite to granulite-facies relations in the Fiskenæsset region, Southern West Greenland. J Geol 100:207–219

Meija J, Coplen TB, Berglund M, Brand WA et al. (2016) Atomic weights of the elements 2013 (IUPAC Technical Report). Pure Appl Chem 88:265–291

Mercier A, Debat P, Saul JM (1999) Exotic origin of the ruby deposits of the Mangari area in SE Kenya. Ore Geol Rev 14:83-104

Myers JS (1985) Stratigraphy and structure of the Fiskenæsset Complex, southern West Greenland. Bull. Grønl. Geol. Unders. 150, 72 pp

Nassau K (1983) The physics and chemistry of color: the fifteen causes of color. John Wiley and Son, New York, 454 pp

Paton C, Hellstrom J, Paul B, Woodhead J, Hergt J (2011) Iolite: Freeware for the visualistation and processing of mass spectrometric data. J Anal At Spectrom 26:2508-2518

Peucat JJ, Ruffault P, Fritsch E, Bouhnik-Le Coz M, Simonet C, Lasnier B (2007) Ga/Mg ratio as a new geochemical tool to differentiate magmatic from metamorphic blue sapphires. Lithos 98:261-274

Polat A, Appel PWU, Fryer B, Windley B, Frei R, Samson IM, Huang H (2009) Trace element systematics of the Neoarchean Fiskenæsset anorthosite complex and associated metavolcanic rocks SW Greenland: evidence for a magmatic arc origin. Precamb Res 175:87–115

Polat A, Frei R, Scherstén A, Appel PWU (2010) New age (ca. 2970 Ma), mantle source composition and geodynamic constraints on the Archean Fiskenæsset anorthosite complex, SW Greenland. Chem Geol 277:1–20

Pornwilard MM, Hansawek R, Shiowatana J, Siripinyanond A (2011) Geo-graphical origin classification of gem corundum using elemental fingerprint analysis by laser ablation inductively coupled plasma mass spectrometry. Int J Mass Spectr 306:57– 62

Porto, S.P.S. & Krishnan, R.S. (1967). Raman Effect of Corundum. The Journal of Chemical Physics 47(3), 1009-1012.

Poulsen MD, Paulick H, Rosa D, van Hinsberg VJ, Petersen J & Thomsen LL (2015) Follow-up on Ujarassiorit mineral hunt finds and outreach activities, South-East Greenland. In: Bennike O, Garde AA & Watt WS(eds) Review of Survey Activities 2014. Geological Survey of Denmark and Greenland Bulletin 33:53-56

Rakontondrazafy AFM, Giuliani G, Ohnenstetter D, Fallick AE, Rakotosamizanany S, Andriamamojy A, Ralantoarison T, Razanatseheno M, Offant Y, Garnier V, Maluski H, Dunaigre C, Schwarz D, Ratrimo V (2008) Gem corundum deposits of Madagascar: A review. Ore Geol Rev 34:134–154

Rossman, GR (2009) The Geochemistry of Gems and Its Relevance to Gemology: Different Traces, Different Prices. Elements DOI: 10.2113/gselements.5.3.159, 4pp.

Rumble D III, Hoering TC (1994) Analysis of oxygen and sulfur isotope ratios in oxide and sulfide minerals by spot heating with a carbon dioxide laser in a fluorine atmosphere. Acc Chem Res 27:237-241

Saminpanya S, Manning DAC, Droop GTR Henderson CMB (2003) Trace elements in Thai gem corundums. J Gemmol 28:399–415

Scholz, M., 2006: Approaches to analyse and interpret biological profile data. PhD Thesis Max-Planck-Institut für Molekulare Pflanzenphysiologie, Potsdam, Germany. 93pp.

Schumacher JC, van Hinsberg VJ, Keulen N (2011) Metamorphism in supracrustal and ultramafic rocks in southern West Greenland and South-West Greenland 64–61.5◦N. Danmarks og Grønlands Geologiske Undersøgelse Rapp 2011/06, 29 pp

Schwarz D, Pardieu V, Saul JM, Schmetzer K, Laurs BM, Giuliani G, Klemm L, Malsy AK, Erel E, Hauzenberger C, Du Toit G, Fallick AE & Ohnenstetter D (2008) Rubies & Sapphires from Winza, central Tanzania. Gems & Gemmol 44:322–347

Sharp ZD (1990) A laser-based microanalytical method for the in-situ determination of oxygen isotope ratios of silicates and oxides: Geochim et Cosmochim Acta 54:1353-1357

Simonet C, Fritsch E, Lasnier B (2008) A classification of gem corundum deposits aimed towards gem exploration. Ore Geol Rev 34:127–133

Siivola J, Schmid R (2007) List of mineral abbreviations. Recommendations by the IUGS Subcommision on the Systematics of Metamorphic Rocks: Web version 01.02.07. http://www.bgs.ac.uk/scmr/docs/papers/paper_12.pdf, 14pp

Smith CP (2014) Ruby Sources, Chart issued by the American Gemological Laboratories (AGL)

Smith CP, Fagan AJ Clark B (2016) Ruby and Pink Sapphire from Aappaluttoq, Greenland. J Gemmol 35:294–306, http://dx.doi.org/10.15506/JoG.2016.35.4.294

Sutherland FL Coenraads RR Schwarz D Raynor LD, Barron BJ & Webb GB (2003) Al-rich diopside in alluvial ruby and corundum-bearing xenoliths, Australian and SE Asian basalt fields. Mineral Mag 67:717–732

Sutherland FL Schwarz D, Jobbins EA, Coenraads RR, Webb G (1998) Distinctive gem corundum from discrete basalt fields: a comparative study of Barrington, Australia, and west Pailin, Cambodia, gem fields. J Gemmol 26:65–85

Sutherland FL, Zaw K, Meffre S, Giuliani G, Fallick AE, Graham IT & Webb GB (2009) Gem-corundum megacrysts from east Australian basalt fields: trace elements, oxygen isotopes and origins, Australian Journal of Earth Sciences, 56:7, 1003-1022, DOI: 10.1080/08120090903112109

Sutherland, FL, Zaw K, Meffre S, Yui T-F, Thu K (2015) Advances in Trace Element “Fingerprinting” of Gem Corundum, Ruby and Sapphire, Mogok Area, Myanmar. Minerals 2015, 5:61-79; doi:10.3390/min5010061

Sutherland FL Graham IT, Harris SJ, Coldham T, Powell W, Belousova EA Martin L (2017) Unusual ruby–sapphire transition in alluvial megacrysts, Cenozoic basaltic gem field, New England, New South Wales, Australia. Lithos 278-281

Szilas K, Hoffmann JE, Scherstén A, Rosing MT, Windley, BF, Kokfelt TF, Keulen NT, van Hinsberg VJ, Næraa, T, Frei R, Münker C (2012) Complexcalc-alkaline volcanism recorded in Mesoarchaean supracrustal belts north of Frederikshåb Isblink, southern West Greenland: implications for subduction zone processes in the early Earth. Precambrian Res. 208–211:90–123

Thirangoon K (2008) Ruby and Pink Sapphire from Aappaluttoq, Greenland – Status of on-going research. GIA Laboratory, Bangkok, http://www.gia.edu/research-resources/news-from-research/Greenland_corundum_03-23-09.pdf 18 pp

Van Gool JAM (2006) Ruby showings on Storø. Geological Survey of Greenland and Denmark (GEUS), Preliminary report with field notes and geologic map, 7 pp

Van Hinsberg VJ, Poulsen MD, Thomsen LL (2017) SEGMENT 2014 field report – Investigations of the metamorphic rocks in the Tasiilaq area. Geological Survey of Greenland and Denmark Report 2017/xx.

Venkateswaran, C.S. (1935). The Fluorescence of Ruby, Sapphire and Emerald. Proceedings of the Indian Academy of Sciences - Section A: Procedings Mathematical Sciences, 2(5), 459-465.

Vysotskiy SV, Nechaev VP, Kissin AY, Yakovenko VV, Ignat'ev AV, Velivetskaya TA, Sutherland FL, Agoshkov AI (2015) Oxygen isotopic composition as an indicator of ruby and sapphire origin: A review of Russian occurrences. Ore Geol Rev 68:164–170

Windley BF, Herd RK, Bowden AA (1973). The Fiskenæsset Complex, WestGreenland, Part 1: a preliminary study of the stratigraphy, petrology, and whole rock chemistry from Qeqertarssuatsiaq. Bull. Grønl. Geol. Unders. 106, 80 pp

Yakymchuk C, Szilas K (2017) Corundum formation by metasomatic reactions in Archean metapelite, southern West Greenland – Identification of exploration vectors for ruby deposits within high-grade greenstone belts. Geoscience Frontiers (in press) 24pp. doi:10.1016/j.gsf.2017.07.008

Zaw K, Sutherland L, Yui T-F, Meffre S, Thu K (2014) Vanadium-rich ruby and sapphire within Mogok Gemfield, Myanmar: implications for gem color and genesis. Miner. Deposita doi:10.1007/s00126-014-0545-0

Appendix A:

Field report on collection of samples in the FC in 2011 (in Danish).

4. Indsamling af rubinprøver fra området ved Fiskenæsset

4.1 Introduktion

Dette arbejde er tidligere afrapporteret i form af et GEUS-Notat til Råstofdirektoratet (RD) 11-MI-10-01, af 4. august 2011. Nedenfor er notatet gengivet, med enkelte redaktionelle ændringer og tilføjelser.

Som led i RD og GEUS' igangværende kapacitetsopbygning vedr. rubiner er der gennemført en fælles indsamling af prøver fra områder ved Qeqertarsuatsiaat. Indsamlingen blev gennemført med helikopter fra Nuuk til lokaliteterne den 29/7 og 31/7, 2011, af Henrik Stendal og Annette Clausen, RD, samt Per Kalvig, GEUS. Der blev givet prioritet til lokaliteter, hvorfra True North Gems (TNG) har indsamlet store prøver, samt til en lokalitet, som GEUS fandt i 2008, benævnt GEUS Bjørnesund 2008, som ligger uden for TNG's licensområde. I alt blev der besøgt 10 lokaliteter, hvoraf det dog kun lykkedes at finde rubiner på 8 af lokaliteterne.

Formålet med indsamlingen af prøverne er at lade dem indgå i tekniske undersøgelser af rubiner fra området, , som sigter på at udvikle metoder til karakterisering af rubiner, de såkaldte "fingeraftryk", for at kunne afgøre, om en rubin har sin oprindelse i Grønland. Især rubinernes kemiske sammensætning undersøges. Herudover undersøges sammensætningen af mikroskopiske indeslutninger i krystallerne. Prøverne skal bruges til at fremstille rubinkoncentrater fra lokaliteterne med henblik på en vurdering af stenenes egnethed som smykkesten (gemmologisk vurdering). Prøverne vil indgå i GEUS' prøvesamling for smykkesten i Grønland, som er under opbygning.

Siden slutningen af 1960'erne har geologer haft kendskab til, at der i området ved Qeqertarsuatsiaat findes mange forekomster af rubiner; der kendes i dag omkring 40 rubinlokaliteter af meget vekslende kvalitet. Disse forekomster er gennem årene fundet af Grønlands Geologiske Undersøgelser (GGU) og GEUS, samt af private efterforskningsselskaber, som eksempelvis Renzy Mines, Platinomino og True North Gems (TNG).

Der er indsamlet ca. 110 kg prøvemateriale, som skal til GEUS for yderligere bearbejdning. Prøverne afsendes fra Nuuk og forventes at ankomme til GEUS i slutningen af august 2011.

4.2 Besøgte lokaliteter

4.2.1 Aappaluttoq

Lokalitet: 63,01067 N / 50,32063 W; 267 moh

Aappaluttoq-forekomsten er den hidtil bedst undersøgte forekomst og udgør hovedforekomsten i TNG’s nylige ansøgning om udvindingstilladelse. På denne forekomst har TNG i 2007 og 2008 udført 65 boringer med en samlet længde på ca. 6457 m, svarende til en gennemsnitlig dybde på ca. 100 m, samt indsamlet ca. 270 tons prøvemateriale i perioden 2006-8. Alle prøver opbevares af TNG og indgår i selskabets undersøgelser i Vancouver.

Aappaluttoq samt basecamp set mod N fra helikopter.

Vi undersøgte det område, hvorfra TNG har udtaget hovedparten af prøverne. De overfladeprøver, som blev indsamlet, indeholder varierende kvalitet af rubiner, fra svagt lyserøde, uigennemsigtige til mere farvemættede, rosa, semi-transparente, 1-2 mm store rubiner. RD/GEUS indsamlede i alt ca. 29 kg bjergartsprøver til tekniske undersøgelser (GEUS Prøvenumre 521101-121).

Aappalutoq forekomsten set mod vest.

Aappalutoq rubin-holdigt lag, hvorfra TNG har udtaget større prøve.

Aappalutoq – set mod øst.

Aappalutoq forekomsten; udtagningssted for større prøve ses i bunden af billede.

Nærbillede af rubinførende bjergart fra Aappalutoq.

4.2.2 Ruby Island / Tasiusarsuaq

Lokalitet: 63,03617 °N / 50,28635° W; 12 moh

Forekomsten, som ligger på en ca. 200 m lang ø, blev fundet i 1965. TNG har i 2005 udtaget en prøve på ca. 3 tons; prøven er savet ud. Lokaliteten er kendt for at indeholde lyserød og dybrød rubin, hvoraf de fleste findes i en phlogopit matrix. Vi fandt flere horisonter med korund og meget bleg/mælket rubin, sammen med mineralerne phlogopit, gedrit, kornerupin, scapolit, sapphirin og lidt pargasit; der blev ikke set gode kvaliteter af rubin, og forekomsten skønnes at være for lille til kommerciel drift.

RD/GEUS indsamlede 2,3 kg bjergartsprøve, som skal indgå i de fortsatte tekniske undersøgelser (GEUS prøvenumre 521142-148).

Lyserøde rubiner i phlogopit- og gedrit rig matrix; grønt mineral er pargasit.

Rubin Ø set mod SØ fra helikopter.

Rubinførende horisonter på Rubin Ø.

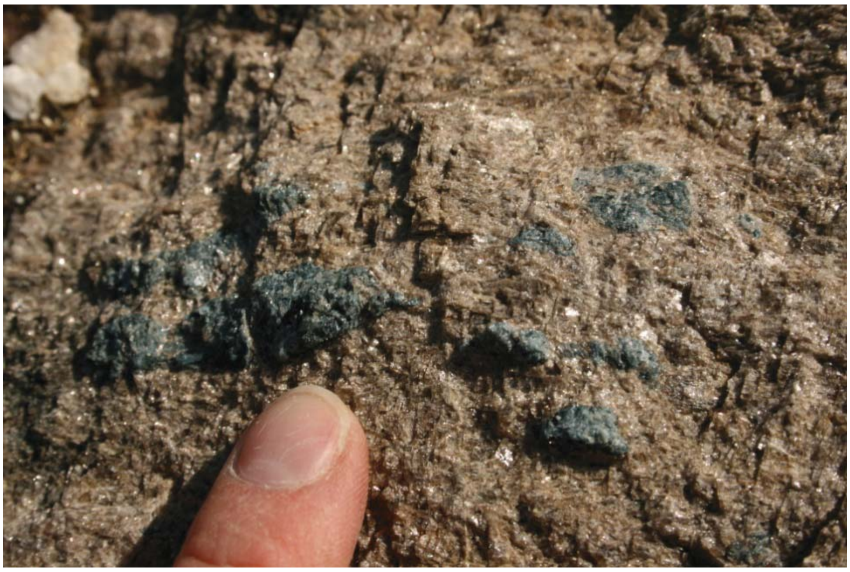

Blålige sappherin krystaller i gedrit-phlogopit matrix.

4.2.3 Siggartartulik

Lokalitet: 62,98671° N / 50,41973° W; 326 moh

I 2004 indsamlede TNG en 3 tons prøve fra Siggartartulik; prøven er savet ud med stensav.

Under besøget fandt vi et par mindre horisonter (mindre end 20 cm tykke og op til ca. 3 m lange), domineret af 'mælkede' svagt lyserøde rubiner; der sås dog også enkelte semi-transparente, lyserøde rubiner.

RD/GEUS udtog ca.13 kg bjergartsmateriale til tekniske undersøgelser (GEUS prøvenumre: 521137-141).

Oversigt over Siggartartulik-forekomsten, set mod vest. De bedste lokaliteter blev fundet i området lige over helikopteren.

Lyserøde rubiner i bjergart fra Siggartartulik.

Rubinførende bjergart hvorfra RD/GEUS udtog de fleste prøver fra Siggartartulik.

4.2.4 Upper Annertussoq

Lokalitet: 63,01189 °N / 50,42929 °W; 310 moh

Upper Annertussoq var den første lokalitet, hvor der blev fundet egentlige rubiner. Forekomsten ligger i et ca. 2 km langt bælte, indenfor hvilket der kendes flere rubin-/korundlokaliteter. TNG udtog i 2005 ca. 3 tons prøvemateriale ved brug af stensav og har rapporteret tilstedeværelse af rubiner og pink rubin i smykkestenskvalitet. Vi så flere horisonter, hver på omkring 30 cm tykkelse; det er uklart, om lagene er repeteret som følge af foldning. Rubinerne er generelt violetfarvede med god farvemætning, men kun meget få har god transparens; de fleste rubiner er mindre end 3 mm, men der blev også set enkelte sten på op til ca. 30 mm. Hovedmineraler synes at være gedrit og phlogopit samt mindre mængder kornerupin, sapphirin samt lidt pargasit.

RD/GEUS udtog ca. 10 kg bjergartsmateriale til tekniske undersøgelser (GEUS prøvenumre 521122-128).

Upper Annertussoq; de bedste horisonter blev set lige i forgrunden samt på nordsiden af den lille sø.

Upper Annertussoq; foran personen på billedet ses lokalitet, hvorfra TNG har udskåret større prøve.

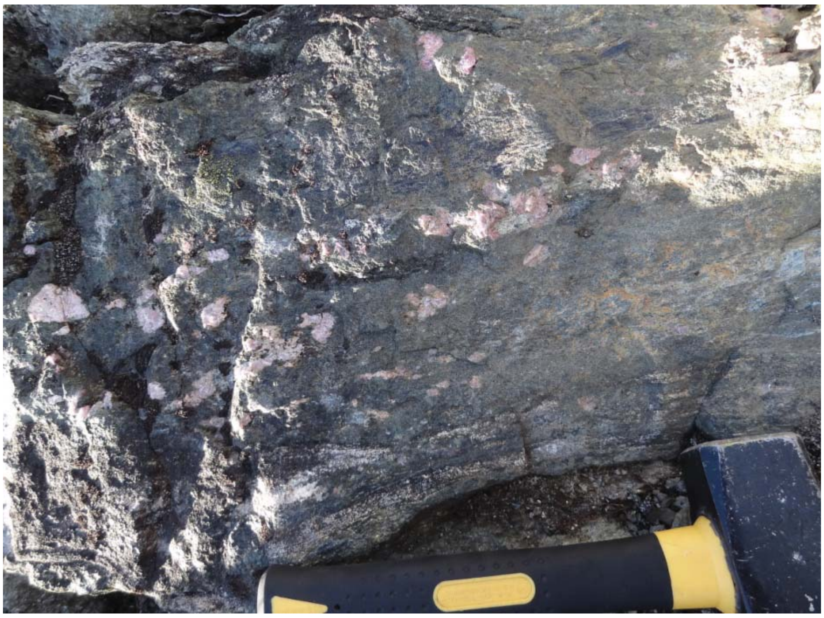

Lyserøde rubiner i bjergart fra Upper Annertussoq.

Nærbillede af lyserøde rubiner fra Upper Annertussoq.

4.2.5 Lower Annertussoq

Lokalitet: 63,00697 °N / 50,47878 °W; 42 moh

TNG udtog i 2005 en prøve på ca. 3 tons; prøven er udtaget med stensav.

Forekomsten består af en enkelt horisont, omkring 1,2 m tyk og 4 m lang, med ret få og små (< 1-2 mm) lyserøde rubiner, som generelt har dårlig transparens. Hovedmineralerne er phlogopit, sapphirin, gedrit og kornerupin. Forekomstens størrelse og kvalitet synes ikke at kunne give grundlag for en kommerciel/mekaniseret udnyttelse.

RD/GEUS indsamlede ca. 6 kg bjergartsmateriale til tekniske undersøgelser (GEUS prøvenumre 521129-130).

Lower Annertussoq set mod Ø – hvor person i rød jakke kan anes.

Lokalitet hvor TNG har udtaget stor prøve.

Rubinførende horisont ved Lower Annertussoq.

Nærbillede af rubinførende bjergarter fra Lower Annertussoq.

4.2.6 Kigutilik

Lokalitet: 62,98217 °N / 50,46949 °W; 197 moh (TNG-koordinat)

TNG har i 2005 og 2006 udtaget henholdsvis 3 t og 30 t bulkprøver fra Kigutilik, og lokaliteten er af selskabet rapporteret som forekomsten med det højeste rubinindhold per ton bjergart (8688 g/t). Det lykkedes ikke RD/GEUS at finde forekomsten på TNG's koordinat; der er efterfølgende opstået usikkerhed om, hvorvidt vi har brugt den rigtige position i vores søgning. Under eftersøgning af Kigutilik fandt vi rubiner/korund på nedenstående koordinat, som ligger syd for Lower Annertusaq, og som på indsamlingstidspunktet blev opfattet som værende Kigutilik:

Lokalitet: 63,98878o° N / 50,47944o °W; 239 moh

Lokaliteten var markeret med blå og orange markeringstape, men der blev ikke set spor af indsamling af større bulkprøver, og det konkluderes, at vi ikke har været på den egentlige Kigutilik-forekomst. Der blev på denne lokalitet set en lille blotning med blege lyserøde, ikke-transparente rubiner, hvoraf de fleste er mindre end ca. 1,5 mm; de største der blev set, var omkring 2-3 mm store. RD/GEUS indsamlede 6,5 kg bjergartsmateriale til tekniske undersøgelser (GEUS prøvenumre 521149-152).

Rubinførende horisont.

Rubinførende enhed koncentreret i foldeombøjning.

Nærbillede af rubiner fra ovenstående foto.

4.2.7 Qaqqatsiaq / Waltons Showing.

Lokalitet: 63,12601° N / 49,82317 °W; 1181 moh

Qaqqatsiaq ligger indenfor TNG's koncessionsområde, og selskabet udtog i 2005 en prøve på ca. 3 tons, hvorfra TNG rapporterer fund af rubiner i både smykkestenskvalitet og næsten-smykkestenskvalitet.

Lokaliteten Qaqqatsiaq består af flere horisonter, som strækker sig fra ca. 800 m til 1300 m. Rubinforekomsterne findes i kontaktområdet mellem en række ultramafiske bjergarter og anorthositer. Forekomsten er kendt for – ud over rubiner – at indeholde en del ret sjældne mineraler, heraf mange som store krystaller. Forekomsten indeholder mange 5-20 cm brede bånd af rød spinel, som kan følges over 5-10 m. Indholdet af rubiner er forholdsvis beskedent: de fleste har ret dårlig transparens og er mindre end 1-2 mm; farven er typisk rødviolet med mellemgod farvemætning. Rubinerne findes i forskellige parageneser, hvoraf phlogopit synes at dominere på den besøgte lokalitet.

På grund af forekomstens unikke mineralogi har den gennem årene været undersøgt af mange forskellige forskere, og forekomsten har stadig stor forskningsmæssig betydning. Det anbefales derfor at 'frede' denne forekomst, så den ikke fremover kan indgå i nogen form for kommerciel mineraludnyttelse.

Udsigt fra Waltons showing – set mod Bjørnesund.

Pargasitrige bånd i Waltons showing.

4.2.8 Qaqat Agulerit = Beer Mountain

Lokalitet: 63,13965 °N / 49,55727° W; 929 moh

Der blev i 1970 fundet to rubinlokaliteter på Qaqat Aqulerit. Det lykkedes os ikke at finde lokaliteterne; Richard Herd beskriver forekomsterne således: Rubinerne findes i (i) en 1 m tyk horisont i anorthositbjergarten; og (ii) 'ruby-bearing gravel'. På landingsstedet blev der observeret en del 5-20 cm chromitbånd med fuchsitmineraliseringer. Der blev udtaget ca. 2 kg bjergartsprøver af dette materiale (GEUS prøvenummer 521154). Det vil bl.a. blive undersøgt om fuchsitmineraliseringerne kan bruges til fremstilling af smykkesten.

Fuchsit- og kromitrige horisonter ved Qaqat Aqulerit.

Nærbillede af ovenstående foto af fuchsit- og kromitrige bånd ved Qaqat Aqulerit.

4.2.9 Bjørnesund TNG

Lokalitet: 63,08451° N / 49,78794° W

Denne lokalitet blev først registreret af TNG i 2006. Der foreligger ikke oplysninger om kvaliteten af de rubiner, der er indsamlet.

Det lykkedes ikke RD/GEUS at finde en lokalitet med korund/safir; der blev dog observeret m-store linser af ultramafiske bjergarter samt anorthosit, som ofte er associeret med rubinmineraliseringer.

4.2.10 Bjørnesund GEUS 2008

Lokalitet: 63,12672 °N / 49,74599 °W; 969 moh

Forekomsten blev fundet af GEUS i 2008 og ligger uden for TNG's licensområder. Efter fundet lukkede RD området for licensansøgninger.

Kig mod øst over rubinforekomsten GEUS 2008.

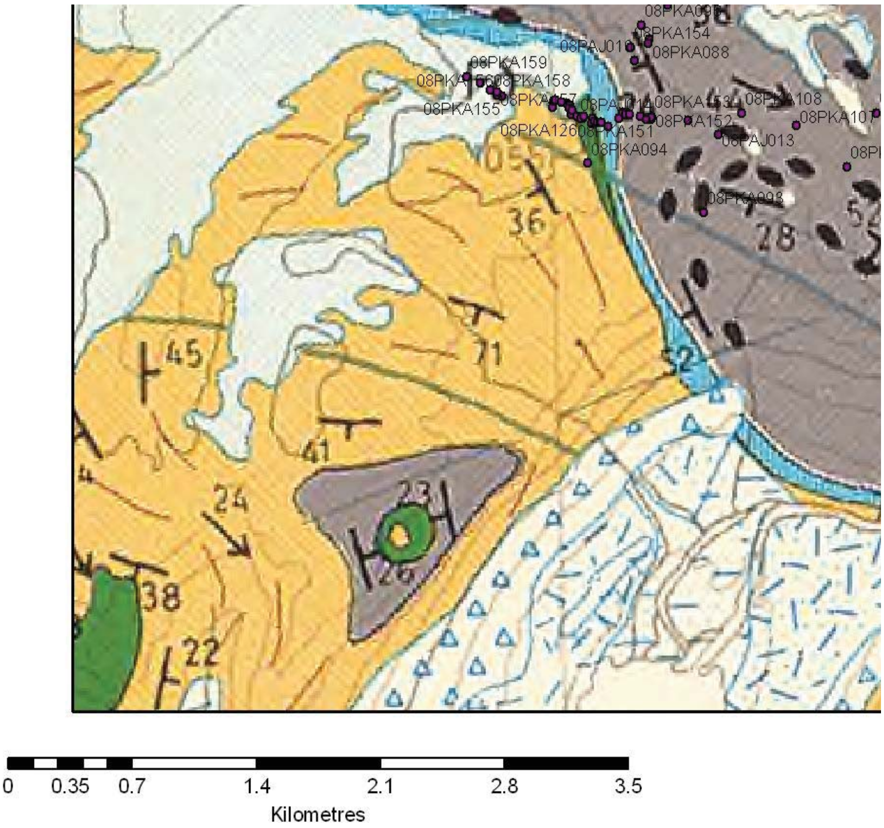

Fig. 5. *Prøvekort for prøver indsamlet af GEUS i 2008.*

Forekomsten danner et ca. 1,5 km langt bælte, hvori der findes et stort antal rubinførende enheder; enhederne varierer i længde fra omkring få meter til mere end 20 m lange og med tykkelser varierende fra 0,3 m til lag af flere meters tykkelse. Kvaliteten varierer, men semitransparente, røde rubiner blev observeret flere steder. Denne forekomst synes i størrelse at være ganske betydelig sammenholdt med de øvrige besøgte forekomster. Det anbefales derfor at overveje, om forekomsten kan danne grundlag for én eller flere småskala-licenser.

RD/GEUS indsamlede ca. 22 kg bjergartsmateriale fra denne forekomst (GEUS prøvenummer: 521131-136).

Rubinførende phlogopite-sapphirin schist (loc. PKA144).

Rubinførende phlogopite-sapphirine schist (loc. PKA153).

***Tabel 3.** Informationer om GEUS 2008 forekomsten, indsamlet i forbindelse med feltarbejdet i 2008.*

Lokalitet	**Prøve**	**Foto**	**Tykkelse (m)**	**Bemærkninger**
PKA 90	513719 513720 513721	020-28	0,5	Ruby, phlogopite; Rubies: 1-5 mm; locally up to 5% Strike: 320/30SW
PKA 91			0,5	
PKA 92			1	
PKA 95	513722 513723	036-37 086		Bands of pseudo tachylite, with plk phenocrysts
PKA 110			1	
PKA 111			0,5	
PKA 112			0,5	
PKA 114			1	
PKA 115			2	
PKA 122			1	
PKA 123			2	
PKA 124			1	
PKA 126			0,5	
PKA 127			2	
PKA 132			2	
PKA 134			1.5	
PKA 135			1	
PKA 136			1,5	
PKA 137			1,5	
PKA 138			0,5	

PKA 139			0,3	
PKA 140			0,5	
PKA 141			5	
PKA 142			2 x 0,5	
PKA 144	513731 513732 513733		2	Phologopite and sapphirin Ruby, phlogopite, sapphirin Ruby, phlogopite, sapphirine
PKA 146			2	
PKA 147			1	
PKA 150			1	
PKA 151			1,5	
PKA 152			2	
PKA 153				Biotite rich peridotite
PKA 155			0,2	
PKA 156			0,2	
PKA 159			0,2	

Tabel 4. *Detaillokaliteter for GEUS 2008 forekomsten, indsamlet i forbindelse med feltarbejdet i 2008*

Lokalitet	**Dato**	**Time**	**Latitute (°N)**	**Longitute (°W)**
08PKA090	14/07/2008	10:52:31	63.12679667	-49.74729500
08PKA091	14/07/2008	11:22:52	63.12661500	-49.74603333
08PKA092	14/07/2008	11:41:46	63.12646167	-49.73842500
08PKA095	14/07/2008	16:14:36	63.12843500	-49.75735000
08PKA110	15/07/2008	17:14:09	63.12716167	-49.74942000
08PKA111	15/07/2008	17:20:27	63.12747833	-49.74927167
08PKA112	15/07/2008	17:22:57	63.12750667	-49.74900333
08PKA114	15/07/2008	17:27:13	63.12740167	-49.74835333
08PKA115	15/07/2008	17:31:18	63.12723500	-49.74742167
08PKA122	15/07/2008	17:40:20	63.12709000	-49.74751000
08PKA123	15/07/2008	17:42:06	63.12699833	-49.74724167
08PKA124	15/07/2008	17:45:05	63.12668667	-49.74662833
08PKA126	15/07/2008	17:47:23	63.12661333	-49.74625000
08PKA127	15/07/2008	17:47:55	63.12669833	-49.74592500
08PKA132	15/07/2008	17:56:36	63.12657000	-49.74496000
08PKA134	15/07/2008	17:58:33	63.12634667	-49.74502667
08PKA135	15/07/2008	17:59:28	63.12644833	-49.74472667
08PKA136	15/07/2008	18:00:46	63.12635833	-49.74443667
08PKA137	15/07/2008	18:01:29	63.12639167	-49.74406667
08PKA138	15/07/2008	18:01:57	63.12635833	-49.74390833
08PKA139	15/07/2008	18:03:57	63.12614667	-49.74318167
08PKA140	15/07/2008	18:06:09	63.12653500	-49.74200667
08PKA141	15/07/2008	18:09:50	63.12685500	-49.74153500
08PKA142	15/07/2008	18:10:29	63.12675167	-49.74125167

08PKA144	15/07/2008	18:15:05	63.12676167	-49.74079167
08PKA146	15/07/2008	18:21:45	63.12674500	-49.74071833
08PKA147	15/07/2008	18:23:44	63.12661667	-49.73959667
08PKA150	15/07/2008	18:27:43	63.12646167	-49.73855500
08PKA151	15/07/2008	18:28:18	63.12652833	-49.73837167
08PKA152	15/07/2008	18:28:54	63.12657167	-49.73826667
08PKA153	16/07/2008	08:11:24	63.12659423	-49.73837856
08PKA155	17/07/2008	11:15:44	63.12774167	-49.75500333
08PKA156	17/07/2008	11:57:09	63.12779000	-49.75559833
08PKA159	17/07/2008	13:03:31	63.12874667	-49.75893833

4.2.11 Lichtenfels

Lichtenfels-lokaliteten blev ikke besøgt på grund af manglende tid, men blev overfløjet. Fra luften ses der tydelig kontakt mellem Fiskenæsset-kompleksets bjergarter og ultramafiske bjergarter, som ofte er det geologiske miljø, hvor der findes rubiner. Forekomsten har været kendt siden 1971 og har i 2005 været undersøgt af TNG, men ligger uden for selskabets eneretskoncession. Forekomsten er af Richard Herd beskrevet som én til to lokaliteter, som mest består af sapphirin, gedrit, hornblende og rubin.

Det anbefales at undersøge forekomsten nærmere for at se, om den evt. kan være af interesse for småskala-licenshavere.

4.3 Separation af rubiner

Som led i en kvalitetsundersøgelse af Fiskenæsset-områdets rubiner er udvalgte prøver indsamlet i sommeren 2011, sammen med prøver fra Siggartartulik uden specifikke koordinater, tre prøver fra Intex AS licensområde, samt en prøve af ukendt herkomst, fundet i et lager i Nuuk, blevet knust og rubiner separeret (se Tabel 5). Prøverne blev knust i 3 trin i kæbeknuser og mellem hvert trin blev materialet sorteret på 2 mm sigte og frie korn (>2 mm) blev frasorteret manuelt.

Tabel 5: *Makroskopisk beskrivelse af prøver fra Fiskenæsset-området. Farvebeskrivelse på grundlag af GIA (http://www.gemval.com/color_grade.html); i prøver med stor farvevariation er bedste farve angivet. Der er store usikkerheder på både farve og transparens som følge af størrelsesfordeling og manglende polering.*

Lokalitet	**GEUS no.**	**Rubin karakteristik**	**Farve**	**Transparens**
Aappalutoq	521101	Rather few and small size	214. Medium dark strongly purplish red	Good
Aappalutoq	521104	Plenty and big size	199. Light reddish purple	Milky
Aappalutoq	521105	Rather few and small size	214. Medium dark strongly purplish red	Good
Aappalutoq	521106	Rather few and small	214. Medium dark strongly	Some good

		size	purplish red	
Aappalutoq	521107		215. Medium dark stronly purplish red; slightly brownish	Some good
Aappalutoq	521108	Plenty and big size	003. Light red; very slightly brownish	Milky
Aappalutoq	521109	Plenty and big size	222. Medium dark slightly purplish red;	Milky
Aappalutoq	521110	Plenty and big size	011. Medium dark red; very slightly brownish	Medium
Aappalutoq	521111	Few and small size	214. Medium dark strongly purplish red	Good
Aappalutoq	521113	Rather plentifyl and medium size	215. Medium dark strongly purplish red; slightly brownish	Medium
Aappalutoq	521120	Plenty and big size	214. Medium dark strongly purplish red	Low
Aappalutoq	521121	Plenty and big size	213. Medium strongly purplish red; slightly brownish	Medium
U. Annertussaq	521123	Plenty and big size	215. Medium dark strongly purplish red; slightly brownish	Milky
U. Annertussaq	521127	Rather few and small size	214. Medium dark strongly purplish red	Milky
L. Annertussaq	521130	Few and small size	207. Light strongly purplish red: very slightly brownish	Low - medium
Bjørnesund 2008	521131	Rather plentiful and small size	209. Medium strongly purplish red; very slightly brownish	Low - medium
Bjørnesund 2008	521132	Rather plentiful and medium size	222. Medium dark slightly purplish red;	Good
Bjørnesund 2008	521134	Plenty medium size	219. medium slightly purplish red; very slightly brownish	Low - medium
Bjørnesund 2008	521135	Plenty medium size	214. Medium dark strongly purplish red	Medium
Siggartartulik	521138	Plenty and big size	199. Light reddish purple	Very low; milky
Siggartartulik	521140	Plenty and small size	221. Midium slightly purplish red; very slightly brownish	Medium - good
Siggartartulik	521158	Plenty and medium size	214. Medium dark strongly purplish red	Medium - good
Siggartartulik	521159	Plenty and big size	221. Midium slightly purplish red; very slightly brownish	Low - medium
Siggartartulik	521160	Plenty and big size	214. Medium dark strongly purplish red	Low
Rubin Ø	521142	Few and small	204. Medium dark reddish purple	Medium - good
Rubin Ø	521144	Medium size	205. Very light strongly purplish red.	Low
Rubin Ø	521148	Very few and small	214. Medium dark strongly purplish red	Medium
Kigutilik	521149	Rather few and medium size	213. Medium strongly purplish red; slightly brownish	Low
Kigutilik	521151	Few and small	214. Medium dark strongly purplish red	Good

Kigutilik	521152	Rather few and small	222. Medium dark slightly purplish red;	Good
Intex	521161	Rahter few and small	215. Medium dark strongly purplish red; very slightly brownish	Very low (omdannede)
Intex	521162	Many big (fragments)	219. medium slightly purplish red; very slightly brownish	Low
Intex	521163	Few and small	212. Medium strongly purplish red; very slightly brownish	Medium
Ukendt	521153	Plenty and big	214. Medium dark strongly purplish red	Low

Yderligere karakterisering vil blive fortsat i 2012. Alle prøver blev forelagt Swiss Gemmological Institute (SGI), Basel, Schweiz, som på grundlag af en hurtig makroskopisk vurdering gav følgende karakteristik: Tvilling-lameller er meget udbredt; en meget stor del har gennemgående sprækker, og rubinerne har et blåligt skær i den røde farve. SGI anbefalede at igangsætte forsøg med varmebehandling evt. suppleret med flux-behandling til at lukke sprækker.

4.3.1 Planlagte undersøgelser

Som led i karakteriseringsarbejdet påtænkes der gennemført følgende undersøgelser på udvalgte prøver (omtalt i Tabel 5): Geokemisk karakterisering; spektroskopi (evt. Raman), fluoressense målinger og bestemmelse af indeslutningstyper.

Appendix B:

Article published in the Review of the Surveys Activities, 2013

Keulen, N. & Kalvig, P. (2013): Fingerprinting of corundum (ruby) from Fiskenæsset, West Greenland. In: Geological Survey of Denmark and Greenland Bulletin 28, 53–56.
Open access: www.geus.dk/publications/bull

Fingerprinting of corundum (ruby) from Fiskenæsset, West Greenland

Nynke Keulen and Per Kalvig

Since the late 1960s, it has been known that pink and red corundum occur in the area near Fiskenæsset (Qeqertarsuatsiaat) in southern West Greenland. Corundum is hosted in the Fiskenæsset complex, which is part of the Archaean basement of the North Atlantic Craton. To date, *c.* 40 corundum localities with a wide range of quality are known in the area – a few localities yield stones of gem quality. The most promising locality, Aappaluttoq, is likely to be mined in the foreseeable future by the Canadian company True North Gems (Figs 1, 2A). Red corundum of gem quality is called ruby; gem quality corundum of other colours (e.g. pink, yellow or blue) is called pink sapphire, yellow sapphire etc., while the blue gem corundum is sapphire. Red, pink and blue corundum are also known in smaller quantities from other areas in Greenland.

The Fiskenæsset complex

The Fiskenæsset complex (Fig. 1) comprises a series of intrusive sheets of anorthosite, leucogabbro, gabbro and ultramafic rocks (Myers 1985), and is interpreted as derived from a supra-subduction setting, while the associated amphibolites stem from a mid-oceanic ridge to island arc basalt precursor (Polat *et al.* 2009). The greater Fiskenæsset region was metamorphosed *c.* 2.85–2.80 Ga ago at mid- to upper amphibolite-facies temperatures and pressures, reaching granulite facies conditions near the village of Fiskenæsset (McGregor & Friend 1992; Schumacher *et al.* 2011). At least one generation of the *c.* 2.71 Ga felsic pegmatite sheets cuts the anorthosite, ultramafic rocks, amphibolite and gneisses and created reaction zones that developed aluminium-rich mineral assemblages derived from the aluminium in the anorthosite rocks (Schumacher *et al.* 2011; Fig. 2B). These reaction zone assemblages, associated with pegmatitic felsic sheets and the ultramafic bodies, include very coarse-grained, radial anthophyllite ± green pargasite ± green or red spinel ± sapphirine ± cordierite (up to 30 cm single crystals) ± pink corundum, and ± phlogopite (Schumacher *et al.* 2011).

This study is a first attempt to find geochemical and mineralogical characteristics that can be used to tie the Greenlandic rubies to their area of origin. This may have practical implications if an operation of rubies and pink sapphires is established in Greenland. Here, we present Laser Ablation Inductively Coupled Plasma Mass Spectrometry (LA-ICP-MS) trace-element geochemical and oxygen isotope data of samples from the Fiskenæsset area and other known localities in Greenland (Storø, Maniitsoq, Kapisillit and Nattivit).

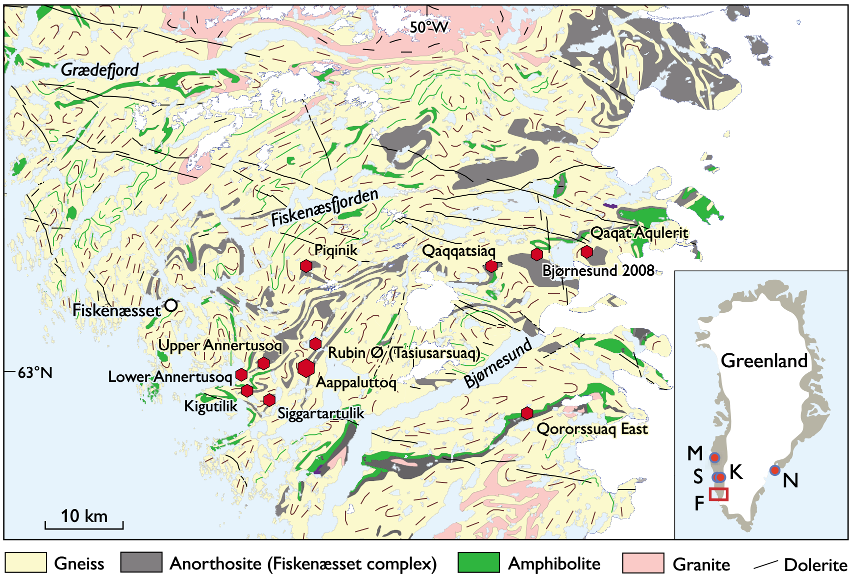

Fig. 1. Simplified geological map of the Fiskenæsset area in southern West Greenland showing the investigated pink and red corundum (ruby) localities in the Fiskenæsset complex. Map after Keulen & Kokfelt *et al.* (2011). **M:** Maniitsoq, **S:** Storø, **K:** Kapisillit, **F:** Fiskenæsset, **N:** Nattivit.

© 2013 GEUS. *Geological Survey of Denmark and Greenland Bulletin 28, 53–56. Open access: www.geus.dk/publications/bull*

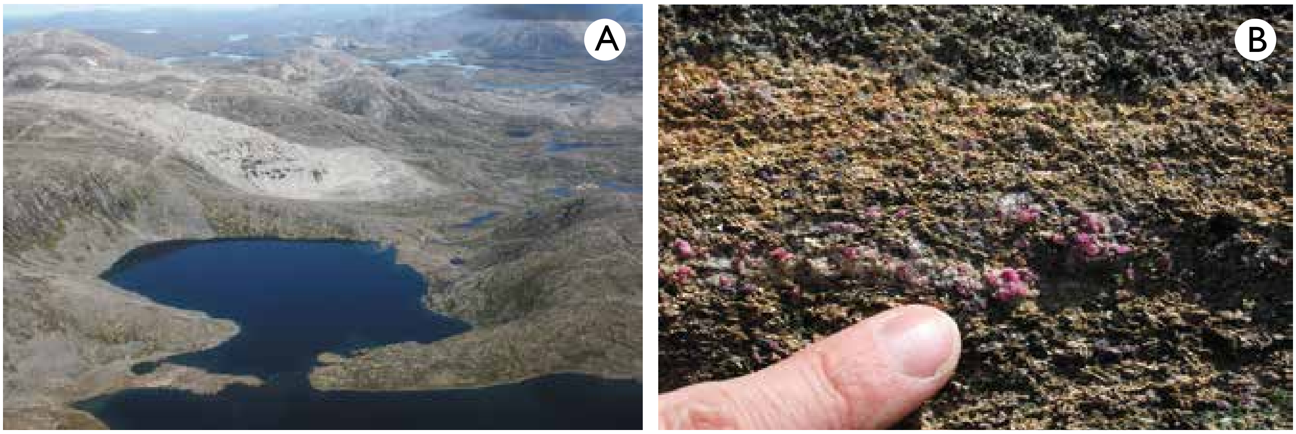

Fig. 2. **A**: Aappaluttoq, Fiskenæsset, seen from a helicopter towards the north. The white-grey rock is anorthosite. **B:** Rubies in their host rock at Tasiussarsuaq, Fiskenæsset, Greenland.

Trace-element geochemistry

Corundum has the chemical formula Al_2O_3 and like most other minerals usually includes very small quantities of other elements in its crystal structure. The amounts of these trace elements and their ratios may depend on the geological conditions during the formation of the corundum and therefore usually vary between individual corundum deposits. Twenty-four different elements were analysed for by means of LA-ICP-MS; however most of them were not detected, including Sn, Nb, and Ta. Our investigations of the Greenlandic corundum were concentrated on the elements Mg, Si, Ti, V, Cr, Fe, and Ga, as these elements are present in significant amounts and are also the most widely documented. We used

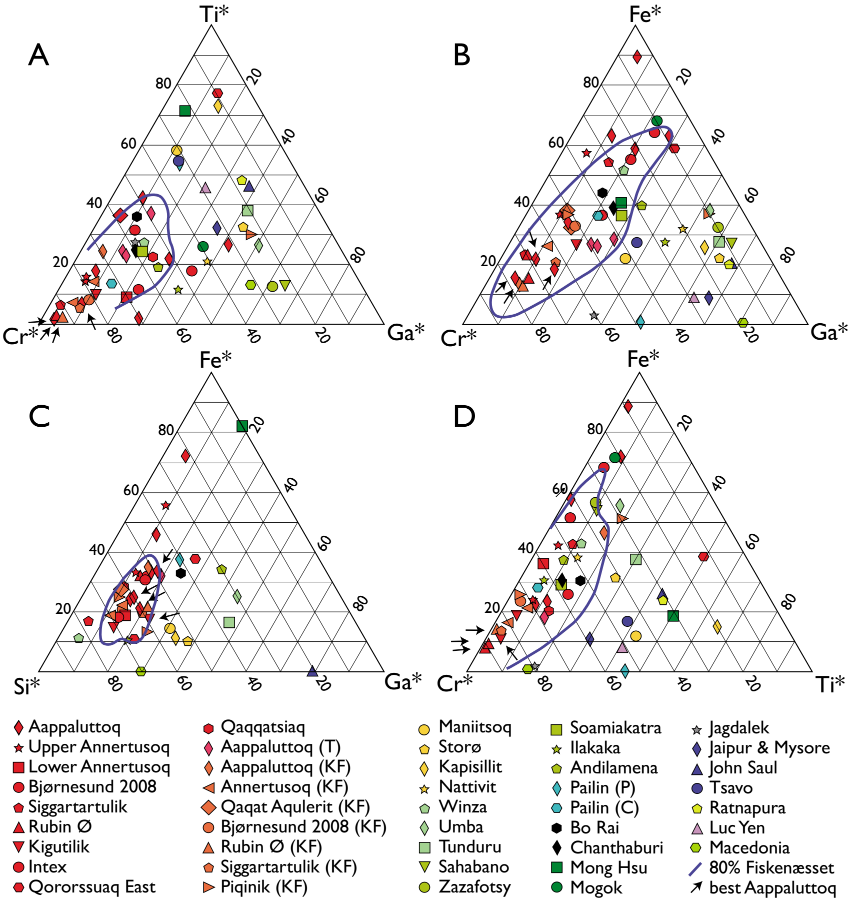

Fig. 3. Normalised trace-element distributions for **A**: Ti-Cr-Ga, **B**: Fe-Cr-Ga, **C**: Fe-Si-Ga and **D**: Fe-Cr-Ti in corundum from Fiskenæsset. The data are compared with data on international and Greenlandic corundum occurrences (Calligaro *et al.* 1999; del Castillo *et al.* 2009; Kalvig & Frei 2010; Pornwilard *et al.* 2011; Rakontondrazafy *et al.* 2008; Schwarz *et al.* 2008; Thirangoon 2008). Different colours show different countries. Initials of the authors' names were used where more than one study of the same locality exist. Diagrams were created with WxTernary (Keulen & Heijboer 2011).

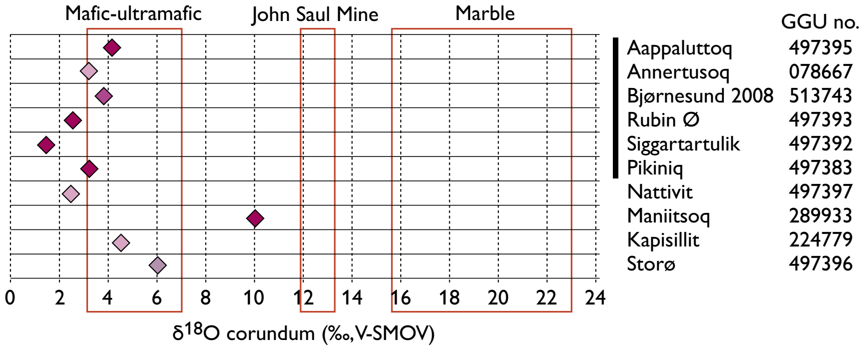

Fig. 4. δ^{18}O values for six samples from Fiskenæsset and four other localities in Greenland. The values are relative to VSMOW (Vienna standard mean ocean water). Colours indicate the approximate colour of the stones. Red boxes and classification as mafic-ultramafic, John Saul mine, and marble after Giuliani *et al.* (2007).

the Laser Ablation Sector-Field Inductively Coupled Plasma Mass Spectrometer (LA-SF-ICP-MS) at the Geological Survey of Denmark and Greenland (Frei & Gerdes 2009), employing an ELEMENT 2 instrument from Thermo-Fisher Scientific and a UP213 frequency-quintupled Nd:YAG solid state laser system from New Wave Research. Data reduction and determination of concentrations were calculated off-line through the software Iolite using the Trace_Elements_IS routine (Hellstrom *et al.* 2008). Further details on the methods are found in Keulen & Kalvig (2013).

Results on the trace-element investigations of corundum grains separated from 21 hand specimens from ten localities in the Fiskenæsset complex are shown with red symbols in the ternary diagrams of Fig. 3. The data for corundum from the Fiskenæsset complex are in good concordance with earlier data from the area (Kalvig & Frei 2010; Thirangoon 2008). In Fig. 3 they are compared with data from other localities in Greenland and from internationally, well-known, ruby occurrences. Samples from Fiskenæsset show a considerably higher amount of Cr (up to 14000 ppm) than samples from other areas in Greenland and most international samples. The Fiskenæsset rubies are relatively rich in Fe and Si, but relatively poor in Ti and Ga, while V and Mg do not show very distinctive values compared to samples from other areas (Kalvig & Keulen, 2011).

In order to use trace-element investigations as a fingerprinting tool for rubies it is necessary to investigate the amount of overlap between samples from Fiskenæsset and other localities. The blue lines in Fig. 3 include 80% (26 out of 32) of the samples from the Fiskenæsset area, based on sample distribution density contouring. Most samples from other localities plot outside the blue line, but an overlapping chemistry is found with samples from Soamiakatra, Ilakaka, and Andilamena in Madagascar, Bo Rai and Chanthaburi in Thailand, Pailin in Cambodia and Winza in Tanzania. Rubies from all these localities are hosted by ultramafic to mafic rocks or are found as placer deposits. This indicates that the trace elements in the rubies derive from the ultramafic rocks that are associated with the anorthosite.

However, if only the four handspecimens with the most transparent and most intensively red-coloured corundum grains from Aappaluttoq, Fiskenæsset, are taken into account, no overlap between these handspecimens and samples from other known ruby occurrences is seen. Corundum from these handspecimens is closest in transparency and colour to the stones that would be sold from a potential mine and therefore represent the Aappaluttoq signature. As these corundum grains have a distinct composition, it can be concluded that trace-element geochemistry with ICP-MS is a helpful tool in fingerprinting rubies from Greenland.

Oxygen isotope geochemistry

Oxygen isotopic composition measurements were performed on ten samples from Greenland at the University of Lausanne, Switzerland using an isotope ratio mass spectrometer, employing a method similar to that described by Kasemann *et al.* (2001), see Kalvig & Keulen (2011) for details.

Six of the samples come from the Fiskenæsset complex. Their δ^{18}O values vary between 1.62 and 4.20‰ for the Fiskenæsset area, which is low compared to the other areas in Greenland (up to 10.03‰ for Maniitsoq) with the exception of one sample from Nattivit (2.41‰; Fig. 4). The δ^{18}O values are also low compared to most other investigated corundum deposits worldwide (Giuliani et al. 2007). The lowermost values (δ^{18}O <3‰) are nearly diagnostic for the Fiskenæsset area – worldwide only the placer deposits at Andilamena and Ilakaka in Madagascar and gem-corundum in a cordieritite from Iankaroka, Madagascar have lower reported δ^{18}O values. Low δ^{18}O values (≤4‰) generally reflect rock types such as mafic rocks, mafic gneiss, basalts, and desilicated pegmatite in mafic rocks (Giuliani et al. 2005), which is in excellent agreement with the mafic to ultramafic setting of the Fiskenæsset rubies. The values for samples from Nattivit, Kapisillit and Storø are also low (2.4, 4.5 and 6.0‰ respectively) and also plot in the mafic–ultramafic field. Unfortunately, no further geological information is available for these specimens and the data can thus not be validated against field observations. The value for Maniitsoq with $\delta^{18}O = 10.03‰$ is typically related to skarns in marble, or to biotitite in gneiss related to shear zones with high fluid activity. The rubies in the investigated sample are assumed to stem from sapphirine-bearing hornblendite. The hornblendite was probably formed in a shear zone with high fluid activity (like the biotitites in Madagascar).

The low $\delta^{18}O$ values are a potentially useful tool for fingerprinting Greenlandic rubies, especially the very low values for the Fiskenæsset complex and Nattivit, as only few other international occurrences have such low values.

Conclusions

High confidence fingerprinting of rubies requires a combination of independent analytical methods such as trace-element analyses, oxygen isotope analyses and other studies. The two methods discussed here are efficient in characterising the Fiskenæsset rubies. The ongoing research focuses on optical and physical characteristics, spectroscopy methods and scanning XRF.

Acknowledgements

This study is part of a collaboration project between the Bureau of Minerals and Petroleum in Nuuk, Greenland and the Geological Survey of Denmark and Greenland. The authors wish to thank Kerstin Bauer and Torsten Vennemann for help with the oxygen isotope analyses.

References

Calligaro, T., Poirot, J.-P. & Querré, G. 1999: Trace element fingerprinting of jewellery rubies by external beam PIXE. Nuclear Instruments and Methods in Physics Research B **150**, 628–634.

Calvo del Castillo, H., Deprez, N., Dupuis, T., Mathis, F., Deneckere, A., Vandenabeele, P., Calderón, T. & Strivay, D. 2009: Towards the differentiation of non-treated and treated corundum minerals by ion-beam-induced luminescence and other complementary techniques. Analytical and Bioanalytical Chemistry **394**, 1043–1058.

Frei, D. & Gerdes, A. 2009: Precise and accurate *in situ* U-Pb dating of zircon with high sample throughput by automated LA-SF-ICP-MS. Chemical Geology **261**, 261–270.

Giuliani, G., Fallick, A.E., Garnier, V., France-Lanord, C., Ohnenstetter, D. & Schwarz, D. 2005: Oxygen isotope composition as a tracer for the origins of rubies and sapphires. Geology **33**, 249–252, http://dx.doi.org/10.1130/G21261.1.

Giuliani, G. *et al.* 2007: Oxygen isotope systematics of gem corundum deposits in Madagascar: relevance for their geological origin. Mineralium Deposita **42**, 251–270.

Hellstrom, J., Paton C., Woodhead J. & Hergt J. 2008: Iolite: software for spatially resolved LA- (quad and MC) ICPMS analysis. In: Sylvester P. (ed.): Laser ablation ICP–MS in the earth sciences: current practices and outstanding issues, 343–348. Mineralogical Association of Canada short course series **40**, 343–348.

Kalvig, P. & Frei, D. 2010: Testing the use of geochemical characteristics of corundum from Greenland as a tool for geographical typing. Danmarks og Grønlands Geologiske Undersøgelse Rapport **2010/68**, 36 pp.

Kalvig, P. & Keulen, N. 2011: Aktiviteter i rubinprojektet 2011 – samarbejdsprojekt med Råstofdirektoratet. Danmarks og Grønlands Geologiske Undersøgelse Rapport **2011/138**, 41 pp.

Kasemann, S., Meixner, A., Rocholl, A., Vennemann, T., Schmitt, A. & Wiedenbeck M. 2001: Boron and oxygen isotope composition of certified reference materials NIST SRM 610/612, and reference materials JB-2G and JR-2G. Geostandards Newsletter **25**, 405–416.

Keulen, N. & Heijboer, T. 2011: The provenance of garnet: semi-automatic plotting and classification of garnet compositions. Geophysical Research Abstracts **13**, EGU 2011-4716.

Keulen, N. & Kalvig, P. 2013: Report of the activities in the ruby project 2012 – a joint project with the Bureau of Minerals and Petroleum. Danmarks og Grønlands Geologiske Undersøgelse Rapport **2013/09**, 25 pp.

Keulen, N., Kokfelt, T.F. & the homogenisation team 2011: A 1:100 000 seamless, digital, internet-based geological map of South-West and southern West Greenland, 61°30′–64°N, *http://geuskort.geus.dk/gisfarm/gis_svgreenland.jsp*. Copenhagen: Geological Survey of Denmark and Greenland.

McGregor, V.R. & Friend, C.R.L. 1992: Late Archean prograde amphibolite- to granulite-facies relations in the Fiskenæsesset region, southern West Greenland. The Journal of Geology **100**, 207–219.

Myers, J.S. 1985: Stratigraphy and structure of the Fiskenæsset Complex, southern West Greenland. Bulletin Grønlands Geologiske Undersøgelse **150**, 72 pp.

Polat A., Appel, P.W.U., Fryer, B., Windley, B., Frei, R., Samson, I.M. & Huang, H. 2009: Trace element systematics of the Neoarchean Fiskenæsset anorthosite complex and associated meta-volcanic rocks, SW Greenland: evidence for a magmatic arc origin. Precambrian Research **175**, 87–115.

Pornwilard, M.-M., Hansawek, R., Shiowatana, J. & Siripinyanond, A. 2011: Geographical origin classification of gem corundum using elemental fingerprint analysis by laser ablation inductively coupled plasma mass spectrometry. International Journal of Mass Spectrometry **306**, 57– 62.

Rakontondrazafy, A.F.M. *et al.* 2008: Gem corundum deposits of Madagascar: a review. Ore Geology Reviews **34**, 134–154.

Schumacher, J.C., van Hinsberg, V.J. & Keulen, N. 2011: Metamorphism in supracrustal and ultramafic rocks in southern West Greenland and South-West Greenland 64°–61.5°N. Danmark og Grønlands Geologiske Undersøgelse Rapport **2011/6**, 29 pp.

Schwarz, D. *et al.* 2008: Rubies and sapphires from Winza, Central Tanzania. Gems & Gemology **44**, 322–347.

Thirangoon, K. 2008: Ruby and pink sapphire from Aappaluttoq, Greenland. Status of on-going research. Unpublished report for True North Gems Co. (In archives of Geological Survey of Denmark and Greenland, GEUS Report File **23642**, 18 pp.).

Authors' address
Geological Survey of Denmark and Greenland, Øster Voldgade 10, DK-1350 Copenhagen K, Denmark. E-mail: *ntk@geus.dk*

Appendix C:

Whole-rock geochemistry data for samples from the FC.

Final Report
Activation Laboratories

Activation Laboratories, Ontario, Canada
Report Date: 12/30/2013

App C.

Analyte Symbol	SiO2	Al2O3	Fe2O3(T)	MnO	MgO	CaO	Na2O	K2O	TiO2	P2O5	LOI	Total	Sc	Be	V	Cr	Co	Ni
Unit Symbol	%	%	%	%	%	%	%	%	%	%	%	%	ppm	ppm	ppm	ppm	ppm	ppm
Detection Limit	0.01	0.01	0.01	0.001	0.01	0.01	0.01	0.01	0.001	0.01		0.01	1	1	5	20	1	20
Analysis Method	FUS-ICP	FUS-ICP	FUS-ICP	FUS-ICP	FUS-ICP	FUS-ICP	FUS-ICP	FUS-ICP	FUS-ICP	FUS-ICP	FUS-ICP	FUS-ICP	FUS-ICP	FUS-ICP	FUS-ICP	FUS-MS	FUS-MS	FUS-MS
522106	49.62	14.9	14.76	0.192	5.42	7.95	3.56	1.12	2.441	0.67	-0.14	100.5	25	2	202	50	50	80
522136	53.71	17.18	8.68	0.125	5.26	6.45	3.42	2	0.88	0.15	1.15	99	13	2	106	90	39	90
522137	47.91	17.51	13.29	0.181	7.71	9.26	3.06	0.38	1.251	0.14	-0.52	100.2	20	< 1	146	70	58	110
522138	47.28	18.12	12.14	0.16	7.35	9.41	3.01	0.36	1.273	0.14	-0.42	98.82	20	< 1	159	80	55	120
522142	63.54	15.99	4.49	0.081	1.21	2.44	4.55	5.14	0.572	0.22	1.25	99.49	7	3	63	< 20	8	< 20
522147	58.16	15.39	11.05	0.248	0.47	2.25	5.29	5.72	0.9	0.18	1.02	100.7	12	12	9	< 20	2	< 20
527261	48.2	17.79	12.6	0.168	6.48	9.34	3.08	0.55	1.537	0.17	0.34	100.2	24	< 1	201	60	54	100
521114	20.34	31.9	3.39	0.061	15.31	6.55	1.28	0.78	0.376	0.02	19.89	99.9	56	1	105	490	10	50
521101	40.56	24.32	5.91	0.078	22.74	0.59	1.5	1.15	0.284	0.01	2.11	99.26	13	< 1	331	6180	19	230
521145	38.12	26.34	1.44	0.026	21.47	6.25	1.01	1.33	0.491	< 0.01	2.45	98.94	27	< 1	171	> 10000	5	100
521147	38.35	27.97	4.14	0.049	16.93	4.95	1.28	1.94	0.377	0.02	2.88	98.88	38	< 1	180	930	12	150
521106	36.45	32.6	5.54	0.074	19.63	0.61	1.22	1.2	0.262	< 0.01	2	99.58	13	< 1	300	5000	17	190
unknown	49.03	13.47	14.24	0.207	6.18	11.23	2.5	0.22	2.143	0.19	0.24	99.65	42	< 1	448	130	55	60

Final Report
Activation Laboratories

Activation Laboratories, Ontario, Canada
Report Date: 12/30/2013

App C.

Analyte Symbol	Cu	Zn	Ga	Ge	As	Rb	Sr	Y	Zr	Nb	Mo	Ag	In	Sn	Sb	Cs	Ba	La
Unit Symbol	ppm	ppm	ppm	ppm	ppm	ppm	ppm	ppm	ppm	ppm	ppm	ppm	ppm	ppm	ppm	ppm	ppm	ppm
Detection Limit	10	30	1	0.5	5	1	2	0.5	1	0.2	2	0.5	0.1	1	0.2	0.1	3	0.05
Analysis Method	FUS-MS	FUS-MS	FUS-MS	FUS-MS	FUS-MS	FUS-MS	FUS-ICP	FUS-MS	FUS-ICP	FUS-MS	FUS-MS	FUS-MS	FUS-MS	FUS-MS	FUS-MS	FUS-MS	FUS-ICP	FUS-MS
522106	50	140	22	1.8	< 5	25	300	35.7	295	10.7	< 2	1.4	< 0.1	2	< 0.2	2	495	31.2
522136	40	80	20	1.6	< 5	58	528	16.1	153	5.1	< 2	0.6	< 0.1	1	< 0.2	3.1	580	25.2
522137	60	100	20	1.6	< 5	6	362	16.5	81	0.3	< 2	< 0.5	< 0.1	< 1	< 0.2	0.4	170	6.9
522138	50	90	20	1.8	< 5	5	379	16	76	0.2	< 2	< 0.5	< 0.1	< 1	< 0.2	0.3	174	7.29
522142	20	60	20	1.7	< 5	141	424	24.8	351	19.1	< 2	1.5	< 0.1	3	0.3	0.9	1223	73.7
522147	20	270	42	3.3	< 5	226	95	102	1223	196	7		< 0.1	11	0.3	6.7	192	152
527261	90	100	21	1.7	< 5	11	355	20.3	101	2.8	< 2	< 0.5	< 0.1	< 1	< 0.2	0.4	222	10.3
521114	< 10	< 30	27	0.6	< 5	41	86	168	48	4.6	< 2	< 0.5	< 0.1	1	< 0.2	2	81	9.91
521101	< 10	100	18	0.6	< 5	50	8	19.5	15	< 0.2	< 2	< 0.5	< 0.1	< 1	< 0.2	3.8	83	0.35
521145	< 10	< 30	22	0.7	< 5	66	42	25.2	19	< 0.2	< 2	< 0.5	< 0.1	< 1	< 0.2	21.1	231	1.8
521147	< 10	50	20	1	< 5	103	31	14.9	24	< 0.2	< 2	< 0.5	< 0.1	< 1	< 0.2	6.9	131	1.93
521106	< 10	70	19	0.5	< 5	53	10	13.1	17	< 0.2	< 2	< 0.5	< 0.1	< 1	< 0.2	3.7	89	0.19
unknown	230	110	21	2.2	< 5	3	210	28.6	109	< 0.2	< 2	< 0.5	< 0.1	1	< 0.2	< 0.1	48	6.31

Final Report
Activation Laboratories

Activation Laboratories, Ontario, Canada
Report Date: 12/30/2013

Analyte Symbol	Ce	Pr	Nd	Sm	Eu	Gd	Tb	Dy	Ho	Er	Tm	Yb	Lu	Hf	Ta	W	Tl	Pb
Unit Symbol	ppm	ppm	ppm	ppm	ppm	ppm	ppm	ppm	ppm	ppm	ppm	ppm	ppm	ppm	ppm	ppm	ppm	ppm
Detection Limit	0.05	0.01	0.05	0.01	0.005	0.01	0.01	0.01	0.01	0.01	0.005	0.01	0.002	0.1	0.01	0.5	0.05	5
Analysis Method	FUS-MS	FUS-MS	FUS-MS	FUS-MS	FUS-MS	FUS-MS	FUS-MS	FUS-MS	FUS-MS	FUS-MS	FUS-MS	FUS-MS	FUS-MS	FUS-MS	FUS-MS	FUS-MS	FUS-MS	FUS-MS
522106	67.8	8.79	35.2	7.47	2.31	7.06	1.18	6.77	1.31	3.74	0.556	3.64	0.519	5.7	0.61	1.7	0.11	< 5
522136	52.3	6.5	24.1	4.54	1.22	3.71	0.56	3.13	0.65	1.74	0.266	1.67	0.249	3.3	0.48	< 0.5	0.33	9
522137	16.4	2.4	10.7	2.85	1.16	3.03	0.53	3.07	0.64	1.71	0.252	1.66	0.266	1.8	0.21	< 0.5	< 0.05	< 5
522138	17.1	2.53	11.2	2.95	1.22	3.08	0.53	3.11	0.62	1.77	0.271	1.71	0.246	1.8	0.16	< 0.5	< 0.05	< 5
522142	149	17.3	59.7	9.77	1.6	6.23	0.87	4.66	0.88	2.6	0.379	2.58	0.378	8.3	1.33	< 0.5	0.79	20
522147	301	36.6	132	23.8	2.88	19.1	3.18	18.4	3.68	11.2	1.77	11.5	1.6	24.8	10.8	2.2	1.21	30
527261	22.9	3.25	14.3	3.57	1.29	3.56	0.64	3.86	0.8	2.11	0.304	2.08	0.319	2.3	0.28	< 0.5	0.18	< 5
521114	34.7	6.58	36.3	18.3	6.32	29.3	5.87	35.5	6.72	17.3	2.44	13.4	1.66	2.5	0.44	< 0.5	0.24	6
521101	0.92	0.16	0.9	0.79	0.323	2.34	0.54	3.81	0.79	2.04	0.26	1.67	0.233	0.3	< 0.01	< 0.5	0.45	< 5
521145	5.46	0.96	5.09	1.95	1.49	3.61	0.71	4.71	0.94	2.61	0.409	2.7	0.349	0.5	0.24	< 0.5	0.42	< 5
521147	4.97	0.8	4.06	1.41	0.643	2.07	0.39	2.58	0.56	1.67	0.244	1.67	0.25	0.6	< 0.01	< 0.5	0.66	< 5
521106	0.35	0.06	0.36	0.45	0.162	1.23	0.33	2.41	0.52	1.45	0.223	1.46	0.2	0.2	< 0.01	0.7	0.45	< 5
unknown	16.5	2.68	13.5	4.36	1.73	5.2	0.92	5.68	1.04	2.95	0.45	2.81	0.386	2.6	< 0.01	82.9	< 0.05	< 5

Analyte Symbol	Bi	Th	U
Unit Symbol	ppm	ppm	ppm
Detection Limit	0.1	0.05	0.01
Analysis Method	FUS-MS	FUS-MS	FUS-MS
522106	< 0.1	2.41	0.62
522136	< 0.1	5.39	3.89
522137	< 0.1	0.44	0.14
522138	< 0.1	0.44	0.13
522142	0.1	14.5	7.11
522147	< 0.1	19.8	6.1
527261	< 0.1	0.89	0.26
521114	< 0.1	8.56	0.92
521101	< 0.1	0.14	0.04
521145	0.9	0.17	0.29
521147	0.3	0.42	0.5
521106	< 0.1	< 0.05	0.04
unknown	< 0.1	0.51	0.14

Appendix D:

Chondrite-normalized plot of rare-earth element analyses from ruby-bearing and related rocks.

Appendix D:

Chondrite-normalized plot of rare-earth element analyses from corundum-bearing and related rocks

Plots of the normalized rare earth elements (REE) of the analysed samples from the FC show an order of magnitude difference among the analysed rocks (Figure A1). The light REEs show the largest variation among all samples, but the heavy REEs show sample 521114 with an order of magnitude higher concentration and the remaining rocks, all of which are grouped tightly at about 10 times chondrite. All the rocks show depletion of the light REE relative to the intermediate and heavy REE, but the diopside normative sample shows higher concentrations of all the REE. The corundum normative rocks have similar heavy REE and slight to more extensive depletion of the light REE (Figure A1). The light REE behave geochemically like Ca, so processes affecting Ca may be seen in the light REE. These REE patterns are consistent with the interpretation that the corundum normative bulk compositions are rocks where more extensive breakdown of plagioclase occurred and more Ca was removed. The high REE content of sample 521114, which is the CaO richest sample, is more difficult to explain. The presence of small amounts of allanite (pegmatite fluid) could explain the overall higher REE content. However, a geochemical study of more rocks would be necessary properly interpret the trace-element variation, which may possibly just represent local differences in the source rocks.

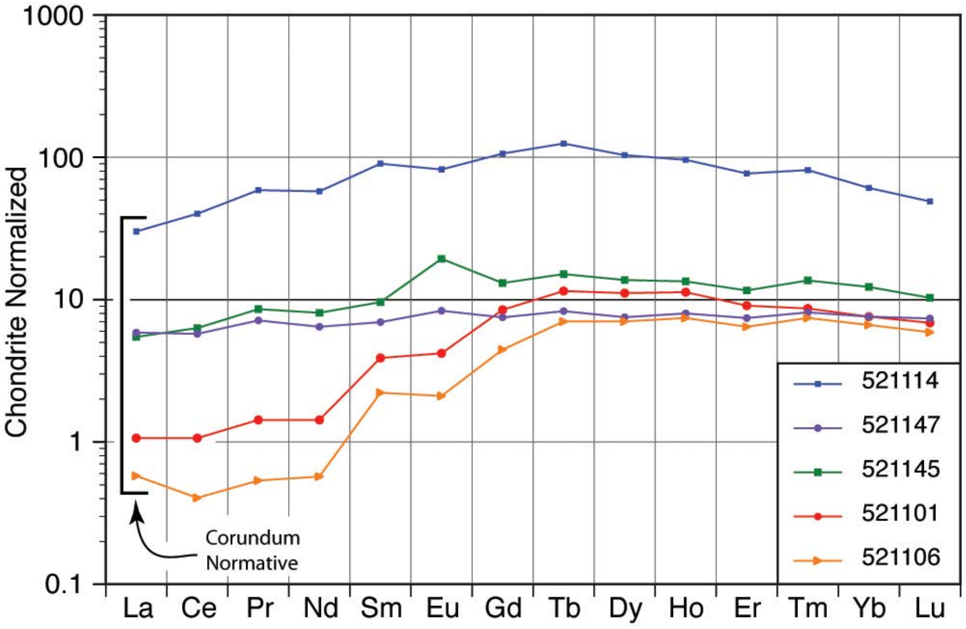

Figure A1: *Chondrite-normalized plot of rare-earth element analyses from corundum-bearing and related rocks.*